AD_____

Award Number: DAMD17-03-C-0122

TITLE: Novel Therapeutic and Prophylactic Modalities to Protect the United States Armed Forces against Major Biological Threat Agents

PRINCIPAL INVESTIGATOR: Serguei Popov, Ph.D.

CONTRACTING ORGANIZATION: George Mason University
Manassas, VA, 20110

REPORT DATE: August 2007

TYPE OF REPORT: Final

PREPARED FOR: U.S. Army Medical Research and Materiel Command
Fort Detrick, Maryland 21702-5012

REPORT DOCUMENTATION PAGE

Form Approved
OMB No. 0704-0188

1. REPORT DATE *(DD-MM-YYYY)*	**2. REPORT TYPE**	**3. DATES COVERED** *(From - To)*
01-08-2007	Final	29 SEP 2003 - 31 JUL 2007

4. TITLE AND SUBTITLE

Novel Therapeutic and Prophylactic Modalities to Protect the United States Armed Forces against Major Biological Threat Agents

5a. CONTRACT NUMBER

5b. GRANT NUMBER
DAMD17-03-C-0122

5c. PROGRAM ELEMENT NUMBER

6. AUTHOR(S)
Serguei Popov, Ph.D.

E-Mail: spopov@gmu.edu

5d. PROJECT NUMBER

5e. TASK NUMBER

5f. WORK UNIT NUMBER

7. PERFORMING ORGANIZATION NAME(S) AND ADDRESS(ES)

George Mason University
Manassas, VA, 20110

8. PERFORMING ORGANIZATION REPORT NUMBER

9. SPONSORING / MONITORING AGENCY NAME(S) AND ADDRESS(ES)
U.S. Army Medical Research and Materiel Command
Fort Detrick, Maryland 21702-5012

10. SPONSOR/MONITOR'S ACRONYM(S)

11. SPONSOR/MONITOR'S REPORT NUMBER(S)

12. DISTRIBUTION / AVAILABILITY STATEMENT
Approved for Public Release; Distribution Unlimited

13. SUPPLEMENTARY NOTES

14. ABSTRACT
We found that secreted virulence factors other than anthrax toxins play important role in anthrax. Our experiments revealed several pathogenic mechanisms relevant to the activity of anthrax proteases and hemolysins in cultured cells and mice challenged with B. anthracis spores. In the reporting period the research was focused on the hemostatic abnormalities manifested in the degradation of von Willebrand factor, release of this factor in response to anthrax proteins, and degradation of the ADAMTS13 protease. The results favor a hypothesis that an anticoagulant activity of secreted pathogenic factors along with the disruption of barrier permeability could be considered as a major cause of hemorrhage during infection. Studies on host cell signaling cascades allowed identify the cell survival pathways as new potential pharmacological targets. Inhibition of AKT pathway in spore-challenged cells indicates a strong contribution of the edema toxin generated cyclic AMP to the lethal outcome of infection. We conclude that in murine model the host response to anthrax infection is an important factor contributing to lethality. This hypothesis is substantiated by the protective effect of adenosine derivative in combination with ciprofloxacin in anthrax-challenged mice. We identified B. anthracis HSP60 protein as a potential TLR2 agonist capable of binding host cell CD91 receptor and inducing host inflammatory response.

15. SUBJECT TERMS
Biological weapons, lethal toxin blocker, protease inhibitors, toll-like receptors

16. SECURITY CLASSIFICATION OF:			**17. LIMITATION OF ABSTRACT**	**18. NUMBER OF PAGES**	**19a. NAME OF RESPONSIBLE PERSON**
a. REPORT	**b. ABSTRACT**	**c. THIS PAGE**			USAMRMC
U	U	U	UU	163	**19b. TELEPHONE NUMBER** *(include area code)*

Table of Contents

INTRODUCTION

This report covers the results obtained during the period from September 2005 till August 2007. In addition to the results presented in the 2006 Annual report, it includes updates on hemostatic abnormalities, toll-like receptor signaling during anthrax infection, and phosphoproteomics analyses of host cell response.

BODY OF THE REPORT

1. Task 1. Synergistic Anti-Toxin/Antibiotic Treatment of Anthrax

Experiments on this task have been completed and reported in the year 2004.

2. Task 2. Anthrax Protease Inhibitors for Therapy of Late-Stage Inhalational Anthrax[1]

2.1. Secreted Neutral Metalloproteases of *Bacillus anthracis* as Candidate Pathogenic Factors

Bacillus anthracis secrets two major virulence factors, lethal toxin (LT) and edema toxin (ET) encoded by megaplasmid XO1. Another plasmid XO2 encodes for the anti-phagocytic capsule,

[1] The abbreviations used are: AT, antithrombin; Cln, cytolytic lipase cereolysin; CBA, collagen binding activity; InhA, EF, edema factor; GST, ECM, extracellular matrix; glutathione S-transferase; HSPG, heparan sulfate proteoglycan; Ig, immunoglobulin; InhA, immune inhibitor A metalloprotease; LT, or LT, lethal toxin; LF, lethal factor; LB, Luria broth; MT1-MMP, membrane-type 1 MMP; MKK, mitogen-activated protein kinase (MAPK) kinase; MMP, matrix metalloprotease; Npr, neutral protease; NMuMG, normal murine mammary gland; PA, protective antigen; *p*NA, *p*-nitroanilide; PMA, phorbol 12-myristate 13-acetate; PTK, protein tyrosin kinase; PKC, protein kinase C; AnlO, anthralysin O; VWF, von Willebrand factor; ULVWF, ultra large von Willebrand factor; uPA, urokinase-type plasminogen activator

which substantially contributes to the virulence of the microbe. LT is necessary for pathogenicity, as deletion of its gene renders the microbe avirulent, while ET-knockout strains are only partially attenuated [1]. LT consists of a heptameric protective antigen (PA) noncovalently associated with lethal factor (LF). LT is a zinc metalloprotease, which cleaves and thus inhibits mitogen-activated protein kinase kinase (MAPKK) family members *in vitro* and *in vivo*, resulting in defective host cell signaling [2,3], with broad implications for the host innate and adaptive immune responses [4,5]. Based on its properties, LF is considered to be a major target for new anthrax therapies[6,7]. Specific LT blockers are expected to complement the existing antibiotic treatments [8], which alone are successful only in 55% of the inhalation anthrax patients [9]. It has been reported that the synthetic inhibitor of LT's proteolytic activity in combination with ciprofloxacin was protective in rabbits [7]. However a number of anthrax pathological features, such as massive hemorrhages, and intensive organ and tissue damage, cannot be explained by the sole activity of LT and ET, indicating the involvement of other virulence factors. Our animal experiments using culture supernatants of the non-toxigenic *B. anthracis* delta Ames strain, demonstrated their hemorrhagic effect in the skin and high toxicity upon intratracheal administration [10]. Consistent with this, several broad-spectrum protease inhibitors, as well as immune sera against anthrax M4 and M9 metalloproteases, displayed high efficacy in the post-exposure treatment of murine systemic anthrax [10]. These observations prompted us evaluate the pathogenic potential of the secreted proteolytic enzymes, which might serve "accessory" functions to LT, and therefore might be required for the full virulence of *B. anthracis*. To our best knowledge, *B. anthracis* extracellular proteases have not been previously characterized with respect to their enzymatic properties, as well as the activity toward pathologically-relevant substrates.

Bacterial proteases may exert tissue damage directly by cleaving the extracellular matrix (ECM) components such as collagen, laminin, fibronectin, or elastin [11,12]. Another general mechanism involves microbial interference with the homeostatic balance between endogenous proteases and their inhibitors, which determines tissue integrity. One of the examples is the effect of *Pseudomonas aeruginosa* elastase on the balance between neutrophil elastase and the inhibitors α_1-protease inhibitor and α_2-macroglobulin [13]. Mammalian plasminogen system can also serve as a target of

bacterial proteases, which can accelerate the urokinase-catalyzed activation of plasminogen and degrade endogenous plasmin inhibitors such as α_2-antiplasmin and α_2-macroglobulin [14]. As a result, the activated plasmin can directly digest laminin, a major glycoprotein of basement membranes, and indirectly further damage tissue barriers by activating latent matrix metalloproteases (MMPs) [15].

In addition to the ECM degradation, bacterial proteases are also involved in the pathogenic cleavage of the host cell surface molecules in a process of ectodomain shedding [16,17]. Shed ectodomains play pivotal roles in diverse pathophysiological events including septic shock, host defense, and wound healing [18, 19, 20]. During infection, secreted pathogenic factors enhance host ectodomain shedding which contributes to epithelial barrier disruption, endothelial damage, and tissue penetration by bacilli. For instance, LasA, a secreted virulence factor of *P. aeruginosa*, enhanced shedding of syndecan-1, which belongs to a family of cell surface heparan sulfate proteoglycans (HSPGs). The resulting soluble syndecan-1 ectodomains enhanced bacterial virulence in newborn mice [16,17]. Quite notably, inhibition of syndecan-1 shedding or neutralization of the shed ectodomain's heparan sulfate prevented lung infection of *P. aeruginosa* [16]. These facts indicate that proteolysis of the ECM and shedding of the cell surface ectodomain can play not only roles in signaling, but also in establishment of infection by acting as mediators of lethality perturbing different mechanisms of the host defense response.

We report here the purification, biochemical properties, and substrate specificity with regard to the ECM molecules, plasma proteins, and cell surface protein syndecan-1, of two neutral Zn-metalloproteases. The first, designated Npr599, is a thermolysin-like enzyme highly homologous to bacillolysins from other *Bacillus* species [21 22]. The second, designated InhA, is a homolog of the *B. thuringiensis* immune inhibitor A. These proteases belong to M4 and M6 families, respectively. Both of these enzymes can serve as possible pathogenic factors enhancing tissue destruction, bacterial invasion, and perturbation of host defense responses. Inhibition of the Npr599 and InhA activities *in vitro* correlates with the protective effects of the anti-protease treatments reported previously [10], indicating that they can be considered as potential therapeutic targets.

Npr599 and InhA are Abundant in Culture Supernatant of B. anthracis delta Ames

In anthrax pathology the extracellular secreted proteins distinct from LT represent virulence factors causing hemorrhage and other tissue damage [23, 24]. We previously detected the toxic properties of anthrax culture supernatants, and the ability of the elastase-like neutral protease (BA3442) belonging to the M4 family to induce hemorrhage in mice [10]. In order to understand molecular mechanisms of anthrax infection and to develop new therapeutic approaches, we undertook purification and characterization of secreted proteases from *B. anthracis*. The delta Ames strain ($pXO1^-$, $pXO2^-$) was cultured in a nutrient-limiting LB medium at 37^{o}C with vigorous agitation until stationary phase. Proteins from the culture supernatant were precipitated with ammonium sulfate and used for the DEAE-cellulose anion exchange chromatography. Two major peaks with enzymatic activities against casein and elastin were eluted from the column in the flow-through fractions (P1), and in the 200 mM NaCl (P2). The P1 and P2 protease fractions were pulled and further purified to apparent homogeneity on a Sephacryl S-200 gel filtration column chromatography. In the reduced denaturing SDS-PAGE, the purified enzymes show a single protein band for P1 with a molecular mass of 36 kDa, and two co-purified protein bands for P2 with molecular masses of 46 and 18 kDa (Fig. 1). The proteases are highly abundant [25] and therefore require a purification rate of only 3.2 over the crude culture supernatant.

To identify the proteases and to determine if the isolated proteins correspond to the particular maturation forms of preproenzymes, we sequenced the N-terminal amino acids by an automated Edman degradation. It was determined that P1 protease contains KPVTGTNAVG as a major sequence and VTGTNAVG as a subsequence. These results identify the sequences as the alternatively cleaved N-terminal parts of the catalytic domain of the M4 thermolysin-like neutral protease (NP_843132), with the calculated MW of 34.1 kDa (observed MW is 36kDa). The full P1 gene (BA0599 in *B. anthracis* Ames genome) encodes the protein, which is 99.3% identical to lactobacillus hydrolase (BAA06144), *B. cereus* neutral protease (AAZ42070, 99.1% identity), bacillolysin (YP034856, 97.7% identity) and bacillolysin MA (BAD60997, 72.3% identity), all of which

belong to the neutral protease family (Npr). This has low homology (33%) with *P. aeruginosa* LasB (DQ150629)[26] (29). We designated P1 as Npr599.

The N-terminal sequences of isolated P2 protease were determined as TGPVRGGLNG for the 46 kDa protein and SNGTEKKSHN for the 18 kDa protein. Both of the proteins originate from the M6 family immune inhibitor A metalloprotease (InhA) 98% similar to that of *B. cereus* and *B. thuringiensis* (30), and encoded by the BA1295 gene. Based on this sequence homology, it is likely that the 18 kDa protein (calculated MW 18.1 kDa) represents the auto-processed product of the InhA, as it has been previously shown for *B. cereus* [27].

Both Npr599 and InhA are Neutral Zn-Metalloproteases

The caseinolytic activities of Npr599 and InhA were assayed in the range of buffers with pH from 4 to 10. The highest activity at 37 °C is found in the Tris-HCl buffer in the interval of pH from 7 to 8, indicating that the isolated enzymes belong to the class of neutral proteases. To estimate the optimal temperature the proteases were assayed for the caseinolytic activity at 21, 37, 50, and 70°C at pH 7.8 in the Tris-HCl buffer. Both enzymes display high activity at 37°C, and remain fully active at 50°C. The effect of various inhibitors on the protease activity is presented in Table 1. Both Npr599 and InhA are rapidly inhibited by metal-chelating agents such as EDTA, 1,10-phenanthroline, while InhA is less sensitive to phosphoramidon and galardin, compared to Npr599. High concentrations of the disulfide bond reducing agent dithiothreitol (10 mM) inhibits both proteases, but milder thiol reducing compounds like β-mercaptoethanol and L-cysteine (at 1 mM) show no substantial activity, which is expected with the absence of cysteine residues in both protein sequences. Of note, the addition of 3.5 μM SDS activates Npr599 approximately 2.4-fold, similar to the effect of Brij 35 on the leukocyte elastase activity reported by Cook and Ternai [28], suggesting that these detergents could mimic a biologically-relevant activation mechanism. Divalent metal ions Cu^{2+}, Fe^{2+} and Zn^{2+} inhibit caseinolytic activities of Npr599 and InhA, whereas Ca^{2+}, Mg^{2+} and Mn^{2+} do not (Table 2). Both enzymes appear to require zinc for hydrolytic activity, since depletion of the metal ion from the active center with 1 mM 1,10-phenanthroline completely abolishes the activity against casein, which cannot

be restored by addition of excess $CaCl_2$ (1 mM). Both Npr599 and InhA contain a HEXXH motif, which is defined as a Zn-binding domain of metalloprotease [29]. Collectively, the above data agree with the primary structure-based identification of Npr599 and InhA proteases to M4 and M6 Zn-metalloenzymes [30], respectively (see above).

Potential Substrates for Npr599 and InhA Include ECM- and Hemorrhage-related Proteins

To evaluate the isolated proteases as pathogenic factors, we next surveyed their target molecules that are related to inflammation and innate immune response. When the internally quenched fluorescent substrates of casein, gelatin and elastin are used as substrates, Npr599 has strong activity for casein (14.1 U/mg) and elastin (17.5 U/mg) and weaker activity for gelatin (6.5 U/mg), while InhA has strong activity for casein (14.3 U/mg) and gelatin (16.3 U/mg) but weaker activity for elastin (4.3 U/mg). Individual kinetic parameters for synthetic collagenase substrate hydrolysis were evaluated by Lineweaver-Burk plot as summarized in Table 3. Among synthetic substrates tested, Mca-Pro-Leu-Gly-Leu-(DNP)Ala-Ala-Arg-NH_2 (k_{cat}=1.8 s^{-1}) and Mca-Pro-Leu-Ala-Nva-(DNP)Dpa-Ala-Arg-NH_2 (k_{cat}=54.5 s^{-1}) are the best turn-over substrates for Npr599 and InhA, respectively. InhA is about 15-fold more catalytically efficient than Npr599 in cleaving the substrate Mca-Pro-Leu-Gly-Leu-(DNP)Ala-Ala-Arg-NH_2 in terms of k_{cat}/K_m.

Since bacterial protease may cause tissue damage by directly degrading host tissues, significant host proteins were tested as substrates of the purified proteases. For example, the extracellular matrix proteins such as fibronectin, laminin, type I and IV collagens, which could be degraded during inflammation and bacterial infections, are candidate targets of *B. anthracis* proteases [11, 31]. Fig 2A shows that indeed both Npr599 and InhA effectively cleave fibronectin and type I collagen, while Npr599 is more active with laminin, and less active with collagen type IV, compared to InhA. In addition to the extracellular structural proteins, α_2-macroglobulin, α_2-antiplasmin and α_1-protease inhibitor are the most important serum protease inhibitors regulating the activity of plasmin and blood elastase [32]. Fig. 2B shows that both of these proteins are partially degraded by the proteases, which could potentially have high pathological relevance. On the other

hand, the purified proteases do not prominently digest immunoglobulins (Ig) G, M, and interferon-□which are important components of humoral and cell immunity (Fig. 2C). In the same conditions, the mucosal IgA is partially cleaved. With regard to the blood coagulation cascade, fibrinogen chains of Aα- and Bβ-type are completely cleaved by Npr599 within 4 h, unlike the γ-chains, which remain visible in the gel. On the other hand, all fibrinogen chains Aα-, Bβ- and γ-chains are completely cleaved by InhA (Fig. 2D). In addition, we further examined if denaturation of collagens leads to enhanced degradation and if the proteases exhibit antiplasmin inactivating activity. Fig. 3A and 3B show that collagens of type I, III and IV become more are more susceptible to proteolysis after denaturation, albeit native collagens are also degraded effectively. Besides, proteolysis of α_2-antiplasmin by Npr599, not by InhA, leads to complete loss of the plasmin inhibitory activity (Fig. 3C).

InhA May Modulate Blood Coagulation Cascade Through Regulation of Plasmin Activity

As mentioned above, bacterial proteases can activate mammalian plasminogen system to induce fibrinolysis and ECM degradation. We next investigated if protease-mediated cleavage of plasminogen generates plasmin activity. As shown in Fig. 2D, InhA is more active than Npr599 in cleaving human plasminogen, and produces a cleavage pattern of 5 major bands similar to that of bacillolysin MA [22]. Then, we analyzed protease-catalyzed plasmin activity using a chromogenic synthetic substrate Val-Leu-Lys-p-nitroanilide. The degradation of plasminogen does not generate the plasmin activity, in contrast to streptokinase of Staphylococcus aureus used as a positive control (Fig. 4A). This demonstrates that neither Npr599 nor InhA itself is a bacterial plasminogen activator. On the other hand, in the incubation of plasminogen with uPA, the addition of InhA elevated the initial rate of uPA-mediated plasminogen activation (Fig. 4B). This result suggests that InhA, but not Npr599, is a modulator of uPA-catalized plasminogen activation. Taken together, direct cleavage of endogenous plasmin inhibitors α_2-macroglobulin and α_2-antiplasmin (Fig. 2B), inactivation of α_2-antiplasmin by Npr599 (Fig. 3C), and InhA's modulating effects on plasmin activity during anthrax infection (Fig. 4), suggest that direct proteolytic effects of the secreted proteases during the

infectious process are likely to prevent initiation of both blood coagulation and clot fibrinolysis through modulation of the host's plasmin-mediated system.

Npr599 and InhA Activate Syndecan-1 Shedding Through Stimulation of the Host Cell's Shedding Mechanism

Proteolytic activity of Npr599 and InhA against components of extracellular matrix prompted us evaluate the effect of these proteases on intercellular interactions in epithelial monolayers. We were specifically interested in the fate of syndecan-1 ectodomains, which are involved in maintenance of barrier permeability, cytoskeleton organization, intercellular signaling, and have been recently implicated as mediators of lethality perturbing different mechanisms of the host defense response [16, 33]. We tested whether anthrax extracellular proteases can modulate syndecan-1 shedding from host cells using a culture of the NMuMG epithelial cells. Fig. 5 shows that both Npr599 and InhA can function as sheddases releasing soluble syndecan-1 molecules into culture media in a time- and dose-dependent manner. Maximum stimulation is reached at a concentration of 250 ng/ml for both Npr599 (~7-fold increase) and InhA (~22-fold increase) (Fig. 5A). Furthermore, shedding activation by Npr599 is rapid and saturable by 8 hrs, whereas InhA is not saturable by this time point (Fig. 5B). At high concentrations (> 250 ng/ml), Npr599 becomes ineffective in the acceleration of syndecan-1 shedding (Fig. 5A). Both Npr599 and InhA are shown to have minimal toxic effects on host cells when tested using LDH release assay (data not shown).

Since ectodomain shedding by host cells is inhibited by a variety of substances active in a number of receptor- and stress-activated signaling pathways, which involve protein tyrosine kinases (PTKs), protein kinase C (PKC), and mitogen-activated protein kinases (MAPKs) [34,35], we next analyzed the effects of the inhibitors of several of these pathways on shedding activity. Shedding by both Npr599 and InhA is strongly inhibited by piceatannol, a specific inhibitor of the cytoplasmic Syk family PTKs (Fig. 6), indicating that the cell PTK activity is involved in the bacterial protease-induced shedding. Suramin is a multi-potent inhibitor [36], which among other activities modulates protein tyrosine phosphatases (PTPs) involved in cell adhesion, integrin signaling and cell cycle progression

[37,38]. Specifically, suramin inhibits several PTPs in the low μM range, and activates them at higher concentrations. Because of low bioavailability, the suramin concentration above 50 μM has to be used for the activation effect [39]. Fig. 6 shows that similar to piceatannol, suramin stimulates syndecan shedding at 20 μM. At higher concentration, suramin effectively inhibits syndecan-1 shedding induced by proteases, supporting the notion that the effects of Npr599 and InhA on shedding are mediated by the host cell sheddase(s) through signaling pathways that involve PTKs and PTPs.

In order to understand if p38, ERK and JNK signaling pathways are involved in protease-mediated acceleration of syndecan shedding, we tested SB202190, an inhibitor of p38; PD98059, an inhibitor of MEK1/2 (ERK pathway); and the JNK inhibitor II. As shown in Fig. 6, low concentrations of either PD98059 or JNK inhibitor (5 μM) show some stimulatory effect on syndecan-1 shedding, but all three of them inhibit the InhA-induced syndecan-1 release in the concentration range of 5 to 50 μM typical for their activity, although Npr599 seems to be susceptible only to the JNK II inhibitor. The metalloprotease (sheddase) inhibitors galardin, phenanthroline and phosphoramidon inhibit the Npr599-activated shedding only partially and do not inhibit the InhA-activated one (Fig. 6). On the other hand, these inhibitors are active in the direct caseinolytic assay (Table 1). For example, phenanthroline at >1 μM completely abrogates digestion of casein but has no activity even at 20 μM with regard to shedding by both proteases. Taken together, these experiments highlight differences between Npr599 and InhA. While the activities of both converge on the activation of PTKs and PTPs, the Npr599, in contrast to InhA, seems to function rather independently of the cellular stress pathways.

Npr599 and InhA Can Further Accelerate Syndecan-1 Shedding Through Direct Proteolytic Cleavage of Ectodomain

To investigate whether Npr599 and InhA directly cleave the ectodomain of syndecan-1, we prepared recombinant rat syndecan-1 tagged with glutathion *S*-transferase (GST) at the amino terminal and expressed in *E. coli* BL21 host cells. The GST-syndecan-1 was purified through

glutathione-sepharose 4B beads. When incubated with Npr599 and InhA, GST-syndecan-1 protein is completely degraded within an hour (Fig. 7A). However LF, a metalloprotease component of lethal toxin, has no significant activity on syndecan-1 proteolysis (data not shown). To identify the degraded fragments, Western blot analysis is performed using anti-GST and anti-syndecan-1 antibody (N-18, Santa Cruz Biotechnology) raised against a 15-20 amino acid peptide, which maps within the first 50 amino acids of syndecan-1 of mouse origin. As shown in Fig. 7B, the major digestion products generated by Npr599 and InhA are approximately of a 32-kDa size, although the mobilities of the fragments are slightly different. This suggests that recombinant GST-syndecan-1 protein is cleaved at the site adjacent to the amino terminus, right after the heparan sulfate attachment sites.

To test how the digestion pattern of the recombinant protein is relevant to that of the syndecan-1 shed from the cell surface, we analyzed the syndecan-1 ectodomains after treatment of NMuMG cells with the purified proteases and *B. anthracis* culture supernatants. Fig. 8 shows that the sizes of the intact ectodomains (with HS chains attached to the core proteins) shed by both purified proteases and the culture supernatant are different from those of the unstimulated or the phorbol ester (PMA)-stimulated cells as the endogenous sheddase activation control [40]. The ectodomains after additional heparinase II- and chondroitinase ABC-digestions (with the core proteins stripped from the HS chains) become similar in size in all cases, and reveal an additional small fragment generated by the proteases, as well as by the culture supernatant. Together with the data on the N-terminal cleavage of the recombinant syndecan-1, these findings suggest that Npr599 and InhA are capable of syndecan-1 shedding through the direct proteolysis of the ectodomain at the site apart from that of the cellular sheddase.

Npr599 and InhA Cleave the Syndecan-1 Fusion Protein at the Asp^{39}-Asp^{40} and Gly^{48}-Thr^{49} Bond, Respectively

Finally, in order to determine the cleavage sites for each protease, recombinant GST-syndecan-1 fusion protein was incubated with Npr599 and InhA and separated on SDS-PAGE. The

major digestion products with GST-tag were trypsinized, and the resulting peptides were subjected to a reverse-phase liquid chromatography nanospray tandem mass spectrometry. Beside peptides with typical trypsin-cleaving amino acids (Lys and Arg), (R)L^{17}QPALPQIVTANVPPEDQDGSGD^{39}(D) (MH^+, 2361.16 Da) was found among the Npr599-digested peptides, whereas a peptide (R)L^{17}QPALPQIVTANVPPEDQDGSGDDSDNFSGSG^{48}(T) (MH^+, 3227.46 Da) was found with a high fidelity among the InhA-digested peptides. These data allow the assignment of Npr599 and InhA cleavage sites in the syndecan-1 core protein to the Asp^{39}-Asp^{40} and Gly^{48}-Thr^{49} peptide bonds, respectively. The HS chains in syndecan-1 are known to be attached at Ser^{37}, Ser^{45} and Ser^{47} (ref [41]). Therefore, the Npr599-induced shedding is expected to generate the N-terminal ectodomain fragments 1-39 with one HS chain, while the InhA-induced shedding would result in a single ectodomain fragment 1-49 containing all three HS chains. The differences in the lengths of the core fragments and the number of attached HS chains may influence the affinity of the detection antibody, and would contribute to the low intensity of the Western blot band in the case of Npr599 digestion, compared to the InhA (Fig. 8).

In the current report, InhA and Npr599 (bacillolysin) have been isolated as major proteases in the culture supernatants of the avirulent delta Ames strain of *Bacillus anthracis* in agreement with previous proteome analysis [42, 43]. It is likely that these proteases are controlled by the tetratricopeptide protein Cot43 [44], and contribute to the activity of LT and other virulence factors. The direct tissue-degrading activities of bacterial proteases are important factors of microbial pathology at all stages of the infectious process. With regard to inhalation anthrax, the hemorrhagic mediastinitis and hemorrhagic thoracic lymphadenitis are typical signs of such an activity [45]. In this study, both Npr599 and InhA have been found to cleave tissue components, such as fibronectin, laminin, type I and IV collagens, with some differences in specificity. Recent analyses confirmed that proteolytic degradation of extracellular matrix proteins in anthrax may play an important role in the development of hemorrhage and damage to endothelial and epithelial barriers [10,46]. In addition to structural damage relating to tissues, we show that Npr599 and InhA specifically cleave α_1-protease inhibitor, a neutrophil elastase inhibitor; α_2-macroglobulin, a universal protease inhibitor; as well as

α_2-antiplasmin, a plasmin inhibitor. Proteolysis of α_2-antiplasmin by Npr599 leads to loss of its plasmin inhibitory activity (Fig. 3C). As a potential consequence, the host protease inhibitor depletion by bacterial proteases may cause extensive tissue damage by disruption of normal host proteolytic balance and abnormal activation of the host neutrophil elastase [47]. This mechanism may be relevant to anthrax, because it has been shown that the intensity of neutrophil infiltration into tissues inversely correlated with the outcome [48]. In addition to this, fibrinogen and plasminogen are degraded by Npr599 and InhA. The *in vitro* cleavage by the proteases does not generate plasmin activity even in the presence of fibrin as an anti-autolytic agent, however the cleavage pattern of plasminogen produced by the purified proteases in our study is similar to that of bacillolysin MA [22]. It is therefore plausible that like bacillolysin, Npr599 and InhA may use the host plasmin for both fibrinolysis and invasion. In support of this suggestion, InhA elevates the initial rate of uPA-mediated plasminogen activation (Fig. 4B), and it remains to be studied if these or other *B. anthracis* proteases can activate the fibrinolytic system during infection, similar to the streptokinase of *S. aureus* [49](52). In a transgene experiment with human plasminogen in mice, streptokinase increased mortality during streptococci infection [50]. Although the loss of the endogenous plasmin inhibitors' activity upon cleavage with Npr599 and InhA has not been examined, it seems likely that the cleavage would cause a shift of hemostatic balance toward the activation of fibrinolysis.

The syndecan-1 shedding activity of *B. anthracis* proteases suggests additional pathogenic mechanisms. Syndecan ectodomains are constitutively shed from culture cells as part of normal cell surface HSPG turnover. Shedding is also activated as one of the host responses to stress, tissue injury, and other external stimuli [16,51] via endogenous metalloproteases [34,35,52] such as MT1-MMP, MMP-7 and MMP-9 [52,53,53, 54]. During disease, the abnormally increased levels of shed syndecans in the bloodstream could modulate susceptibility to infection or even become toxic [16,17]. For instance, shed syndecan-1 can tightly bind to host enzymes cathepsin G and neutrophil elastase and consequently decrease the affinity of these proteases for their physiological inhibitors [55]. This effect would further increase the neutrophil damage discussed above.

Our previous experiments have shown that secreted factors of *B. anthracis*, such as LT, pore-forming toxin anthralysin O (AnlO), and cytolytic lipases ClnA and AnlB accelerate the normal process of host cell syndecan-1 ectodomain shedding. Secreted α- and β-toxins of *S. aureus* also induce syndecan-1 shedding [34]. Our data increase the repertoire of *B. anthracis* sheddases and further support the notion that microbial shedding could exploit the host cell response to a variety of bacterial stress factors, which are likely to cause a cumulative effect of a pathogenic proportion. The experiments with inhibitors in this and previous reports [17,22,34] demonstrate that the accelerated shedding can involve different signaling pathways, thus reflecting the specific nature of the particular inducer, but seems to converge on the stimulation of cytoplasmic tyrosine kinases ultimately leading to the activation of cellular sheddase. On the other hand, our study presents evidence that shedding of syndecan-1 can also occur through the direct ectodomain cleavage by *B. anthracis* proteases. The recombinant syndecan-1 is susceptible to digestion, with the cleavage sites located at positions Asp^{39}-Asp^{40} and Gly^{48}-Thr^{49} in the case of Npr599 and InhA, respectively. In contrast, both constitutive and PMA-induced host-mediated syndecan-1 shedding are expected to result in cleavage at a juxtamembrane site located in the region adjacent to the putative transmembrane domain of syndecan-1 [53]. The results of the immunoblotting experiments using syndecan ectodomain shed from the NMuMG cells are in agreement with direct and host-mediated shedding taking place simultaneously. The effect of chemical inhibitors of proteolysis, such as phenanthroline, on shedding (Fig. 6) indicates that the contribution of direct cleavage is relatively minor for InhA, although it seems to be more important for Npr599. In support of this, piceatannol as the inhibitor of the endogenous mechanism at the highest tested concentration of 50 μM demonstrates some residual shedding (27% and 7% for Npr599 and InhA, respectively), which might be attributed to the direct effect of bacterial proteases. Previously it has been shown for the *P. aeruginosa* shedding enhancer LasA, a known metalloprotease virulence factor stimulated shedding independently of its strong elastolytic activity [17]. Recently, thrombin and plasmin have been reported to accelerate syndecan-1 and -4 shedding by a combination of direct and receptor-mediated mechanisms [54]. However our observation is the first example of bacterial proteases mimicking the direct shedding effect of host

proteases. Future therapeutic interventions targeting anthrax proteases should take into account the plural nature of their biological activity.

2.2. Anthrax Protease InhA is a Bacterial von Willebrand Factor-Cleaving Metalloprotease

We suggest that soluble syndecan ectodomain shedding induced by anthrax proteases or in response to activation, injury, or stress [56,57,58,59] may influence blood coagulation in a manner similar to the administration of soluble heparin. Although heparin has been a subject of intensive study, the reported experimental results are highly variable and even contradictory due to the intrinsic heterogeneity of the heparan sulfates deriving from differences in their origin and in the manufacturing processes (often proprietary). When rapidly administered intravenously, unfractionated heparin (UFH) reduced platelet counts and prolonged bleeding times, creating a platelet deficiency. *In vitro*, low doses of heparin are more apt to reduce platelet aggregation, and high doses are more likely to increase it. Platelets aggregate in response to most agonists, including ADP, adrenaline, collagen, and platelet activating factor.[60]

Another aspect of heparin influence on blood coagulation is its interaction with the glycoprotein von Willebrand Factor (VWF). After blood vessel injury, VWF is the only multimeric protein involved in platelet adhesion to the extracellular matrix under conditions of shear stress generated by blood flow along the vessel wall. VWF is composed of identical 250-kD subunits, with the multimer typically exceeding 10,000 kD. Each subunit has a single 24-kD A1 domain that binds to the amino-terminal 45-kD segment of platelet receptor GpIbα [61]. Increased tethering of platelets to endothelium can be caused by elevated levels of ULVWF polymers as a result of activation by microbial factors. The examples are Rickettsial infection of cultured cells[62,63] and *in vivo*,[64] Rocky Mountain spotted fever,[65] human cytomegalovirus,[66] herpes virus,[67,68] and *H. pylori.*[69] Deficiency of the protease ADAMTS13, which specifically cleaves VWF, is another possible mechanism. ADAMTS13 may be inactivated by thrombin and plasmin,[70] as a result of which the pro-thrombotic inflammatory response of the ECs would be expected to promote an increase in the amount of

ULVWF. Patients with sepsis-induced DIC display lower molecular weight forms of ADAMTS13 in plasma, suggesting its cleavage by proteases in addition to decreased synthesis in the liver.[71] ADAMTS13 deficiency is also associated with enterohemorrhagic *E. coli* infection.[72] Therefore it was intriguing to test whether ADAMTS13 can serve as a substrate for anthrax proteolytic enzymes.

InhA Degrade ULVWF Multimers in a Temperature-dependent Manner.

The cleavage of VWF by ADAMTS13 in vitro is stimulated by high fluid shear stress or by mild denaturation of VWF with urea or guanidine hydrochloride, suggesting that conformational changes in VWF are necessary to expose the domain A2 cleavage site or ADAMTS13-binding sites. In addition, VWF proteolysis in plasma is elevated in denaturing conditions without $BaCl_2$ at subphysiological temperature (e.g. at 22℃). To investigate if Npr599 and InhA facilitate VWF proteolysis in denaturing condition at subphysiological or physiological temperature, human normal plasma was incubated with the proteases in the absence or presence of urea at room temperature or 37℃. At room temperature, ULVWF is cleaved by ADAMTS13 in plasma in the presence of urea (Fig. 9A, lane 14). In this condition, LB culture supernatant (Fig. 9A, lane 8) and InhA (Fig. 9A, lane 11) further enhanced ULVWF cleavage. Plasma ULVWF was cleaved to a smaller extent by Npr599 (Fig. 9A, lane 3) and InhA (Fig. 9A, lane 5) at room temperature in the absence of urea. On the other hand, both Npr599 and InhA enhanced the cleavage of ULVWF at 37℃ in the presence of urea (Fig. 9B, lanes 10 & 11). However, ULVWF is not cleaved by the plasma at 37℃ even in the presence of urea (Fig. 9B, lane 14).

VWF monomer was also analyzed in 6% SDS-PAGE gel under reducing condition after incubating with proteases. As shown in Fig. 10, Npr599 cleaved VWF monomer only at 37℃ to a lesser extent. However, InhA cleaves VWF monomer at both room temperature and 37℃. EDTA completely inhibits Npr599- and InhA-dependent VWF cleavage at 37℃ (Fig. 10C). These suggest that Npr599 and InhA enhance plasma ULVWF cleavage at 37℃ in the presence of urea in a temperature-dependent manner. In addition, to investigate the fate of ADAMTS13, an endogenous VWF-cleaving metalloprotease in plasma, normal plasma was incubated with proteases in the

absence of denaturant. Western blot analysis showed that InhA effectively degrades ADAMTS13 proteins (Fig. 10D). This suggests that InhA-dependent VWF proteolysis is not affected by endogenous ADAMTS13, and implies a strong disturbance of hemostasis during anthrax infection.

Npr599 and InhA cleave a synthetic VWF substrate FRET-VWF73, and InhA degrades native VWF

Recently, a minimal synthetic ADAMTS13 substrate FRETS-VWF73, which contains cleavage site of VWF A2 domain, was developed for fluorescent energy transfer (FRETs) assay. The peptide substrate corresponds to residues Asp^{1596}-Arg^{1668} and contains the Tyr^{1605}-Met^{1606} bond that is cleaved by ADAMTS13. First of all, it was intriguing to check whether FRET-VWF73 can be used as a substrate for VWF's Npr599- or InhA-dependent proteolysis. Therefore, FRETS assay was performed using a fluorescence spectrophotometry in the presence of Ca^{2+} (Table 4). Proteolysis of FRETS-VWF73 was dependent on both enzyme and substrate concentrations (Fig. 10A). The rate of proteolysis by Npr599 and InhA displayed a linear or a hyperbolic dependence on the substrate, respectively. The reaction demonstrated typical Michaelis-Menten kinetics with K_m or k_{cat}, as summarized in Fig. 10B. The K_m and k_{cat} of Npr599 were derived to 2.3- and ~3-fold lower than ADAMTS13, respectively. However, InhA showed a similar substrate affinity (K_m), approximately 18-fold and 15-fold increase of turnover rate (k_{cat}) and catalytic efficiency (k_{cat}/K_m) compared with ADAMTS13, respectively. These results suggest that InhA is specific and fast in VWF cleavage, at least, within A2 domain. To further determine the cleavage sites of native VWF by Npr599 and InhA, we treated native VWF with the proteases and sequenced the N-terminal amino acids of its fragmented products. Native VWF was degradable by InhA, but not by Npr599, under a mild denaturing condition (1.5 M urea). Treatment of InhA produced two major bands (fragments II and III), which were sequenced to be SLSCR and VLQRC, respectively. Because cysteine residue is not able to be detected in automated Edman degradation, the 4^{th} amino acid of fragment II and the 5^{th} amino acid of fragment III assumed to be cysteine according to database of VWF protein sequence. Fig. 11 summarizes the localization of cleavage sites of VWF by InhA. This assignment was further

supported by LTQ-MS analysis (data not shown). ADAMTS13 cleaves at a position Tyr^{1605}-Met^{1606} of A2 domain, while InhA does at a position Leu^{1664}-Val^{1665}. This is consistent with cleavage pattern of plasma VWF in a Western blot analysis in terms of molecular weights of fragments. Overall, these results suggest that anthrax protease InhA mimics endogenous plasma VWF-cleaving protease ADAMTS13.

Npr599 and InhA abolish VWF's collagen-binding activity

The binding of VWF to the collagen is the first step in the initiation of primary hemostasis. The native conformation of VWF is essential for the interaction with collagen, but limited reduction of multimers to their dimeric form results in decreased binding to collagen. In order to measure the binding of protease-treated VWF to the collagen, collagen-binding assay (CBA) was performed using normal human plasma and human placenta type III collagen. In the absence of urea, no significant inhibition of VWF binding to collagen by anthrax protease treatment was observed in different concentrations (data not shown). However, in the presence of 1.5 M urea, Npr599 and InhA strongly inhibited VWF binding to collagen in a concentration-dependent manner (Fig. 5A). LF did not show any inhibition of the binding in different concentration (0.01 -10 μg/ml). Incubation of proteases with *o*-phenanthroline results in total abolishment of Npr599- or InhA-dependent CBA inhibition (Fig. 5B). This suggests that Npr599 and InhA modulate VWF binding to the collagen matrix by VWF proteolysis in the presence of urea, in which native conformation of VWF is changed to protease-susceptible state.

Npr599 and InhA bind to VWF

With regard to inhibition of VWF binding to the collagen, we tested if the proteases interact with VWF, because an endogenous VWF-cleaving protease ADMATS13 binds to VWF through its spacer domain. Fig. 12A shows a protease-transferred PVDF membrane stained with naphthol blue. In VWF overlay analysis as shown in Fig. 12B, Npr599 strongly binds to VWF, while InA is weakly bound to VWF, displaying relatively strong binding of C-terminal truncated fragment (18 kDa)

compared to catalytic domain-containing fragment (46 kDa). When human collagen type III was used as a positive control, strong binding to VWF was observed. Cleavage and binding properties of Npr599 and InhA to VWF mimic ADAMTS13, an endogenous VWF-cleaving metalloprotease that binds to its substrate. This result suggests that Npr599 binding to VWF may, in turn, modulate VWF-mediated platelet aggregation. We speculate that this feature of Npr599 is related to prolonged bleeding time, a typical manifestation of anthrax infection.

InhA inhibits ristocetin-induced platelet aggregation

Proteolysis of VWF impairs ristocetin-induced platelet aggregation (RIPA) by disturbing interaction between VWF and its platelet receptor glycoprotein (GP) Ibα. In order to investigate effect of Npr599 and InhA on RIPA, plasma VWF was preincubated with the proteases in the presence of urea and then formalin-fixed platelets and ristocetin were added to induce platelet aggregation. Platelet aggregation by different concentrations of plasma was examined under the microscope. Npr599-treated plasma showed a similar RIPA activity as control plasma; however, InhA completely inhibited platelet aggregation (Fig. 13C and D, *inlets*). Quantification of RIPA was performed by a flow cytometry using anti-CD41 antibody to detect free platelets. Flow cytometric method is much more sensitive and quantitative than conventional aggregometry in detecting the early stages of platelet aggregation. As shown in Fig. 13, preincubation of plasma with Npr599 and InhA inhibits RIPA up to 32% and 84%, respectively, compared with none-treated control. LF exhibited no significant decrease in RIPA. On the other hand, preincubation of InhA with 5 mM *o*-phenanthroline blocks inhibitory effect of InhA on RIPA (Fig. 13E). This suggests that inhibition of platelet aggregation by InhA-treated VWF is caused by VWF fragmentation, but not by InhA binding to VWF as shown above (Fig. 12).

Anthrax proteases induce and then degrade VWF multimers from HUVEC cells

Human umbilical vein endothelial cells (HUVECs) are known to secrete ULVWF multimeric strings after stimulation with histamine or Shiga toxins of *E. coli* O157:H7. To investigate whether

anthrax pathogenic factors stimulate secretion of ULVWF multimers in HUVECs, AnlO and culture supernatants were used as shown in Figs. 14, 15. However, ULVWF induced by culture supernatants showed a dimeric form. As a positive control, human normal plasma (1:10 dilution) was used for ULVWF multimer analysis. When VWF monomer was analyzed in reducing condition, only supernatant after AnlO treatment showed clear monomer band in Western blot. Culture supernatant induced release of VWF proteins from HUVECs; however, monomer was not detected in this analysis. From this observation, it is possible to speculate that proteases in culture supernatants can digest ULVWF multimers secreted from HUVECs.

ADAMTS13 and ULVWF are depleted in plasma of spore-challenged mice

The *in vitro* data presented above prompted us to test if stimulation of VWF release suggested by the HUVEC cell model and concomitant degradation of both VWF and ADAMTS13 by secreted proteases reflected the features of anthrax infection *in vivo*. Mice (DBA/2) were challenged with *B. anthracis* spores of either the toxigenic Sterne $34F_2$ strain [$pXO1^+$, $pXO2^-$] or the atoxigenic delta Sterne strain [$pXO1^-$, $pXO2^-$]. Blood samples were drawn every 24 h post challenge. In the conditions of our experiments, the delta Sterne strain caused no clinical signs of infection or detectable bacteremia, while about 50% of Sterne-challenged mice died at day 3 post infection with massive proliferation of bacteria in the spleen and liver [6]. The proteolytic activities of culture supernatants for both strains tested with casein as substrate were similar (± 10%) (data not shown).

ADAMTS13 was significantly depleted from serum during infection at day 3 post Sterne spore challenge and at day 2 post delta Sterne spore challenge. All Sterne-challenged animals died by day 5, but all delta Sterne-challenged mice survived after they recovered the level of ADAMTS13 at day 3 post challenge (Fig. 16A) consistent with the non-virulent nature of the delta Sterne strain. In both challenge groups the animals responded to infection with the activation of ADAMTS13 gene transcription in the liver, where the protein is synthesized. The expression of the gene returned to normal upon recovery in the case of the delta Sterne-challenged mice (Fig. 16B). In contrast, the aggravating condition of the Sterne-challenged mice was accompanied by a steady increase in the

ADAMTS13 gene transcription (up to ~2.8-fold at day 3 post challenge). The profile of the ADAMTS13 transcription was mirrored by the amount of VWF antigen recognized by a specific antibody in plasma of infected mice (Fig. 16B), perhaps indicating an increased physiological demand of the host to maintain hemostasis in response to ADAMTS13 depletion and the elevated levels of VWF.

Taking into account the capacity of secreted proteases to degrade ADAMTS13 and VWF, we suggested that the multimerization state of VWF in the plasma of challenged animals would be indicative of the infectious process severity. When plasma samples from spore-challenged mice were analyzed on a SDS-agarose gel, Sterne spore-challenged mice displayed significant reduction of high MW multimers starting at day 3 (Fig. 17A). This indicated the onset of intensive proteolysis of VWF multimers before death in the case of Sterne spore challenge. The delta Sterne spore-challenged mice showed a gradual decrease of multimer amount (Fig. 17B). By day 5, all Sterne-challenged animals died, while all delta Sterne-challenged mice survived. The survived mice were able overcome the loss of intact VWF, although the recovery of hemostatic parameters in these mice took about 4 more days (data not shown).

As expected, the Sterne-challenged mice demonstrated early dramatic loss of VWF capable of collagen binding (Fig. 18A) in spite of the increase in the total amount of circulating VWF antigen (Fig. 18B). In the case of delta Sterne challenge, there was a partial loss of the collagen-binding capacity of circulating VWF with a trend to recover a normal function of VWF (Fig. 18A). Overall, VWF antigen levels showed an inverse correlation with collagen binding activity in the plasma for both *B. anthracis* strains (Fig. 18C), indicating the accumulation of functionally defective VWF during infection. The above observations in challenged mice are consistent with the *in vitro* data obtained with purified enzymes although direct demonstration of Npr599 and InhA roles *in vivo* requires further experimentation.

Secreted metalloproteases Npr599 and InhA are candidate *B. anthracis* virulence factors capable of degrading a variety of biologically important substrates. In this report we extended

analyses of these proteases to cleavage of VWF and its natural regulator ADAMTS13. The choice of these proteins was determined by their important roles in hemostasis along with the observations on severe DIC-like coagulopathy in anthrax infection [24 73 74]. For example, VWF-deficient mice develop spontaneous bleeding in intra-abdomen and massive hemorrhage in the neck and head [75]. On the other hand, accumulation of ULVWF multimers in ADAMTS13 knockout mice results in a prothrombotic state [76]. In humans the ADAMTS13 deficiency may lead to a condition known as Thrombotic Thrombocytopenic Purpura (TTP). As a result of the abnormal processing of ULVWF, most patients with TTP develop platelet-rich thrombi in the microvasculature, renal failure, neurologic disfunction, and 90% of them ultimately die [77]. Recently, Ono *et al.* [78] demonstrated that sepsis-induced DIC was associated with a severe secondary ADAMTS13 deficiency. In these patients, the amount of antigen and enzymatic activity of ADAMTS13 were decreased to less than 20% of their normal level and were accompanied by increased multimerization of VWF.

Currently, DIC in anthrax has no mechanistic explanation. A previous study in LT-injected mice suggested that blood vessel leakage and hemorrhage led to DIC and circulatory shock as underlying pathophysiological mechanisms [79]. However, there were no reports related to ADAMTS13 and/or VWF pathologies in anthrax. Our findings point toward possible roles of metalloproteases Npr599 and InhA in a life-threatening anthrax coagulopathy. We demonstrate that these proteases are capable of cleaving VWF *in vitro*. Specifically, InhA cleaves VWF at least at three sites, two of which are located within the A2 domain of the molecule, including the one in the immediate proximity to the endogenous ADAMTS13 cleavage site. The cleavage pattern suggests that InhA could be more potent than ADAMTS13 and therefore could cause a significant reduction of ULVWF multimers in the blood. Normally, VWF is cleaved rapidly by ADAMTS13 in the conditions of high fluid shear stress but is resistant to cleavage under static conditions [80]. Our data show that InhA is capable of cleaving VWF in static conditions without urea, as well as in conditions where the protein is partially unfolded by urea. Hemorrhagic lymphadenitis and meningitis are common pathologic features of inhalation anthrax, and it seems plausible that during anthrax pathogenesis the InhA may contribute to

hemorrhage by cleaving VWF and therefore reducing the capacity of the host to repair vascular damage.

One of the VWF functions is to bridge platelets to exposed reactive surfaces at sites of vascular injury. In this process, the collagen binding domain is involved in anchoring of VWF to damaged vessels. We found that the InhA-mediated degradation completely abrogated collagen binding of VWF. In addition, binding of VWF to platelets in the presence of ristocetin was strongly inhibited by InhA, but not by Npr599 or LF, the proteolytic component of LT.

We also found that in human plasma, InhA effectively degraded not only VWF but ADAMTS13. Various proteases have been shown to degrade ADAMTS13 *in vitro*. Thrombin, plasmin, and granulocyte elastase generated during DIC can cause inactivation of ADAMTS13 [81 82], and InhA is the first bacterial protease implicated in this process. In addition, in the experiments with HUVECs we found that InhA, hemolytic protein AnlO, as well as *B. anthracis* proteins secreted in the culture media induced a strong release of VWF accompanied by its concomitant cleavage. When microvascular endothelial cell layers are damaged by pathogen infection or trauma, ULVWF multimers secreted from endothelial cells bind to the ECM components including the collagen. GP-1bα receptor of platelets interacts with ULVWF multimers resulting in subsequent growth of hemostatic plug formation. In these circumstances the ADAMTS13 deficiency is expected to be pro-thrombotic because it increases the VWF multimerization. In contrast, VWF deficiency is associated with spontaneous bleeding [83]. When both ADAMTS13 and VWF can be degraded by InhA, the hemostatic consequences of its proteolytic activity are difficult to predict based only on the *in vitro* results and may depend on a specific biological setting. Our experiments with human plasma show that in the presence of InhA the pattern of VWF cleavage does not contain bands typical for ADAMTS13 activity and therefore suggests that InhA can cause a fast preferential degradation of ADAMTS13. This however may not correctly reflect the situation *in vivo* because a balance between pro- and anti-thrombotic VWF-associated processes in anthrax infection may depend on a number of factors, such as individual host susceptibility, differential expression and distribution of pathogenic proteins within the infected host, blood flow hydrodynamics in the vessels of different size, etc. This

consideration may, at least in part, explain variability of hemostatic abnormalities often observed between patients and even inbred experimental animals, as well as the paradoxical simultaneous presence of hemorrhage and thrombosis in the same patient.

To confirm that our *in vitro* observations were relevant to situation *in vivo*, we investigated the role of VWF and ADAMTS13 in anthrax murine model during systemic infection. Available data demonstrate that InhA (encoded by BA0672 and BA1295 genes) can be detected in the sera of infected animals as active protein. In mice challenged with a lethal dose of Sterne spores the protein levels of ADAMTS13 were significantly reduced on day 3 although mRNA levels remained steadily elevated until death (>50% of animals died by day 3). Reduction in both the ULVWF amount and the capacity of VWF to bind collagen coincided with the depletion of ADAMTS13 and remained low through the entire course of infection with Sterne spores while the antigen level of VWF continued to grow. Overall, the results of the virulent Sterne challenge indicated the onset of the overwhelming proteolysis of circulating ADAMTS13 and ULVWF before death. In comparison, all animals challenged with the same dose of non-virulent delta Sterne spores experienced similar but less severe symptoms, demonstrated recovery from disease, and ultimately all survived. In the case of both strain challenges the deficiency of ADMATS13 did not induce an increase of ULVWF levels in anthrax plasma. Furthermore, a decrease of ADAMTS13 showed no correlation with either degradation of ULVWF or antigen level. It is therefore plausible that, similar to experiments with human plasma *in vitro*, during infection the secreted proteolytic factors of *B. anthracis* quickly deplete ADAMTS13 and take a complete control over the fate of circulating VWF. Fig. 18C shows that gradual reduction in the collagen binding capacity of VWF correlates with increased total amount of VWF antigen in plasma, which may reflect systemic endothelial injury and consequent activation. Before death, the animals demonstrate almost a complete loss of VWF binding capacity which therefore might be considered as a marker of lethality.

Currently, it seems to be firmly established that systemic anthrax is associated with overt or probable DIC in human patients [24], as well as in the recently developed baboon model [73] showing a significant increase in vascular permeability coincident with hemostatic imbalances manifested by

TP, transient leucopenia, and microthrombosis. The latter is a typical feature of anthrax but the mechanism of its formation is unknown. Thrombosis is commonly attributed to the increase in ULVWF but not the VWF fragmentation found in our experiments. Nevertheless, increased fragmentation of VWF has been reported during the acute disease phase in patients with HUS and TTP in association with thrombosis, suggesting a permissive role of fragmented VWF in the formation of microvascular thrombi [84]. A recent comparison study with normal and $VWF^{-/-}$ mice strongly suggested the existence of a ligand for platelet GP-Ibα other than VWF during thrombus formation in the injured vessels [85]. Furthermore, thrombus formation observed in fibrinogen-deficient mice and in mice doubly deficient for fibrinogen and VWF showed the existence of a novel platelet aggregation pathway independent of both fibrinogen and VWF [86 87]. These results allow explain the formation of microvascular thrombi under VWF fragmentation in anthrax, but the precise role of VWF in anthrax thrombosis requires further studies.

In summary, our results demonstrate a new proteolytic mechanism of hemostatic imbalance in anthrax, which affects both the levels and activities of VWF and its natural regulator ADAMTS13 in plasma of spore-challenged mice, correlates with the severity of infectious process, and could contribute to hemorrhage and thrombosis typical in challenged animals and anthrax patients. The experiments with human plasma and purified anthrax proteases indicate that InhA and Npr599, but not LT, could be considered as pathogenic factors effectively compromising functions of VWF and ADAMTS13 in the repair of vascular damage and regulation of platelet recruitment to injured endothelium.

2.3. Antithrombin Depletion in Spore-challenged Mice

Sepsis is the systemic response to infection and is caused by the activation of host defense mechanisms. Severe sepsis is triggered by diverse pathogens that lead to secretion of pro- and anti-inflammatory cytokines, activation and mobilization of leukocytes, activation of coagulation and inhibition of fibrinolysis which can lead to organ dysfunction, hypoperfusion or septic-induced

hypotension [88] [89] [90]. During sepsis there is activation of both the coagulation cascade and the endothelial cell localized anticoagulant pathway. Both of these systems have opposing effects on systemic inflammation and can cause dire consequences when using anticoagulant therapy as a treatment strategy [91]. We hypothesized that neutrophil elastase, the heparin sulfate proteoglycans of shed syndecan and AT form a complex and initiate fibrinolysis and fibrin degredation products in anthrax patients (Fig. 19).

Antithrombin (AT) is a plasma-derived, single chain glycoprotein which is a serine protease inhibitor. AT controls the activity of thrombin and the inhibition of several other proteases of the coagulation cascade. AT has potent anticoagulant activity which has been found to be significantly enhanced by heparin and vessel wall-associated glycosaminoglycans (GAGs). The plasma levels of AT sharply decrease in sepsis, which has been previously shown to cause a dramatic imbalance in hemostasis and homeostasis resulting in an excess of activated factors [92].

Disseminated intravascular coagulation (DIC) is an acute condition that can arise from a variety of situations including some surgical procedures, septic shock, poisonous snakebites, liver disease and postpartum. With DIC, clotting factors are activated and then used up throughout the body. This creates numerous blood clots and at the same time leaves the patient vulnerable to excessive bleeding [93]. These clinical features are similar to the edema, thrombosis and vascular leakage seen in anthrax patients [94]. In the rat model for DIC [95] the profibrinolytic response is almost immediately followed by a suppression of fibrinolytic activity which is caused by a sustained increase in the plasma level of plasminogen activator inhibitor (PAI) in the blood. Other indicators of DIC are the sharp increase of thrombin-AT complex (TAT) which has been shown to increase as much as 70% in the rat model of DIC [95]. Elevated D-dimers are the breakdown products of a fibrin mesh characteristic of the final step in the generation of a thrombus in conditions such as deep vein thrombosis, pulmonary embolism and DIC [96]. Plasma levels of D-dimers in the rat model of DIC show a 50-fold increase as early as 4 h post challenge [95]. The aims of this part of our study was (i) to characterize blood coagulation abnormalities and their contribution to the septic response in

Bacillus anthracis spore challenged mice and (ii) to examine the role of neutrophil elastase and syndecan shedding in AT depletion in anthrax pathogenesis.

B. anthracis spore challenge impairs fibrinolysis in mice

D-dimers: Our data shows significant increase in D-dimers as early as 24 h post spore challenge in both Sterne and Δ-Sterne mice (Tables 6,7 and Fig.19). This indicates early aggressive hemostatic changes associated with fibrin formation and fibrinolysis. The thrombotic response is irrespective of exotoxin activities and therefore may be due to the host's own coagulopathic response to the septic challenge.

The plasminogen activation system (PAS) is tightly regulated in the plasma through its inhibitors, PAI-1and 2, and alpha-1-protease inhibitor (α1-PI) [97 98 99]. PAI-1 is the main regulator of endogenous fibrinolysis by inhibiting the serine proteases tissue plasminogen activator (tPA) and urokinase plasminogen activator (uPA) [100]. PAI-1 is synthesized by a number of tissues, mainly the vascular endothelial cells which are released into the circulating bloodstream. In plasma, PAI-1 complexes and neutralizes tissue plasminogen activator (t-PA) under normal conditions. Clinical studies have shown that septic patients with low plasminogen activity have increased levels of PAI-1, indicating a shift toward inhibition of fibrinolysis in patients with fulminate liver failure and death [101]. In our experiments, PAI-1 is increased 2-fold in Sterne challenged mice (days 1-3) and 3-fold in Δ-Sterne challenged mice (day 2). We tested if the increased levels of PAI were associated with a concomitant activation of PAS. uPA is elevated on day 2 post Sterne challenge and there is no significant change in the Δ-Sterne challenged mice except a decrease on day 3 (Tables 6,7). These data suggest that activation of PAS may be relevant to virulence, because consequently all Sterne challenged mice died and the Δ-Sterne challenged mice recovered from the infection.

PAI-2 does not normally appear in the plasma, and the detectable levels of PAI-2 in septic shock patients are associated with poor prognosis. PAI-2 is thought to be an inhibitor of uPA which participates in cell migration, wound healing and tissue infiltration [101]. Our results show that levels of

PAI-2 in the plasma rise faster and remain higher in the Sterne-challenged mice compared to the Δ-Sterne-challenged mice.

α1-Protease inhibitor , also known as α_1-antiplasmin, is the major circulating serine protease inhibitor with high activity toward the neutrophil serine proteases such as neutrophil elastase [102]. Most of the circulating α_1-PI is synthesized by the liver and is released rapidly during the acute phase response to inflammation or infection [103] [104]. Our results show an increase in α_1-PI in plasma as early as 24-hours post challenge in both Sterne- and Δ-Sterne-challenged mice (Tables 6, 7) indicative of the early acute phase response during anthrax infection. Later in infection, the levels of α_1-PI drop below normal in the case of Sterne challenge, although the Δ-Sterne-challenged mice seem to recover and maintain α_1-PI at the level close to normal. α2-Protease inhibitor (α_2-PI), also known as α_2-antiplasmin, is a serine protease inhibitor which is the main physiologic inhibitor of fibrinolytic plasmin in the blood. α_2-PI is synthesized in the liver and rapidly inactivates plasmin resulting in the formation of the stable plasmin-α_2-antiplasmin (PAP) complex [105] [106] [107]. Our data do not show a significant change of the α_2-PI levels in the plasma. Increase of PAP concentration in blood is typically indicative of a coagulation activation in response to fibrinolysis in sepsis [108]. The main role of fibrinolytic system is the removal of fibrin. Activation of fibrinolysis, which may reflect a self-defense mechanism against vascular injury, has been found in acute stroke, myocardial infarction, unstable angina and arterial fibrillation [105] [108] [109] [110]. Our data show PAP levels increased in Sterne (day 3) and Δ-Sterne (day 2 and 3) indicating a fibrinolytic response to increased coagulation (Tables 6, 7). This pro-coagulant state could contribute to multiple organ dysfunction often seen in anthrax associated sepsis since fibrin deposition in the microvasculature contributes to hypoxygenation of tissues.

TAT levels are often used to assess consumption of the coagulation inhibitors in the blood. As seen in Tables 6 and 7, TAT levels initially decrease on day 1 in both Sterne and Δ-Sterne spore-challenged mice with a significant increase in TAT levels on day 3. This marked consumption of AT indicated that it could be associated with a depletion of AT levels in blood.

AT is depleted in plasma of spore-challenged mice

Reduced AT activity in the blood is often considered as one of the most important diagnostic indicators in sepsis [111] [112]. Fig. 20 shows that levels of AT in the plasma of spore-challenged mice decrease dramatically during 24-120 h post challenge for both Sterne and Δ-Sterne spore-challenged mice. Survival of mice at 72-120 h post challenge is associated with increase in the level of circulating AT. The slow recovery of AT in the blood is usually a result of liver dysfunction [95]. In order to determine if the reduced AT levels are caused by low expression of *AT* in the liver of *B. anthracis* spore challenged mice, we used RT-PCR of liver tissue homogenates. The results show a steady increase in the *AT* expression after Sterne challenge compared with a relatively small transcriptional response in delta Sterne-challenged mice (Fig. 21). Therefore, we suggest that AT depletion is not caused by suppression of its gene expression in the liver, and that AT proteolysis takes place in the plasma. One of the mechanisms for proteolytic inactivation of AT is activation of neutrophil elastase, which can take place in the presence of heparan-sulfated proteoglycans, such as heparin [113]. Therefore we tested the expression of syndecan-1 and -4 in the liver.

Syndecan-1 and -4 expression in the liver

It has been previously found that major pathogens such as *Staphylococcus aureus* and *Pseudomonas aeruginosa* cause ectodomain shedding of syndecan as a major virulence factor [114] [115]. Studies on *B. anthracis* virulence factors also confirmed that syndecan shedding is abnormally increased in the course of the infectious process [198]. Fig. 22, 23 show that Sterne spore-challenged mice respond to infection with a significant increase in syndecan-1 and 4 expression while delta Sterne challenge stimulates the expression of syndecan-1 only. This finding is consistent with the mechanism in which stimulation of syndecan expression may represent a compensatory response to its increased shedding during the infectious process.

AT interacts with shed syndecan-1, syndecan-4 and neutrophil elastase

We suggested that shed syndecan can activate neutrophil elastase (NE), which is produced in granulocyte precursor cells and released upon surface activation, phagocytosis, or cell death [116] [117]. NE is known to inactivate AT by a specific and limited proteolytic cleavage. This inactivation reaction is greatly accelerated by an active anticoagulant heparin subfraction with high binding affinity for antithrombin (AT) [113]. Our data show that NE level in blood is increased at 24 - 48 h post challenge (Fig. 24). This increase coincides with the appearance of the high molecular weight NE complexes and the disappearance of AT indicating possible interaction of these proteins (Fig. 24). Consistent with an increase in NE is a decrease in the amount of α_1-PI detected by Western blot in plasma of Sterne-challenged mice indicating a consumption of the NE inhibitor.

To investigate interaction of AT with neutrophil elastase and shed syndecans, the overlay assay was conducted using isolated proteins (AT and NE) with the culture supernatant of murine mammary gland (NMuMG) epithelial cells as a source of shed syndecans. Purified AT was blotted on a nitrocellulose membrane and overlaid with NE, AnlO-treated NMuMG culture supernatant, and α_1-protease inhibitor. To detect AT-protein interaction on the membrane, we used specific antibodies against AT, NE, syndecan-1, syndecan-4 and α1-protease inhibitor (Fig. 25). The results show that AT interacts with NE as well as syndecans, but not with α_1-AT, and are consistent with the hypothesis on the role of NE in syndecan-mediated AT degradation.

Shed syndecans accelerate NE-mediated AT proteolysis

Fig. 26 shows that both heparin and culture supernatants of nMuMG cells containing syndecans accelerate proteolysis of AT. Higher proteolysis is detected with the NuMG supernatant after AnlO treatment leading to increased syndecans' shedding. To further confirm the role of shed syndecans in NE acceleration, the culture supernatant was treated with anti-syndecan-1 and anti-syndecan-4 antibodies, and the activity of the immunodepleted supernatants was tested in the AT inactivation assay. As shown in Fig. 26, immunodepleted culture supernatant recovered more AT activity than the undepleted control in a concentration-dependent manner.

This data suggest that *B. anthracis* could cause a rapid pro-coagulation shift in hemostasis through the acceleration of syndecan shedding leading to the activation of NE and decrease in AT level in blood.

This study was aimed to evaluate coagulation and fibrinolysis factors in the anthrax murine model. The current data demonstrate that infection with toxigenic *B. anthracis* elicits many features of sepsis, therefore the lethal role of the host response may have been previously underestimated. The broad spectrum of AT's capacity to inhibit almost all coagulation factors renders it the most important serpin in hemostasis. A significant decrease in AT (below 70%) leads to a dramatic imbalance in hemostasis and homeostasis resulting in an excess of activated factors [118]. AT has two distinct and independent actions in patients with inflammatory and pro-coagulatory diseases, namely interference with pathologic coagulation and inhibition of inflammation [118]. From the preliminary data, we propose the inactivation of AT in anthrax pathogenesis is caused by neutrophil elastase, shed syndecan and AT forming a complex in the blood. Thus, we hypothesize that AT's heparin binding site may be blocked by soluble shed syndecan causing the anti-inflammatory properties of AT to be hindered leading to the septic response in the mouse model. Further research into the host septic response during *B. anthracis* infection may provide a novel pathologic mechanism which may ultimately contribute to new therapeutic and detection strategies to decrease mortality in anthrax patients.

2.4. Kinomics analyses of the lung epithelial cell response to anthrax challenge

This section describes our results on the analyses of phosphoprotein signaling in the cells exposed to *B. anthracis*, in order to elucidate the mechanisms of pathogenic factors' activity in anthrax. We also refer to the previously reported results, which have been reevaluated based on the new hypotheses.

Effective prophylaxes and treatments of infectious diseases remain a challenging task in spite of the tremendous advances in antibiotic and chemo therapies during the last century. The ever evolving microbial world effectively adapts to new drugs and generates previously unknown species. This not only limits the choice of effective therapeutics but puts additional requirements for timely and accurate diagnoses. The need for new approaches to combat infections is especially evident in the areas of biodefense addressing a threat of biological weapon attacks with highly-virulent agents, which might have been additionally engineered to resist existing vaccines and therapeutics. *Bacillus anthracis*, a causative agent of anthrax is a typical example of such a threat. Inhalation of the anthrax spores can cause a severe infection, and historically 92% of people with this form of exposure to anthrax died regardless of the treatment they received [119]. Although patients in the U.S. attack in 2001 were less likely to die, the mortality rate of inhalation anthrax (55%) remains unacceptably high. Both antibiotic- and vaccine-resistant recombinant variants of *B. anthracis* have been reported.

Conceptually, the solution of the problem requires not only the development of new antimicrobials targeting the causative agent, but also the effective approaches mitigating the pathogenic consequences of the host response to infection. The latter could be attained using systems biology tools allowing to reveal the inter-relations between pathogenic virulence factors, host immune responses, cytokine and chemokine autocrine and paracrine feedbacks, and effect of and on cellular signaling pathways. One of the goals promising several important prophylactic and therapeutic benefits would be to boost the innate immune to pathogen during the early stages of infection, and to correct the homeostatic imbalance during the disease progression. There seems to be a possibility to design broad-spectrum therapeutics based on the commonalities in the host responses to different pathogens, including the antibiotic-resistant ones. Currently, the drugs approved for inhalation anthrax treatment remain limited to fluoroquinolone and tetracycline classes of antibiotics, which are ineffective against the septic shock condition often manifested in the hypoxic organ failure and circulatory collapse [120]. The virulence of *B. anthracis* is mainly attributed to its lethal and edema toxins (LT and ET, correspondingly) encoded by the XO1 plasmid, as well as the anti-

phagocytic capsule encoded by the XO2 plasmid, although the events leading to death of infected animals and patients remain incompletely understood [121]. A considerable effort has been devoted to the development of specific inhibitors of the proteolytic activity of lethal toxin, however promising results in animal models have been reported only recently [122]. Targeting of other anthrax proteolytic factors in mice has also demonstrated high level of protection during the post-exposure treatment [123]. We however for the first time attempted to explore the therapeutic efficacy of pharmacological modulation of the host response during anthrax infection, in addition to the classical antibacterial and antitoxin methods.

As a means of determining potential novel therapeutic targets we first sought to understand the impact of anthrax infection on host signaling pathways using cell culture conditions that mimic a human exposure route. In the case of inhalation anthrax, the outcome of the spore interaction with the epithelial surface of the lungs has long been recognized as one of the factors contributing to bacterial virulence. Persistence of the dormant spores in the lungs remains a challenging problem in the current antibiotic-based prophylaxis of anthrax [124], as exposed persons are required to take antibiotics for at least 60 days. Human lung epithelial cells were used as the *in vitro* model of early inhalation exposure, and cell signaling events were monitored before and during exposure to the germinating anthrax spores and vegetative cells. We then employed a novel protein microarray platform developed in our laboratory for multiplexed analysis of phosphorylation-driven cell signaling cascades recently used by us for tissue-based cancer studies[125].

Using this technology, which takes advantage of the large and growing number of antibodies that only recognized proteins when they are phosphorylated, it is possible to quantitatively and sensitively measure over 100 kinase substrates from a few thousand cells. To more specifically identify cell signaling pathways that are causally important/related to the infectious process directly, we performed the signal pathway profiling using a toxigenic anthrax strain Sterne ($pXO1^+$, $pXO2^-$) and compared the impact of bacterial exposure on lung epithelial host cell signaling with the isogenic, non-pathogenic anthrax strain delta-Sterne ($pXO1^-$, $pXO2^-$). The use of a pathogenic and non-pathogenic

strain provides a means to identify the pathogenic host responses due to the expression of anthrax virulence factors encoded by the pXO1 plasmid.

Importantly, previous studies have failed to utilize these isogenic matched strains and typically report results using only virulent strains or toxins [126,127,128,129,130]. This approach also provides for the opportunity to study the late bacteremic stages of infection, when anthrax-encoded secreted toxins along with other pathogenic factors are thought to be involved in the damage to the host vital organs with high epithelial content, such as lung, liver, spleen, and kidney. Therefore data collected and results generated by the exposure of primary lung epithelial cells to a pathogenic and non-pathogenic strain could be of general guidance regarding therapeutic mitigation of anthrax, and validating the biological significance of our findings in animal models systems (e.g. spore challenged mice).

The dynamics of cell signaling phosphorylation in the Human Small Airway Epithelial Cells (HSAECs) after exposure to anthrax spores was tested using 43 different antibodies (see Supplement) validated as specific in our previous studies, and which were selected based on their ability to broadly monitor molecular networks involved in host response pathways most likely to be affected by bacterial exposure: survival, apoptosis, inflammation, growth, and differentiation and immune response. Two separate independent experiments were performed, and an average of the measurements were analyzed. Of the 43 different signaling endpoints measured, 24 appeared to be statistically changed upon exposure to either strain, and 6 of the most important responses were additionally tested and verified using western blot analysis. The most prominent changes in the lung epithelial responses consist in the inhibition by the pathogenic strain, compared to the non-pathogenic strain, of the pro-survival signaling pathway, namely the phosphorylation of mitogen-activated protein kinases (MAPKKs) ERK1/2 (p44/42 MAPK) along with their downstream target p90 RSK; other members of the MAPK family, such as the stress-activated kinases p38 and JNK; and global regulators of survival pathways serine/threonine kinases AKT1/2 (Fig.27). Consistent with our observations, the up-regulation of phosphorylation of ERK and AKT kinases is commonly accepted as serving a more protective role, which is directed to the elimination of non-pathogenic bacteria [131, 132, 133]. AKT is a pluripotent mediator of a number of cellular processes, and one of the most

important mediators of cell survival, providing a crucial link between the PI3 kinase and the anti-apoptotic mediators [134]. Down-regulation of ERK and AKT phosphorylation in the epithelium upon exposure to the pathogenic anthrax strain compared to the non-pathogenic strain points to a pathogenic mechanism leading to suppression of epithelial survival and abrogation of protective functions of epithelial cells. Although MAPKKs are well known as specific targets of lethal toxin (LT) proteolytic activity [135, 136] and implicated in the induction of apoptosis by LT in macrophages and epithelial cells [137, 138], the finding that phosphorylation of AKT in target host cells is affected by anthrax exposure is novel. AKT is also a regulator of glycogen synthesis *via* the phosphorylation of glycogen synthase kinase 3 (GSK3), and its inactivation might be directly relevant to the abnormal glucose levels observed in anthrax patients and experimental animals exposed to anthrax.

Another possible connection between AKT signaling and anthrax pathology is the adenylate cyclase activity of edema toxin (ET). Cyclic AMP (cAMP) and its effector, cAMP-dependent protein kinase (PKA), are an integral component of a variety of intracellular signaling pathways. In many cell types, an increase in levels of intracellular cAMP diminishes cell growth and has inhibitory effects on AKT signaling by blocking its coupling between AKT and its upstream regulators [139, 140]. We therefore speculated that the adenylate cyclase activity of the ET could be relevant to the downregulation of AKT phosphorylation observed with the toxigenic strain. The results shown in Fig. 28 provide evidence to confirm this hypothesis. HSAECs exposed to different concentrations of ET demonstrate an initial increase in the AKT phosphorylation, which is followed by the opposite trend for at least 8 h, and then returns to the levels close to normal within 24 h. At the same time, LT does not influence the AKT phosphorylation in HSAECs (data not shown). This pattern of AKT phosphorylation change is in agreement with the cAMP-mediated physiological response of experimental animals to the prolonged intravenous infusion of epinephrine [141, 142]. A vasoconstriction of the terminal arterioles and venules persists until the venules gradually become hyporeactive and dilate, resulting in terminal shock. Vascular collapse has long been recognized as a major contributor to anthrax terminal condition, and recent reports reconfirmed it [121].

Taken together, the above observations suggested that pharmacologically correcting the altered host cell intracellular signaling, could affect the lethal outcome in anthrax-challenged animals. Although none of the individual in vitro models can account for the entire complexity of the host-pathogen infectious process in the whole organism, we determined that HSAECs would be of value for testing therapeutic approaches that target the host cell response. According to the conclusions made by Smith *et al.*[143], we reasoned that such an approach should include at least three components capable of correcting the signaling abnormalities caused by the activities of both major toxins, LT and ET, in addition to the antibiotic ciprofloxacin, which would target the bacterial proliferation. Based on our previous findings demonstrating apoptosis induced by LT in both cultured macrophages and livers of anthrax-challenged mice, as well as the protective effect of apoptosis inhibition with a general caspase inhibitor z-VAD (z-Val-Ala-Asp(OMe)-fluoromethylketone) and a specific caspase-1/4 inhibitor YVAD (acetyl−tyrosyl-valyl-alanyl-aspartyl−chloromethylketone) in both of these models [144], we chose to test the effect of YVAD in combination with ciprofloxacin. Recent evidence regarding different infectious agents indicates that caspase-1-mediated generation of IL-1β represents an important inflammatory consequence of apoptosis [145,146]. It has also been reported that cAMP-mediated pathways produce pro-apoptotic signaling for several cell types such as cardiomyocytes [141]. Fig. 29 shows that only four doses of the inhibitor administered at the days +1 through +4 post infection protect up to 70% of animals in the combination therapy with ciprofloxacin (at days +1 through +10). In these conditions, when the beginning of treatment was delayed till day +1 post infection in order to better model the real clinical setting, the antibiotic alone protected only 30% of animals.

Based on our observation of decreased host cell AKT phosphorylation as a result of exposure to the pathogenic anthrax strain, we next explored the effect of pharmacologically altering the cAMP-mediated host cell AKT signaling under the hypothesis that the activated phosphorylated levels of this important mediator could result from both the physiological stress on the host cells from the infectious process itself as well as the biological activity of ET. To the best of our knowledge, cAMP, and as a consequence, AKT activation has never been previously tested as a target of the

anti-anthrax therapy. Thus, we explored the pharmacological stimulation of the adenosine A3 receptors (A3ARs) known to directly control and influence overall cAMP levels in the cell. Specific agonists of A3ARs such as IB-MECA [N6- (3-iodobenzyl) adenosine-5'-N-methyluronamide] and its Cl-substituted derivative Cl-IB-MECA, beside affecting and down-regulating cAMP, predictably enhance phosphorylation of ERK1/2, AKT and GSK-3β (S9) in mice [147, 148] These A3ARs also display other biologic effects, which seem to be potentially beneficial for anthrax treatment such as cardioprotection during hypoxia [149], inhibition of apoptosis, protection from endotoxemia [150] and colitis [151], as well as decreased mortality, renal and hepatic injury in sepsis [152]. In our experiments, treatment with Cl-IB-MECA at optimal dose of 0.15 mg/kg shows a remarkable 40% protection even without antibiotic (Fig. 29C). Combinations of different Cl-IB-MECA doses with ciprofloxacin are more effective than the antibiotic alone. A statistically reliable ($p<0.05$) difference is observed with the 0.3 mg/kg dose of Cl-IB-MECA. Based upon these dosing determinants, we further investigated triple combinations of YVAD, Cl-IB-MECA and ciprofloxacin (Fig. 29 E, F) which target generation of IL-1β, A3AR, and bacterial growth, respectively. While combinations of YVAD, Cl-IB-MECA, tested at two doses, are marginally protective, a very strong synergistic effect resulting in up to 90% protection takes place with ciprofloxacin. These results indicate that the down-regulation of the ERK and AKT survival axis as observed in host lung epithelial cells is not a simple correlative finding, but is casually important in disease pathogenesis and overall anthrax-induced mortality. These findings also indicate that an optimal combination post-exposure anthrax therapy based entirely on the modulation of the host response to infection could be highly effective, and highly synergistic with the current state-of-care antibiotic, ciprofloxacin. The cultured lung epithelial cells challenged with anthrax spores serve as sensors of infection, and are sensitive to pathogenic factors encoded by the toxigenic plasmid pXO1. The ability to broadly measure the activation and phosphorylation of cell signaling pathways using a novel proteomic provided critical information about which specific signaling networks, out of the myriad of potential candidates, were altered. The use of isogenic matched non-pathogenic and pathogenic strains for host challenge studies also proved highly valuable for the facile determination of specifically affected networks. Ultimately, the information

gleaned from the in vitro cell line experiments provided a rationale for the pharmacological approach used in the animal model. The mouse studies revealed that the pathway effects observed in cell culture were not a simple correlative finding, but underpinned the most important direct biological outcome of anthrax exposure: mortality.

Among these pathways, interference with the cell survival program through modulation of MAPK and AKT activation may represent an important part of anthrax pathogenic strategy. This is in agreement with the recent report on the inhibition of T lymphocyte AKT phosphorylation *in vivo* by LT [153], and allows rational explanation of some poorly understood pathophysiological features of anthrax. Liver damage and cardiovascular collapse are considered to be the major causes of death of anthrax toxin-challenged animals. Our results demonstrate that enhanced GSK-3β phosphorylation at low MOI is followed by its downregulation at higher number of bacteria. We show that ET through generation of cAMP is able to modulate AKT, and this suggests, based on the fact that GSK-3β is a specific substrate of AKT kinase activity, that the downstream activity of GSK-3β regulating glycogenolysis by liver and skeletal muscles may be responsible for the glucose level perturbation in anthrax [154]. LT has also been shown to modify transcription of the GSK-3β-mediated genes in macrophages by unknown mechanism [126]. The physiological effects of cAMP on liver and other organs mimic stimulation of the vascular adrenergic receptors (ARs). The epinephrine-like activity of culture filtrate from *B. anthracis* and other observations, such as the “sudden death” phenomenon commonly observed in anthrax patients, have long implicated the involvement of central nervous system (CNS) in the action of anthrax toxins, and indicated the existence of unknown low-molecular-weight, endogenously produced AR agonist [142, 155]. We suggest that his role could be attributed to cAMP produced either as a mediator of physiological stress under the control CNS and/or as a result of ET enzymatic activity. The finding that cAMP–mediated signaling through AKT is a key axis for mediating anthrax pathogenesis, could also at least partially explain the protective effect of β-AR agonist isoproterenol, which was able to prevent live-threatening drop in blood pressure caused by intensive vasodilation in monkeys administered lethal doses of crude anthrax toxin [156]. Elevation of cAMP can quickly improve endothelial barrier function however the

prolonged generation of cAMP by ET is expected to result in the opposite effect leading to low oxygenation of blood and ultimately contributing to septic shock. Indeed, current therapies based on the protective role of cAMP for the vasculature barrier function often fail [157]. Another potential factor is a cardiomyocyte hypercontracture and toxicity upon chronic exposure to cAMP, which mimics the well-known effect of catecholamines, including norepinephrine, through β1-AR [141]. In addition, the coordinated action of LT as the inhibitor of p38 signaling is expected to abrogate the anti-apoptotic effect of β2-AR stimulation coupled to PI3 kinase and AKT [158], because this anti-apoptotic effect is mediated through p38 [159].

In conclusion, we present experimental evidence of a highly effective post-exposure treatment strategy for anthrax which targets the host response, mediated through specific pro-survival pathways. The inhibitors we tested have no direct antimicrobial or anti-toxin function, and demonstrate a synergistic effect on survival in combination with a low antibiotic dose. Instead of blocking the enzymatic activity of anthrax toxins, both the caspase inhibitor and the A3AR agonist are expected to modulate host cell inflammatory and apoptotic signaling mediators [152]. A paradigm where infectious disease pathogenesis is controlled by modulating host response represents an exciting approach to combating pathogenic organisms, including weaponized versions where agents such as anthrax are purposefully engineered to resist conventional anti-microbial therapies. These findings warrant extending the results obtained in mouse models shown in this study to primate models that most closely relate to human exposure. Based on these findings, it seems intriguing to expand the application of the phosphoproteomic approach for signal pathway and molecular network analysis used here to other infectious agents, and to explore the correlative relations between in vitro and in vivo models.

Task 3. Toll-Like Receptor (TLR)-Neutralizing Antibodies And Soluble TLRs As Specific And Broad-Spectrum Protection Against Biological Weapons

Task 3 had been initially formulated by Dr. K. Alibek based on the hypothesis that TLR

signaling by LT plays a pathogenic role during anthrax infection. During research on this Task presented in the previous reports, we found that TLR signaling *in vitro* was effectively inhibited by the toxigenic infection. These finding strongly argued against the initial hypothesis and prompted us to evaluate a potential contribution of TLR signaling in anthrax. We also found that proteins from culture supernatants of the atoxigenic strain can cause activation of TLR-2 signaling, and therefore we undertook isolation and characterization of potential TLR anthrax agonists.

3.1. Isolation and Characterisation of *B. anthracis* TLR signaling products

Production of TNF-α by bacterial exoproducts in RAW264.7 cells

To test the TNF-α production by bacterial exoproducts through TLRs, mouse macrophage RAW264.7 cells were treated with *B. anthracis* delta Ames culture supernatants, TX-114 extracts of cells or supernatants, and positive control (LPS and Pam_3CSK) in DMEM media supplemented with 5% fetal calf serum. Using a TNF-α ELISA kit, the production was measured in each conditioned media. LB culture supernatant (protease-positive) shows no TNF-α production, while LB culture supernatant in the presence of 0.5% glucose (protease-null) shows high TNF-α production (Fig. 30). TX-114 extracts from the cell pellet and 0.5% glucose-LB supernatant show high TNF-α production, a similar level of LPS and Pam_3CSK treatment.

Protease-positive culture supernatant (obtained in the absence of glucose in culture medium) abrogates LPS- and Pam_3CSk- mediated TNF-α production

Next, we examined the effect of protease activity on TNF-α production in RAW264.7 cells. RAW264.7 cells were treated with different concentrations of LPS or Pam_3CSK and 1 μg/ml of supernatants, and TNF-α production was determined after 24 hrs incubation using an ELISA. LPS- and Pam_3CSK-mediated TNF-α production was abrogated by protease-positive culture supernatants as shown in Fig. 31. However, protease-null supernatant (LB 0.5%G) shows no decrease of TNF-

α. This suggests that secreted proteases modulate TLR-mediated TNF-α production in RAW264.7 cells. We found that secreted proteases can partially degrade TNF-α released upon TLR stimulation (data not shown), however it remains to be determined if secreted proteases can also interfere with the LPS or Pam_3CSK signaling pathways.

TLR-2 agonists from culture supernatants and Triton X-114 extracts of cells

PAMP molecules against TLR-2 were fractionated using Sephacryl S-200 column chromatography after TX-114 extraction (Fig. 32) [Amersham GE Sephacryl S-200HR, flow rate=1.3 ml/min, fraction volume 5 ml]. Fraction number 20-21 from TX-114 extract of supernatant showed the same retention time and protein profile in SDS-PAGE (data not shown) as the fraction number 21 from supernatant itself (Fig. 33). Each fraction was examined for TLR2-mediated NF-kB activation in HEK293/TLR2/CD14 cells. Two major fractions from supernatants activate NF-kB activity effectively. In order to see TNF-α production of each fraction, the active fractions were combined and treated to mouse macrophage RAW264.7 cells in DMEM media containing 5% FBS. The conditioned media was also subjected to TNF-α ELISA analysis. As shown in Fig. 27 (*right bottom panel*), fraction number 21 (Fr. #21) and 46-53 (Fr. #46-53supt) activated TNF-α. During concentration, fractions #46-53 were precipitated from the solution. The precipitates (Fr. #46-53ppt) activate the TNF-α production as well. Cell extracts with TX-114 were also fractionated using sephacryl S-200 chromatography in the same conditions as that used in the fractionation of supernatant. As shown in Fig. 34, gel filtration profile of the bacterial cell extract differs from that of supernatants, suggesting the existence of different PAMP molecules. Lipoteicoic acid, lipoprotein and peptidoglycan can be extracted by TX-114 from the cell membrane and wall. In next step, we are going to identify the each component from different fractions using LC/MS analysis.

Exoproducts of B. anthracis may induce apoptosis of mouse macrophage RAW264.7 cells

Bacterial exoproducts regulate apoptosis or proliferation of macrophage cells. To check apoptosis of RAW264.7 cells, the cells were treated with culture supernatants and positive control

(LPS and Pam_3CSK). Then nuclei were stained with DAPI to see chromatin morphology under fluorescent microscope. Fig. 35 shows DNA condensation or fragmentation by both culture supernatants in the absence and the presence of glucose. LB media alone shows an even DAPI staining of nuclei, whereas LPS and Pam_3CSK represent chromatin condensation and faint DAPI staining, indicating macrophage apoptosis. To see morphology of the cells, the pictures of RAW cells were taken under light microscope after bacterial exoproducts. Cells treated with culture supernatant from LB (+ 0.5% glucose) show a similar morphology with Pam_3CSK-treated cells (Fig. 36). Fraction number 21 (Fr. #21) induce more severe cell damage compared with other treatments. More quantitative estimation of apoptosis needs to be done using Anexin V staining or TUNEL assay. Fraction #46-53 (Fr#50supt and Fr#50ppt) shows an elongated shape of the cells, suggesting a cell differentiation.

Identification of TLR agonists of fraction numbers 20-21 from culture supernatants

Fractionation of TX-114 extracts of culture supernatants (containing glucose 0.5%) allowed to test fractions #20-21 with regard to the TLR-2-dependent NF-kB activation. The fraction showed at least four protein bands in a SDS-PAGE in a range of MW 90 – 60 kDa. Protein bands were excised from the gel and digested with trypsin (Promega) according to published procedure [199]. Tryptic peptides were analyzed by the reverse-phase liquid chromatography nanospray tandem mass spectrometry using a linear ion-trap mass spectrometer (LTQ, ThermoElectron) and a 100 µm × 10 cm-long fused silica capillary column (Polymicro Technologies) with a laser-pulled tip, packed with 5 µm, 200 Å pore size C_{18} resin (Michrom BioResources). After sample injection, the column was washed for 5 min with a mobile phase A (0.4% acetic acid) and peptides were eluted using a linear gradient of 0% mobile phase B (0.4% acetic acid, 80% acetonitrile) to 50% mobile phase B in 30 min at 0.25 µl/min, then to 100% B in an additional 5 min. The LTQ mass spectrometer was operated in a data-dependent mode, in which each full MS scan was followed by five MS/MS scans where the five most abundant molecular ions were dynamically selected for collision-induced dissociation using a normalized collision energy of 35%. Tandem mass spectra were searched against *Bacillus anthracis*

database (the National Center for Biotechnology Information) with SEQUEST. For a peptide to be considered legitimately identified, it had to achieve cross-correlation scores of 1.5 for $[M+H]^+$, 2.0 for $[M+2H]^{2+}$, 2.5 for $[M+3H]^{3+}$, and a maximum probability of randomized identification of 0.001. The LTQ-MS analysis of fraction #20-21 is summarized in the Table 5. S-layer protein Sap precursor and 60 kDa chaperonin protein (groEL) were detected as major components of the fraction. Minor components are included leucine dehydrogenase and peptidase M20/M25/M40 protein. Analysis of seroreactive proteins using sera from *B. anthracis* immunized animals suggested that Sap has an immunogenic potential [160]. Recent study presented that S-layer proteins Sap and EA1 were found to produce protective effect and could be regarded as additional immunogenic factors [161].

To isolate PAMP molecules from culture supernatants, 1 ml of 10X concentrate of the culture filtrate in LB containing 0.5% glucose was loaded onto a Sephacryl S-200 chromatography. The TLR2-dependent NF-kB activation of each fraction was tested in HEK293/TLR2/CD14 cells by transfection with NF-kB-luciferase reporter (Fig. 37). To see the protein purity, the fractions 36-44 were separated in a 12% SDS-PAGE gel. Proteins that are enriched in the activity are located in around 60 kDa. When Annexin V staining was performed using mouse macrophage RAW264.7 cells, the fraction 39 increased apoptosis of the cells, compared to control (Fig. 38). Previous MS analysis suggested that the proteins include 60-kDa chaperonin (GroEL; heat shock protein 60) and leucine dehydrogenase. According to the literature, heat shock protein (HSP60) elicits a potent proinflammatory response in cells of innate immune system through TLR-2/TLR-4, and/or independent signaling [162,163, 164, 165].

Toxigenic Sterne strain but not atoxigenic deltaSterne strain secrets HSP60 in LB culture

To investigate whether toxigenic or atoxigenic *B. anthracis* strain secrets BaHSP60 into culture media, Sterne, deltaSterne, and deltaAmes strains were cultured in LB media in the absence or presence of glucose to induce or suppress protease production. Culture supernatants and cells were separated by centrifuge and the cells were extracted in 3 mg/ml of lysozyme and 0.1% Triton X-100 in PBS solution. The culture supernatants and cell extracts were subjected to SDS-PAGE

analysis and Western blot with ant-GroEL antibody. Fig. 39 shows Western blot analysis for BaHSP60 secretion into culture supernatants. Sterne and deltaAmes secret BaHSP60 into the culture medium while deltaSterne does not (Fig. 39A). Addition of glucose to the culture medium does not affect the BaHSP60 secretion, suggesting that secreted proteases do not interfere with expression and secretion of BaHSP60 proteins. All cell extracts from Sterne, deltaSterne and deltaAmes show BaHSP60 band (3 9B and C). Although BaHSP60 was not found in culture supernantants of deltaSterne, suggesting downregulation of BaHSP60 secretion by deltaSterne strain.

Spore challenge of atoxigenic strain deltaSterne induces endogenous HSP60 in HBMEC

To examine whether spore challenge of the *B. anthracis* induces endogenous or bacterial HSP60 in human brain microvascular endothelial cells (HBMECs), spores of toxigenic Sterne and non-toxigenic deltaSterne were inoculated onto HBMEC monolayer with 10^4 ~ 10^7 spores/ml in 96-well plate. Supernatants from 5- or 24-h cultures were collected by centrifugation. The culture supernatants were used for Western blot analysis by probing with anti-GroEL (specific for endogenous and bacterial HSP60) and anti-HSP60 (specific for endogenous human HSP60) antibodies. As shown in Fig . 10 (*top, left panel*), 10^6~10^7 spores/ml of both Sterne and deltaSterne induce HSP60 production in HBMEC cocultures at 5 h and 24 h. To figure out whether HSP60 protein is endogenous or bacterial, the culture supernatants were analyzed by anti-HSP60 antibody. First, in order to examine specificity of the anti-HSP60 antibody, bacterial culture supernatants in LB media and cell extracts were analyzed in Western blot with the antibody. Anti-HSP60 antibody did not cross-react with bacterial HSP60 as shown in Fig. 40 (*top, right panel*). On the other hand, anti-HSP60 antibody reacts strongly with BaHSP60 from deltaSterne spore-challenged HBMEC culture supernatants and faintly with the Sterne spore-challenged one. Relative expression of bacterial and endothelial HSP60 was calculated by densitometry analysis. Band intensity was measured by AlphaEaseFC software after scanning the blot. Relative expression was determined from the intensity of GroEL / the intensity of BaHSP60 or the intensity of BaHSP60 / the intensity of GroEL to

show relative bacterial BaHSP60 or endothelial HSP60 expression, respectively. As the result, toxigenic Sterne produces 23 times more bacterial than endothelial HSP60, while atoxigenic deltaSterne produces 22 times more endothelial than bacterial HSP60. This result implies that the toxigenic Srerne stain, but not atoxigenic deltaSterne, might have a specific mechanism to bypass a stress response of the host cells.

BaHSP60 was expressed in E. coli and purified from the cells

The BaHSP60 gene of *B. anthracis* was amplified from its chromosomal DNA by PCR with specific oligonucleotides. The primers were as following: HSP60F, GCA AAA GAT ATT AAA TTT AGT GAA and HSP60R, CAT CAT TCC GCC CAT ACC GCC. PCR amplification was performed using a Taq polymerase premix (Invitrogen) with 200 nM of primers. The amplicon was ligated into expression plasmid pTrcHis2-TOPO (Invitrogen), and then transformed into *E. coli* DH5α. Positive clones were confirmed by restriction enzyme digestion with *Pst*I and *Hind*III as shown in figure. Three positive clones (#5, #7, and #8) were selected out of 15 colonies (Fig. 41).

Protein expression was induced with 1 mM isopropyl-β-D-thiogalactopyranoside (IPTG) for 5 h. As shown in Fig. 42, clones #7 and 8, but not #5 efficiently expressed BaHSP60 proteins by IPTG. 50 ml cultures were prepared and the six His-tagged fusion proteins were purified under native conditions by Ni^{2+}-nitrilotriacetic acid affinity chromatography (Probond, Invitrogen). Briefly, the bacteria were lysed with a Barocycler (Pressure Biosciences) with an automatic program according to the manufacturer's recommendation. The lysates were loaded on a column equilibrated with lysis buffer containing 10 mM imidazole. After being washed with lysis buffer containing 20 mM imidazole, proteins were eluted with a buffer containing 250 mM imidazole. Protein-containing fractions were desalted on an Econo-Pak DG10 coulmn (Bio-Rad), equilibrated with PBS, as described in the manufacturer's protocols. As shown in Fig. 42B, the BaHSP60 proteins isolated from cultures of clones #7 and #8 were of high purity.

Synergistic effect of BaHSP60 and LPS

HSPs are highly conserved and ubiquitously expressed proteins that are normally hidden within the cell and function as molecular chaperons of nascent or aberrantly folded proteins in different cellular compartments. Among them, it has been shown that HSP60 possesses that an intrinsic immunostimulatory potential, which is mediated by TLRs. However, it has been suspected that contamination of HSP60 with bacterial endotoxins including LPS may cause this effect. Recent report demonstrated that HSP60 colocalizes with CD14 receptor as well as LPS binding sites and that HSP60 specifically binds bacterial LPS (*JBC* **282**, 4669, 2007). Both HSP60 and LPS synergistically stimulate innate and adaptive immune responses indicated by enhanced IL-12p40 production in bone marrow-derived dendritic cells and macrophages. Therefore, we tested whether recombinant *B. anthracis* HSP60 (rBaHSP60) stimulates TLR signaling with LPS synergistically, and whether HSP60 levels increase in plasma of spore-challenged mice.

To examine NF-κB transcriptional activation through TLR-2 or TLR-4, rBaHSP60 proteins purified from Ni-NTA column were used to stimulate HEK293 cells stably transfected with TLR-2 and CD14 or TLR-4 and MD-2/CD14 genes. The overnight cultured cells (~80% confluent) were transfected with NF-kB-luciferase reporter plasmid pNiFty-luc (0.2 μg/well) in a 96 well plate using lipofectamine 2000 according to manufacturer's recommendation. Next day, different concentrations of purified rBaHSP60 in serum-free media were added into transfected cells, and then further incubated overnight. The reporter luciferase activity was assayed using a Promega luciferase assay kit. As shown in Fig. 43, purified rBaHSP60 activates NF-kB transcriptional activity through both TLR-2 and TLR-4 in a concentration-dependent manner. However, the activity through TLR-4 is completely inhibited by polymyxin B, while the activity through TLR-4 is not. LPS itself also activates the NF-kB transcriptional activity through TLR-2, which is not apparently inhibited by the polymyxin B treatment, as shown in Fig. 43 (lower left panel). From these experiments, we could not distinguish rBaHSP60 effect on TLR-2 activation from the effect of LPS contamination. Therefore, the purified rBaHSP60 proteins were passed through polymyxin B-agarose column to remove the contaminant LPS. 2 ml of the protein solution (614 μg) were incubated with 1 ml of polymyxin B-agarose beads (P1411, binding capacity 200-500 μg LPS per ml) at room temperature for 1 h. The resulting beads

were loaded on a disposable column and the flow-through was collected. The protein concentration of the flow-through was 102 μg (~ 17% of recovery yield). This data suggest that rBaHSP60 binds tightly with LPS, which presumably originated from the *E. coli* DH5α host. To investigate TLR activation by LPS-free rBaHSP60, we performed the NF-kB transcriptional activation experiments using HEK293/TLR-2/CD14 or HEK293/TLR-4/MD-2/CD14 cell line. As described above, the cells were transfected with pNiFty-luc reporter and treated with rBaHSP60 and rBaHSP60 + LPS (1 ng/ml). Before treatment, the mixtures were incubated at room temperature for 1 h to allow them form a complex. In the absence of LPS, rBaHSP60 could not activate either TLR-2 or TLR-4 signaling as shown in Fig. 44, 45. However rBaHSP60 synergistically activated TLR2 in the presence of LPS in a concentration-dependent manner. On the other hand, LPS-free rBaHSP60 did not show any synergistic effect on TLR-4 signaling in combination with LPS above the level of LPS activation (Fig. 45). This data suggest that the inflammatory activity of BaHSP60 may be dependent on the presence of unidentified specific factor mimicking LPS during anthrax infection.

HSP60 levels are increased in plasma of spore-challenged mice

To investigate whether HSP60 levels increase in plasma during anthrax infection, we performed immunoblot analysis using plasma of spore-challenged mice. Plasma proteins (~50 μg) were separated on a 4-20% SDS-PAGE gel and transferred onto a nitrocellulose membrane. The membrane was probed with anti-*E. coli* GroEL antibody, as described above. As shown in Fig. 46, HSP60 levels in plasma increased up to 3 fold compared to unchallenged control in both deltaSterne- and Sterne-challenged mice. In this assay we could not distinguish endogenous HSP60 from bacterial HSP60. Endogenous HSP60 is released from cells upon various cellular stresses and necrotic cell death. Human HSP60 has a strong capacity to stimulate proinflammatory responce by release of TNF-α, NO, and IL-6, therefore endogenous murine HSP60 is a likely inflammatory factor in the infected mice.

rBaHSP60 induces TNF-α and IL-6 in RAW264.7 cells

To investigate a possible function of BaHSP60 in anthrax infection, we performed ELISA analysis of proinflammatory chemokines TNF-α and IL-6 in murine macrophage RAW264.7 cells. The purified rBaHSP60 or its combination with LPS was treated RAW264.7 cells overnight, and culture supernatants were collected. The culture supernatants were tested with mouse TNF-α and IL-6 ELISA kit (ELISA Optia, BD Pharmingen) according to manufacturer's protocol. As shown in Fig. 47, rBaHSP60 protein induced secretion of TNF-α and IL-6 in RAW264.7 cells in a dose-dependent manner. Co-treatment of rBaHSP60 with LPS did not result in a synergistic activation of TNF-α or IL-6 secretion. This result is at odds with the synergistic TLR-2 activation by rBaHSP60 and LPS in HEK293 cells and suggests that secretion of TNF-α and IL-6 by rBaHSP60 may be independent of LPS, TLR-2 or TLR-4. Further studies are necessary to investigate whether the secretion of cytokines involves TLR-2 or TLR-4 as receptors for HSP60 signaling.

rBaHSP60 binds to and induces apoptosis of HBMECs and macrophages

To examine whether rBaHSP60 binds to HBMECs representing the cells of the blood-brain barrier, the protein (1 μg/ml) was incubated with the cells in a serum-free medium for 1 h. The cells were washed 3 times with PBS and fixed with 4% paraformaldehyde for 10 min. Afterwards, the cells were incubated anti-His antibody (1 μg/ml) or anti-*E. coli* GroEL antibody in the presence of 5% goat serum followed by staining with FITC-conjugated goat anti-mouse or Cy5-conjugated goat anti-rabbit secondary antibody, respectively. In fluorescent microscopic analysis, rBaHSP60 binds to the cell surface of HBMEC (Fig. 48). His-tagged rBaHSP60 appears to concentrate in distinct membrane regions when stained with the anti-His antibody, similar to the effect observed previously in bone marrow-derived macrophages (*JBC* **282**, 4669, 2007). However when the anti-*E. coli* GroEL antibody was used, the cells were stained with rBaHSP60 relatively evenly, without a distinct concentration on cell surface (Fig. 49). Interestingly, rBaHSP60-treated cells show kidney bean-like structure of nuclei indicative of apoptosis (Fig. 50). The protein also binds to the murine macrophage-like RAW264.7 cells and causes membrane ruffling detectable in the phase contrast

image (Fig. 21). Taken together, these results suggest that rBaHSP60 binds to and induces apoptosis of HBMEC and macrophages.

To further investigate apoptosis of HBMEC we used terminal transferase dUTP nick-end labeling to detect apoptotic cells (TUNEL assay). The cells were incubated for 2 h in a complete serum-free media in the presence of 12 μg/ml of rBaHSP60 with or without 1 ng/ml LPS. The cells were fixed with 4% paraformaldehyde for 1 hr, permeabilized with 0.1% Triton X-100 in 0.1% sodium citrate for 2 min on ice, and incubated in a reaction mixture including enzyme and substrate for 1 hr at room temperature. As shown in Fig. 51, rBaHSP60 and LPS used separately induced low level of apoptosis of HBMEC. However when rBaHSP60 and LPS were combined to treat the cells, apoptosis was synergistically increased (Fig. 52).

rBaHSP60 increases production of inflammatory cytokines, activates of NF-κB, and stimulates cyclooxigenase-2 in HBMECs

We examined production of inflammatory cytokines in HBMECs to investigate a possible role of BaHSP60 in brain endothelial cell activation. ELISA kits (BD Bioscience, BD OptEIA) were used to determine cytokine secretion in culture media. We were able to detect increases in GM-CSF, IL-8 and IFN-γ when the cells were incubated with rBaHSP60 for 3 days (Figs. 53-55). In the presence of LPS (1 ng/ml), production of GM-CSF was somewhat inhibited as seen in Fig. 53. There was no significant change in the production of IL-8 in the LPS-treated cells compared to untreated cells. This data suggest a potential role of inflammatory cytokines such as IL-8 and GM-CSF in the inflammation of BBB regions through stimulation of neutrophil or macrophage infiltration.

Transcriptional factor NF-κB is a critical regulator of genes involved in inflammation. To examine an NF-κB dependence of the rBaHSP60 signaling we transfected NF-κB-luciferase reporter plasmid (pNiFty) into HBMECs using 0.2 μg/well of plasmid and 0.5 μl/well lipofectamine 2000 in a 96-well plate. Transfected cells were treated with different concentrations of rBaHSP60 overnight and analyzed for luciferase activity. NF-κB-mediated transcriptional was increased by rBaHSP60 in

the absence of LPS (Fig. 56). Although LPS alone activated NF-κB transcriptional activity, there was no synergistic effect with rBaHSP60.

It is well recognized that macrophage and endothelial cells release lipid mediators, including prostaglandins (PGs) and leukotriens that promote inflammation (*Toxicology* 160: 111, 2001; *Annu. Rev. Immunol.*, 15: 323, 1997; *Am. J. Physiol. Cell Physiol.*, 283: C1267, 2002). The synthesis of PGs is dependent on the activity of cyclooxygenase (COX), an oxidoreductase that converts arachidonic acid into the common PG precursor, PGH_2. Two isoforms of the enzyme have been identified, a constitutive form COX-1 and an inducible form COX-2 that is thought to be important in inflammation. We, therefore, examined if COX-2 was induced by rBaHSP60 in HBMECs. The cells were stimulated by rBaHSP60 (5 μg/ml) for 0, 6, 12, 24 and 36 h in XM media containing 5% FCS. At each time point, cell extracts were prepared with RIPA lysis buffer and used in Western blot by probing with rabbit anti-human COX-2 antibody. A 4-fold Induction of COX-2 observed within 6 h suggests an inflammatory role of BaHSP60 in brain endothelial cells (Fig. 57).

CD91 is a receptor for BaHSP60 in HBMEC

To identify the receptor for BaHSP60, 10 μg/ml of the antibodies against cell surface receptors were added into HBMEC culture, 2 h prior to the addition rBaHSP60 (3 μg/ml). IL-8 production from 24-h culture supernatants was measured by a commercial ELISA kit (BD Bioscience). Antibodies against TLR-2, TLR-4 and CD14 did not block but increased the IL-8 production. However the anti-CD91 antibody significantly decreased IL-8 production. Co-treatment with the anti-TLR-2 and anti-CD91antibodies, as well as the anti-TLR-4 and anti-CD91antibodies did not cause a substantial effect compared to the CD-91 antibody (Fig. 58). This result suggested that CD91 can play a role of BaHSP60 receptor in HBMEC. To confirm this suggestion we used CD91 purified from human placenta (BioMac, Leipzig, Germany). CD91 (2 μg) was separated on a 4-12% SDS-PAGE gel and transferred onto a nitrocellulose membrane. The membrane was blocked with 3% bovine serum albumin (BSA) in Tris-buffered saline (TBS) for 1 h at room temperature. rBaHSP60 (1.3 μg/ml) in 3% BSA/TBS was added to the membrane and incubated overnight at 4

℃. The membrane was washed 4 times with TBS and an alyzed by with anti-GroEL antibody. As a loading control, CD91 protein (2 μg) was transferred to the membrane and analyzed by with a mouse monoclonal anti-CD91 antibody (Abcam, 5A6). As shown in Fig. 59 (*left panel*), CD91 preparation contains several fragments, form which two fragments indicated by arrows bound BaHSP60. Although this result suggested a direct interaction of BaHSP60 and CD91 on a solid membrane, it was still unclear if direct interaction would take place in solution. Therefore, we performed immunoprecipitation analysis using an anti-CD91 or anti-HSP60 (GroEL) antibodies. CD91 and rBaHSP60 (2 μg each) were incubated in 100 μl of PBS for 3 min at 4 ℃, anti-CD91 antibody (2 μg) or anti-GroEL antibodies (10 μg) were added, and the solutions adjusted with PBS to 500 μl final volumes were incubated for 1 h at 4 ℃. Neg ative controls included no antibodies. Protein-A/G-agarose beads (20 μl of 50% slurry) were added to each solution and incubated overnight at 4 ℃ with a gentle agitation. The bead s were washed 4 times with PBS and bound proteins were eluted with 2X SDS sample buffer with 30 mM DTT. The samples were loaded on a 4-12% Nu-PAGE and 6% Tris-Glycine SDS-PAGE for detection with the 1:1 mixture of anti-HSP60 and anti-CD91 antibodies. As shown in Fig. 59 (*right panel*), CD91 and GroEL antibodies precipitated rBaHSP60 and CD91 proteins, respectively.

rBaHSP60 activates AKT and suppresses MAPK signaling in HBMECs

It has been previously reported that bacterial HSP60 proteins induced IL-8 *via* activation of ERK, p38 and c-Jun N-terminal kinase (JNK) MAPKs in gastric epithelial cells. Therefore we tested the role of MAPK in the IL-8 production by *B. anthracis* upon HSP60 stimulation. HBMECs were treated with rBaHSP60 (3 μg/ml) and a time-course of MAPK-dependent phosphorylation was measured to assess the activation of these kinases. AKT activation was observed at 30 min, and persisted until 120 min. Of particular interest, ERK suppression was observed after 60 min of treatment. In addition, p38 and JNK suppression were also observed after 10 and 20 min, respectively (Fig. 60A and B). This effect of BaHSP60 to HBMECs contrasts with the activation of

ERK and p38 by the *Helicobactor pylori* HSP60 to gastric epithelial cells and monocytes (*J. Med. Microbiol.* **56**: 154-164, 2007; *Infect. Immun.* **73**: 1523-1531, 2005).

To identify whether AKT signaling is responsible for IL-8 secretion, the effect of LY294002 (50 μM), a specific PI3 kinase inhibitor, as well as MAPK inhibitors such as PD98059 (MEK1/2 inhibitor, 50 μM), SB202190 (p38 inhibitor, 10 μM), and JNK inhibitor (15 μM) were investigated with rBaHSP60 stimulation in HBMEC cells. The cells were preincubated with inhibitors for 2 h before rBaHSP60 treatment and then further cultured for 36 h. IL-8 production was measured from culture supernatants as described above. PI3K inhibitor LY294002 significantly inhibited IL-8 production (67% reduction compared with control) in HBMEC cells (Fig. 61). MEK1/2 inhibitor PD98059 and p38 inhibitor SB202190 reduced IL8-production to 32% and 22% relative to control without rBaHSP60 treatment. However JNK inhibitor increases IL-8 production (174% of control). Since PI3K is an upstream mediator of AKT signaling, this result is consistent with activation of AKT phosphorylation by rBaHSP60. In other words, PI3K inhibition induces AKT inactivation resulting in IL-8 reduction. Overall, these results suggest that AKT and MAPK signaling is involved in modulation of IL-8 production in HBMEC through TLR-2 and CD91 receptors.

We conclude that culture supernatants of *B. anthracis* contain TLR-2 agonist capable of NF-kB activation in HEK293 cells. The activity was not inhibited by polymyxin B, a LPS antagonist. However the proteolytic activity of secreted proteases is capable of inhibiting the LPS- and Pam_3CSK-mediated TNF-α production in murine macrophage RAW264.7 cells. We identified *B. anthracis* Heat Shock Protein 60 (BaHSP60) as a bacterial TLR-2 activator induced in the host cells in response to spore challenge.

Toxigenic spore challenge of HBMEC cells in culture induces mainly bacterial chaperonin BaHSP60, while the atoxigenic delta Sterne spores predominantly induce an endogenous HSP60 from HBMEC cells. This suggests that toxigenic Sterne strain might possess a mechanism to bypass a host stress response through the induction of HSP60.

We found that recombinant BaHSP60 can tightly bind bacterial LPS, and that both compounds synergistically activate TLR-2. It remains to be studies if TLR-2-stimulating activity of BaHSP60 depends on the presence of unidentified specific factor mimicking LPS during anthrax infection.

Stimulation of RAW264.7 cells with HSP60 induces apoptosis and a pro-inflammatory response, including including TNF-α, IL-6, GM-CSF, IL-8 and IFN-γ independently with LPS. In addition, COX-2 is transiently induced by rBaHSP60 in HBMEC cells. This suggests that the induction of chemokines facilitates inflammation of blood-brain barrier regions through neutrophil infiltration or an increase in macrophage numbers.

CD91 (LDL receptor-related protein; LRP1) was identified as a receptor for BaHSP60. Anti-CD91 antibody inhibits IL-8 secretion in HBMEC cells and BaHSP60 bound CD91 directly. Co-treatment with anti-TLR-2 and anti-CD-91 antibody further decreases IL-8 production, indicating that TLR-2 could play a role of CD91 co-receptor inducible by BaHSP60. BaHSP60 down-regulates phosphorylation of ERK, p38 and JNK, and up-regulates AKT. Inhibitors for PI3K, MEK1/2 and p38 decrease IL8-production in HBMEC cells.

We propose that BaHSP60 serves as a danger signal to the innate immune system through production of endogenous inflammatory cytokines through TLR-2 and CD91 receptors.

3. 2. Transcriptional Responses of THP-1 Macrophage-Like Cells to Infection with Anthrax Toxigenic and Non-Toxigenic Spores.

The results presented above indicate that the secreted products of the atoxigenic delta Ames strain are capable of inducing apoptosis while the TLR signal is abrogated. This effect has not been previously described, and apoptosis in anthrax is considered as the attribute of lethal toxin expressed during virulent infection. In the anthrax literature, currently existing hypothesis suggests that macrophage apoptosis is a result of two concomitant events, including the TLR-4 activation by AnlO and lethal toxin (LT) enzymatic activity [166]. It has also been suggested that the edema toxin

(ET) has the anti-apoptotic effect through the TLR-4 activated pathways[167]. In our 2005 report and in the above section of the current report, we presented evidence against the TLR-4 role in anthrax. Therefore, it seemed important to test further if the TLR genes are activated during infection in macrophages, and if the presence of toxins is required for apoptosis.

Highly pathogenic strains of *Bacillus anthracis* contain two plasmids, pXO1 and pXO2 encoding major virulence factors of this Gram-positive bacillus. LT and edema toxin (ET) genes reside on the pXO1, while the anti-phagocytic capsule is encoded by pXO2. LT is necessary for pathogenicity, as deletion of its gene renders the microbe avirulent, while ET-knockout strains are only partially attenuated [168]. Capsule substantially contributes to the virulence of the microbe but unencapsulated strains, such as Sterne (34F2), are still capable of causing death in experimental animals. Therefore, the $pXO1^{+}$, $pXO2^{-}$ Sterne strain serves as a convenient experimental toxigenic model of highly virulent strains. LT consists of a heptameric protective antigen (PA) noncovalently associated with lethal factor (LeF). LT is a zinc metalloprotease, which cleaves and thus inhibits mitogen-activated protein kinase kinase (MAPKK) family members *in vitro* and *in vivo*, resulting in defective host cell signaling [169] [170], with broad implications for the host innate and adaptive immune responses.

During inhalational exposure to *B. anthracis*, the spores may enter alveoli where they become deposited on mucosal surfaces. In the initial interactions with the host, the spores can either germinate on the epithelium, or within hours can be engulfed by phagocytes, such as macrophages or dendritic cells [171]. Both LT and ET are expressed upon germination within the macrophage phagosome [171] and seem to play important roles in suppressing the bactericidal innate immune mechanisms of the epithelium and the intra-phagocytic environment [172]. In a currently accepted model of anthrax, some of the phagocytosed spores *en route* to the mediastinal lymph nodes survive and multiply within the phagolysosome, kill the cell, and become released into the lymphatic system. In the following process of hemorrhagic lymph node destruction, the bacteria gain access to the bloodstream and quickly become systemic by spreading to the spleen and other internal organs [173] [174]. According to this mechanism, lung phagocytes such as macrophages and dendritic cells are

critically involved in the initiation of the disease, and their response to anthrax spores, among other factors, determines whether the exposure to aerosolized spores results in the infectious process [175].

Macrophages were the first cell type discovered to be sensitive to LT [176], however their sensitivity in vitro reversely correlates with the lethal effect of LT in experimental animals [177]. This "anthrax paradox" did not get a satisfactory mechanistic explanation till it was discovered that macrophages exposed to LT undergo the process of programmed, apoptotic death [178]. Subsequently, it was found that certain cell types, such as human peripheral blood monocytes with the LT-resistant phenotype could become sensitive in the conditions of growth media deprivation leading to a cellular stress [179]. This finding was indirectly supported, when it was shown that the stress factors may include a broad range of the bacterial Toll-like receptor agonists of different nature, including the pore-forming hemolysins or endotoxin [166]. The liver contains the majority of the body's resident macrophages called Kupffer cells. Transcriptional analyses of the livers of mice lethally infected with anthrax spores revealed strong upregulation of apoptotic and inflammatory genes and allowed the suggestion that sensitive macrophages, and perhaps other cell types, undergoing apoptotic death may serve as sensors alerting the immune system and mounting the protective response[144,179]. This hypothesis implies that apoptosis of macrophages may be induced as a part of a normal host response to infection. In these circumstances, one of the plausible pathogenic roles of LT would be to delay or avoid the apoptotic mechanism recognizing infection by making the processes of intra-macrophage growth and survival immunologically silent. This is consistent with the recently discovered properties of LT as a suppressor of inflammatory mediator production by the inhibition of pathogen/stress response signal transduction pathways such as p38 [180 181]. Alternatively, the apoptosis of a large number of cells at the terminal stages of disease accompanied by high toxemia may reach pathological proportions and ultimately kill the host. In support of this, treatment of the spore-challenged mice with the pan-caspase inhibitor z-VAD had a protective effect whether the inhibitor was used alone or in combination with ciprofloxacin [6].

In order to get additional insight into the macrophage responses to anthrax spores and the role in this process of the pXO1 plasmid-encoded virulence factors, including LT, we undertook a

transcriptional analysis of the phagocytic THP-1 cells of monocyte origin, which has been previously used in anthrax studies [182]. In our model, the THP-1 cells were exposed to the spores of the toxigenic Sterne strain (called the virulent strain), and the transcriptional responses were recorded. In the parallel experiments, the cells were treated with spores of the atoxigenic delta Sterne strain (called the avirulent strain). We present the results of a comprehensive principle component analysis of the THP-1 cell response to the virulent *vs* avirulent strains of *B. anthracis* allowing us to differentiate between infections by both strains. Finally, we compare host responses of genes of interest using both ANNOVA statistical, and realtime PCR analyses. Our results confirm certain aspects of cellular response previously reported, but also shed light on new factors delineated between virulent and avirulent infections.

Our experiments involved the challenge of unstimulated human macrophage-like monocyte cell line THP-1 by either virulent or avirulent strains of *B. anthracis* Sterne in the conditions modeling the early macrophage-spore interactions on the mucosal surface, and the analyses of the monocyte mRNA to determine the global response patterns. The system models the initial exposure of spores, followed by stimulation of, phagocytosis by, and infection of THP-1 cells. The microarray results for cells challenged at different times and MOIs, show time- and dose-dependent responses for both strains of *B. anthracis* evaluated (Fig. 62). Principle component analyses (PCA), which allow visualize simple trends in collected data within several dimensions of analysis result in the appropriate groupings with respect to chip replicates and treatment conditions (Fig. 62). The results of the 2-hour challenges by virulent Sterne strain spores at both MOIs do not differ significantly from control samples, all falling within the same quadrant of our PCA, in contrast to the cell responses to 2-hour challenges by delta Sterne spores. This demonstrates that macrophages respond to the avirulent infection faster, compared to the virulent one, in agreement with the hypothesis that the initial general response of macrophages to the virulent spores is suppressed due to the presence of the LT-expressing plasmid [171]. At the 4-hour time point, there are significant and discernable differences between Sterne and delta Sterne-challenged cells, indicating a clear distinction between pathogenesis and cellular responses to each strain. The strain-specific separation at higher MOIs

and time points becomes so distinct that it may be useful in delineating virulent *vs.* non-virulent strains. Further confidence in our gene chip data was obtained using realtime PCR (Fig. 63), which demonstrates the results overall correlating to the microarray data within the experimental variations of both data sets.

Fig. 64 shows clustered heat maps of important biological processes, molecular functions, and cellular component modules. In general, our results for both strains appear consistent with the macrophage and innate immune activation programs described in response to other bacterial pathogens [183] [184]. Activation of innate and other immune defenses, and inflammatory responses are typically observed for both spore strains, but in general the activation is greater in the case of the virulent Sterne spore challenge model (Fig. 64a) in spite of the overall initial delay noticed in the 2-hour challenges. Several of the NF-κB-controlled programs are upregulated similarly between both strains, indicating that they are pXO1-independent, while the others could be considered as characteristics of virulence. The most striking differences seen between strain challenges in our clustering analyses consist of a series of modules that are activated at the 4-hour time points in the Sterne spore treatments, while no activation is seen in any of the delta Sterne treatments. Among these modules, there are important signaling pathway processes, including at least 10 phosphatase modules, DNA modification modules, and transcriptional regulation ones. In addition, the pathways involved in eicosanoid and prostaglandin-type metabolism are similarly affected, which agrees with reports of drastic changes in prostaglandin levels during toxigenic-anthrax pathogenesis in mice (Cherkasova et. al., 1991). Other cellular component functions encompassing catabolic and metabolic components do not show much variation between strains, similar to nucleotide/nucleic acid and ATP metabolism and catabolic processes (Fig 35b, c). Interestingly though, the cytochrome oxidase and oxidoreductase modules appear highly activated early in the avirulent delta Sterne strain challenge, in comparison to the Sterne strain, marking the suppression of the transcriptional-level mitochondrial activation as an important virulence feature. Previous reports have indeed implicated LT in the dysfunction of mitochondria in murine macrophages and human peripheral blood

monocytes [137] [185], but our observation demonstrates that during infection the process cannot be solely ascribed to the action of toxin.

Our results are consistent with the transcriptional analysis of the murine macrophage RAW 264.7 cells by Bergman *et al.* (2005) [186]. In response to *B. anthracis* Sterne spore challenge the authors reported transcriptional activation of immune modules, induction of Nf-κB, along with the apoptotic inhibitor GADD45b. However in the absence of the background information regarding the plasmid-negative strain the contribution of the pXO1 gene complex cannot be precisely evaluated. Similarly, both the resting or *Salmonella* lipopolysaccharide-stimulated RAW 264.7 cell cultures exposed to LT in the reports by Bergman *et al.* (2005) and Tucker *et al.* (2003) [187] seem to be inadequate models of the biological context of LT function. Our results indicate that the THP-1 monocytes present significant immunological responses during both toxigenic, and non-toxigenic challenge. In contrast, both of the above-mentioned studies did not observe any significant changes in the unstimulated macrophages exposed to LT, while in the case of stimulated macrophages, LT caused a typical immune suppression attributed to the modulation by LT of the host immune response to antigenic components of the infecting bacteria.

To further examine specific differences in host response to each strain, ANOVA analysis was carried out on individual genes involved in the cell survival and apoptosis-related events (Table 8). This analysis allows us to observe the differential expression of a particular gene at the particular time and MOI, where the only difference is the presence or absence of pXO1 in the *B. anthracis* strain. In our analysis, positive numbers indicate that the expression levels are higher in the avirulent spore treatment, while negative numbers reflect a shift in expression level favoring the virulent spore treatment. Some of the most notable transcriptional differences are seen in the case of apoptotic inhibitors such as CFLAR (FADD-Like Apoptosis Regulator) and GADD45b, which appear to be expressed higher in the virulent spore treatments (Table 8a). This may correlate to the higher induction of the Nf-κB1 gene seen in our ANOVA analysis in the case of the virulent strain (Table 8a). Along with initiating cellular immunological responses, Nf-κB has been indicated to induce both apoptotic and survival processes [188]. Contrasted against this are the cell cycle genes, which seem to

favor expression in response to the avirulent challenge (Table 8b), indicating an initial shift towards proliferation and differentiation.

The role of TNF-α, the primary mediator of the cellular inflammatory response, has attracted significant attention in anthrax studies. Recent data indicate that its systemic levels during infection, or upon LT challenge in animals and cell cultures, are either undetectable or transient [189] and therefore cannot be considered as a primary cause of death, as it was previously suggested [190]. Nevertheless, some data suggest that the TNF-α response may play an important function in the local host antibacterial defense [191]. In our gene chip and realtime PCR results, TNF-α is significantly expressed in a time- and concentration-dependent manner during infection by both strains (Fig. 65). However the level of expression of TNF-α appears much higher in the cells challenged with virulent spores after 4 h. This is also reflected in the ANOVA analysis of stress and inflammatory response genes (Table 8a), including several ones associated with TNF-α induction. These genes show a marked upregulation in the case of virulent Sterne spore treatments relative to the avirulent delta Sterne ones (Table 8c). CXCL2, the chemokine precursor to macrophage inflammatory protein-2α (MIP-2α) is also increased in Sterne spore-challenged cells, pointing to a higher innate response to the toxigenic strain. Interestingly, the level of expression of the apoptosis inhibitor transcribed by CFLAR is not affected upon challenge by the non-toxigenic strain, but does show significant up-regulation in the Sterne strain infection as a response to the presense of pXO1 virulence factors.

In both of our toxigenic, and non-toxigenic models of macrophage challenge, the majority of cells remained viable within 4 h, but ultimately proceed to apoptosis and/or necrosis within 12 to 24 h of infection, as measured by flow cytometry, DNA laddering experiments, Trypan Blue assays, and visual inspection (data not shown). Our results on TNF-α gene induction suggest that in our experiments it may substantially contribute to the apoptotic death, which has been indicated to proceed through either a TNF receptor 1 (TNFR1)-dependent pathway including activation of caspase-8, or a mitochondrial-induced pathway [192] (Fig. 66). One possible interpretation of our results is that the host cells respond with the increased level of TNF-α to the expression of the pXO1 gene products, thus sensitizing the macrophages to apoptosis [193]. In turn, the bacterial pathogenic

factors counterbalance this bactericidal response by the induction of CFLAR. In agreement with this, neither the TNF-α nor the CFLAR genes are preferentially upregulated by the avirulent strain when compared to the virulent strain (Fig. 64, Table 8a). At the same time, as discussed above, gene ontology modules corresponding to the alternative mitochondrial apoptosis are also down-regulated in comparison to the avirulent strain (Fig. 64). As a net result, the virulent strain challenge displays less TNF-α-dependent apoptotic transcriptional activation, and suggests that the pathogenic function of the pXO1-encoded factors may consist in the inhibition of the protective apoptotic response of the host.

Several lines of evidence support this hypothesis. Previous analyses of anthrax-infected RAW 264.7 cells [186] identified overexpression of ornithine decarboxylase (ODC), a normal biosynthetic enzyme involved in the conversion of putrescine to the polyamines spermine and spermidine. Since the overproduction of polyamines by ODC has been implicated in preventing apoptosis, this led the authors to speculate that ODC overexpression was involved in suppressing macrophage apoptosis. In the case of other bacterial infections, apoptosis has been generally considered as a protective host response. Mycobacterium infections have been indicated to subvert apoptotic induction by the inactivation of TNF-α [194]. There is additional evidence that the delay of apoptosis may play roles in some successful viral and fungal infections as well [195] [196]. Recent findings that anthrax LT inhibits the p38 signaling in macrophages and dendritic cells [166] are consistent with the protective role of this stress-activated pathway for survival of the host as a multicellular organism for the expense of the apoptotic elimination of stressed cells [197].

In summary, our results did not reveal a TLR gene upregulation upon anthrax infection in THP cells, and support the notion that anthrax apoptosis does not require the activity of toxins. These cells display a significant innate response of host macrophage-like cells to both virulent and avirulent infection. In general, the early response is suppressed, consistent with the activity of toxigenic strains. Observed genotypic responses that are specific for the pXO1-positive strain are consistent with mitochondrial damage, prostaglandin level disruption, and phosphatase induction. The production of CFLAR may help protect against TNF-α induced caspase-8 dependent apoptosis,

particularly since TNF-α induction is higher in the case of virulent strain. This delay of apoptosis during anthrax infection could allow for more successful bacterial survival and dissemination, resulting in systemic disease, in agreement with the above mentioned report on the induction of genes for GADD45b and the apoptotic inhibitor ODC. This supports a hypothesis that in anthrax the suppression of apoptosis in macrophage-like cells may contribute to disease virulence, and that apoptosis itself may represent a protective response to infection.

MATERIALS AND METHODS

Microbial Strain, Cultivation, and Supernatant Preparation. The non-encapsulated, non-toxigenic *B. anthracis* strain (delta Ames, pXO1$^-$, pXO2$^-$) was kindly provided by Dr. J. Shiloach (National Institutes of Health, Bethesda, MD). To obtain a culture supernatant, a 1 liter of Luria Broth (LB) was inoculated with the overnight seed culture (50 ml), incubated at 37 ^oC with vigorous agitation until the cells had reached stationary phase, and centrifuged at 17,000 *g* for 10 min. The supernatant was removed and passed through a 0.22 μm cellulose acetate filter.

Purification. All operations during enzyme purifications were performed at 4 ^oC unless otherwise indicated. Solid ammonium sulfate was added to 940 ml of culture supernatant until 75% saturation. The precipitated proteins were then collected by centrifugation at 17,000 g for 20 min, dissolved, and dialyzed against 50 mM Tris-HCl (pH 7.6) containing 3 mM sodium azide. The resulting proteins were loaded onto a DEAE-cellulose anion exchange column (bed volume 60 ml) equilibrated with 50 mM Tris-HCl (pH 7.6) containing 3 mM sodium azide. Elution was achieved stepwisely with 10, 50, 100, 200, 500, and 1,000 mM NaCl in the same buffer. The substances of two peaks were collected: a flow-through (P1) and a 200 mM NaCl eluate (P2). The P1 and P2 protease fractions were loaded onto a Sephacryl S-200 gel filtration column equilibrated with 20 mM Tris-HCl (pH7.6), 150 mM NaCl, and eluted at flow rate of 1.3 ml/min. Fractions (5 ml) were collected and protease activity was assayed.

Protease Assay. Protease activity was assayed during purification using EnzChek Ultra Protease kit for casein hydrolytic activity, EnzChek Gelatinase/Collgenase kit for gelatin hydrolytic activity, and EnzChek Elastase kit for elastin hydrolytic activity, respectively, according to manufacturer's recommendation (Molecular Probes). Brielfy, 5 μl of supernatant or fractions in 45 μl of digestion buffer were mixed with 50 μl of fluorescein-labeled substrate, then fluorescence intensity was measured after 1 hour-incubation at 37 ^oC using 485 nm excitation and 510 nm emission

wavelengths. One unit of protease activity was defined as the amount of protease required to liberate 1 mmole of the fluorescent dye from substrate-dye conjugates in 1 min.

Characterization of the Proteases. To study the effect of pH on the protease activity, the proteases were assayed at 37 ^{o}C in buffers with various pH containing 0.1 M NaCl; 50 mM sodium acetate-acetic acid buffer (for pH 4-5.5), MES-NaOH buffer (for pH 6-7), and 50 mM Tris-HCl (for pH 7.5-10). Optimal temperature was determined by measuring caseinolytic activity of the protease at 21, 37, 50, and 70^{o}C for 1 h (without the temperature-pH correction). For testing the effect of inhibitors on the protease activity, the proteins were pre-incubated with inhibitors, divalent ions, or other reaction components in 10 mM Tris-HCl, pH 7.8 for 30 min at room temperature. Then, equal volume of 2x casein substrate was added, followed by further incubation at 37^{o}C for 1 h.

SDS-PAGE and Determination of Protein Concentration. Proteins were separated by Tris-glycine SDS-PAGE using 10% or 14% gels under reduced and denatured conditions. The gels were stained using Coomassie brilliant blue R-250 and then destained. Protein concentration was determined colorimetrically using the BioRad Protein Assay (Bradford) dye reagent and the bovine serum albumin as standard.

N-terminal Amino Acid Sequencing. Partial N-terminal amino acid sequencing of the purified proteases was performed on polyvinylidene difluoride-electroblotted proteins at the Midwest Analytical Inc. (St. Louis, MO) using an automated Edman degradation sequencer from Applied Biosystems (Foster City, CA).

Substrate Digestion by Proteases. Approximately 0.2 μg of proteases was incubated for 4 h at 37 ^{o}C with various proteins in 20 mM Tris-HCl (pH 7.4) containing 1 mM $CaCl_2$ and 1 mM $MgSO_4$. Denaturation of human collagens type I, III, and IV was performed at 95℃ for 2 min. Plasmid for recombinant rat syndecan-1 expression with a GST-tag at the N-terminus was kindly provided by Dr.

Eok-Soo Oh (Ewha Womans University, Seoul, Korea). Recombinant syndecan-1 protein was partially prepared from a host *E. coli* BL21 (DE3) cells using a glutathione-sepharose affinity column. Digested substrates were separated by SDS-PAGE.

Determination of Kinetic Parameters. Synthetic collagenase substrates (0.4 - 25 μM) were prepared in assay buffer (50 mM Tris-HCl, pH 7.5, 1 mM $CaCl_2$, 0.01% Tween-20). Collagenase assay was carried out in the substrate solution by incubating with 4 nM of enzymes at 37℃. Fluorescence was measured using $\lambda_{excitation}$ = 320 nm and $\lambda_{emission}$ = 390 nm. Initial velocities were obtained from plots of fluorescence *versus* time, using the data points corresponding to less than 40% full hydrolysis. The slopes of these plots were divided by the fluorescence change corresponding to complete hydrolysis and then multiplied by the substrate concentrations to obtain initial velocity in units of μMs^{-1}. N-(3-[2-furyl]acryloyl)-Leu-Gly-Pro-Ala-hydrolyzing activity was measured by continuously monitoring the decrease in absorbance of the substrate at 324 nm after the addition of enzyme.

Assay for Plasmin and Plasminogen Activation. Plasmin activity was assayed by monitoring the Val-Leu-Lys-*p*NA hydrolysis in a molar enzyme to □$_2$-antiplasmin ratio of 0.3 in 50 mM Tris-HCl, pH 7.5 and 1 mM $CaCl_2$. □$_2$-Antiplasmin was preincubated with proteases at 37^{o}C for 4 h. Plasminogen activation in the presence of plasma fibrin was assayed by monitoring the Val-Leu-Lys-*p*NA hydrolysis. Human plasminogen (8.3 μg) was incubated at 37 ^{o}C with 2 μg of the protease or streptokinase (positive control) in 50 μl of 50 mM Tris-HCl, pH 7.5, 1 mM $CaCl_2$. The resulting reactions were diluted 20-fold and added to 100 μM Val-Leu-Lys-*p*NA (50 μl) in the presence of fibrin. Urokinase-type plasminogen activator (uPA)-catalyzed plasminogen activation was carried out with 200 U/ml uPA, 0.1 U/ml plasminogen, 100 μM Val-Leu-Lys-*p*NA, and either 2, 5 or 10 μg/ml of the purified proteases in a 100 μl reaction volume. The release of *p*NA from the chromogenic substrate was monitored at 405 nm.

Analysis of Shedding in Cultured Cells. Syndecan-1 shedding from NMuMG cells was assayed as described previously [198]. Briefly, cells were grown up in Dulbecco's modified Eagle's medium in 96-well plates, cultured to 1 day post confluence, then stimulated with indicated proteins using serum-free media. After stimulation, culture supernatants (100 μl) were collected and acidified with 900μl of acidification buffer (150 mM NaCl, 50 mM NaOAc, 0.1% Tween-20, pH 4.5). Samples were applied to Immobilon NY+ membrane using *Bio-Dot* microfiltration apparatus (Bio-Rad). Washing with acidification buffer, the membrane was then blocked in milk and incubated with rat anti-mouse syndecan-1 antibody followed by incubating with goat anti-rat HRP-conjugated secondary antibody. The membranes were developed using *ECL Plus* Western Blotting Detection kit (Amersham Biosciences) and Kodak BioMax Light Film (Sigma). The results were quantified by scanning the exposed film, and evaluating the intensity of exposed dots by software AlphaEase FC (Alpha Innotech). Results were expressed as the amount of syndecan-1 shed relative to control using a calibration curve generated by two-fold dilutions of culture supernatants from mouse epithelial cells treated with Anthralysin O as a positive control for shedding as determined previously [56]. For each set of measurements the mean and the 95% confidence intervals were calculated using the Student *t*-test.

*Western Blot of Syndecan-1 Ectodomains***.** Conditioned media from stimulated NMuMG cells for 4 h with purified proteases (250 ng/ml) or phorbol myristate acetate (PMA, 1 μM) were collected, and 1.3% (w/v) potassium acetate and 3 volumes of 95% EtOH were added to the media. After keeping overnight at -20 ^{o}C, samples were dissolved in digestion buffer (100 mM Tris-HCl, pH 8.0, 0.1% Triton X-100, 5 mM EDTA, and 1 mM phenylmethylsulphonylfluoride (PMSF) and half volume of each samples were digested with 20 mU/ml heparinase II and 20 mU/ml chondroitin sulfate ABC lyase at 37 ^{o}C overnight. These digested and undigested samples were fractionated by SDS-PAGE using 4-20% gradient gels, electrophoretically transferred to Immobilon NY+ nylon membrane. Membrane was probed with monoclonal rat anti-mouse syndecan-1 antibodies (281-2, BD

Pharmingen), and then horse raddish peroxidase-conjugated goat anti-rat IgGs, and developed by the ECL detection method.

Mass Spectrometry. Protease-treated proteins were separated by SDS-PAGE. Protein bands were excised from the gel and digested with trypsin (Promega) according to published procedure [199]. Tryptic peptides were analyzed by the reverse-phase liquid chromatography nanospray tandem mass spectrometry using a linear ion-trap mass spectrometer (LTQ, ThermoElectron) and a 100 µm × 10 cm-long fused silica capillary column (Polymicro Technologies) with a laser-pulled tip, packed with 5 µm, 200 Å pore size C_{18} resin (Michrom BioResources). After sample injection, the column was washed for 5 min with a mobile phase A (0.4% acetic acid) and peptides were eluted using a linear gradient of 0% mobile phase B (0.4% acetic acid, 80% acetonitrile) to 50% mobile phase B in 30 min at 0.25 µl/min, then to 100% B in an additional 5 min. The LTQ mass spectrometer was operated in a data-dependent mode, in which each full MS scan was followed by five MS/MS scans where the five most abundant molecular ions were dynamically selected for collision-induced dissociation using a normalized collision energy of 35%. Tandem mass spectra were searched against rat database (the National Center for Biotechnology Information) with SEQUEST [200]. For a peptide to be considered legitimately identified, it had to achieve cross-correlation scores of 1.5 for $[M+H]^{+}$, 2.0 for $[M+2H]^{2+}$, 2.5 for $[M+3H]^{3+}$, and a maximum probability of randomized identification of 0.001.

Proteolysis of VWF and ADAMTS13 in human plasma. Human normal plasma (1:10 dilution) was incubated with culture supernatants or purified proteases Npr599 and InhA of *B. anthracis* delta Ames in the absence or presence of urea (final 1.5 M). Purification of Npr599 and InhA from culture supernatants was performed as described previously. After overnight incubation at room temperature (arbitrary 21℃) or 37℃, the resulting products in the native SDS sample buffer were separated by 1% agarose-SDS Tris-glycine gel for multimer analysis and by 6% SDS-PAGE gel under reducing condition (32 mM dithiothreitol) for monomer analysis. The VWF fragments were

visualized and Western blotted with HRP-conjugated rabbit antihuman VWF antibodies (P0226, Dako, NJ) in a 1:2000-dilution after transferring to a PVDF membrane. For proteolysis of ADAMTS13, 50 μL human plasma (1:10 dilution) was incubated with 0.2 μg of Npr599, InhA, or LF in 5 mM Tris-HCl, pH 8.0 at 37℃ overnight. The samples were analyzed by Western blotting using anti-ADAMTS13 antibody (BL154G, Bethyl Laboratories, TX).

Proteolysis of a synthetic peptide FRETS-VWF73. FRETS-VWF73 (SFR-3224-s, Peptides International, KY; final 2 μM) was incubated with plasma, purified Npr599, or InhA in 100 μL of reaction buffer (5 mM Tris-HCl, 25 mM $CaCl_2$ and 0.005% Tween-20, pH 6.0). The reaction was incubated at 37℃ for specific times, and change of fluorescence (an excitation 355 nm and an emission 460 nm) was monitored. Initial velocities were obtained from plots corresponding to less than 20% and 70% full hydrolysis against Npr599 and InhA, respectively. The slopes of these plots were divided by the fluorescence change corresponding to complete hydrolysis and then multiplied by the substrate concentrations to obtain initial velocity in units of $\mu M \cdot s^{-1}$. Individual kinetic parameters were calculated using Lineweaver-Berk plot and $k_{cat} = v_{max}/[E_T]$, where $[E_T]$ is total enzyme concentration.

N-terminal sequencing of VWF fragments. Purified native human VWF (Sigma) was incubated with InhA in a buffer consisting of 5 mM Tris-HCl, pH 7.5, 1 mM $CaCl_2$ and 1.5 M urea at 37℃ overnight. The products were loaded onto 4-12% SDS-PAGE gel and separated under reducing condition (32 mM DTT). After transferring the proteins to PVDF membrane, automated N-terminal sequencing was performed using automated Edman degradation sequencer (Applied Biosystems, Foster City, CA) at the Midwest Analytical, Inc (St. Louis, MO).

Collagen binding assay. Acid-soluble collagen type III from human placenta (C4407, Sigma, MO) was dissolved in 3% acetic acid. The collagen solution (100 μL) was rapidly diluted to a final concentration of 20 μg/ml in PBS, and then immobilized on a microplate MaxSorp (Nunc) for 1 hr at

room temperature. After coated, the plate was blocked with 5% BSA in PBS. Plasma (1:80) was incubated with proteases (10, 1, 0.1, 0.01 μg/ml) in the absence or the presence of 1.5 M urea at 37℃ for 3 hrs, and the reaction was stopped by add ing 5 mM EDTA. For assaying VWF's collagen-binding activity (VWF:CBA) of mouse plasma, the plasma (10 μg) was dissolved in 100 μL of PBS. The plasma samples were loaded on the collagen-coated plate for 1 hr at room temperature. After the plate was washed 5 times with PBS containing 0.05% Tween 20 (PBST), HRP-conjugated VWF antibody in dilution 1:2000 was added and incubated for 1 h at room temperature. After washing with PBST, the reaction was visualized by the addition of ELISA developing solution (100 μL) followed by stopping reaction with the addition of 2 M H_2SO_4 (50 μL). The absorbance was read at 450 nm on a microplate reader. Experiments using *o*-phenanthroline were similarly performed except that proteases were preincubated for 5 min with 5 mM *o*-phenanthroline. As a negative control, BSA was used instead of collagen, and the optical density of sample was subtracted by optical density detected in BSA-coated well.

VWF overlay assay. Proteases were electrophoretically transferred to a PVDF membrane. The membrane soaked into PBST overnight at 4℃ and incubated with normal human plasma (diluted 1:20 with PBST) for 1.5 h at room temperature. After the plasma had been washed with PBST five times for 4 min, the membrane was incubated with HRP-conjugated anti-VWF antibody (1:2000) for 1 h followed by HRP reaction.

Ristocetin Cofactor-induced platelet aggregation (RIPA) assay. RIPA assay was performed using a Helena ristocetin cofactor assay kit (Helena Laboratories, TX). Two-fold diluted plasma (100 μL) was incubated with 0.2 μg proteases in 1.5 M urea at 37℃ overnight. 10 μL of protease-treated plasma was added to 80 μL platelets (~ 3×10^5/ml) and 1 mg/ml ristocetin. Thereafter, the mixture was incubated for 10 min with vigorous orbital shaking. To assess microscopic analysis, the aggregates were fixed with 1% paraformaldehyde for 10 min and examined under microscope. Quantification of platelet aggregation was assessed by expression of platelet marker CD41 in flow

cytometry. Ristocetin cofactor-induced platelet aggregates was incubated with PE labeled anti-CD41 antibody (eBioscience, CA) for 10 min. Fixing step was followed by adding 2% paraformaldehyde for 10 min, and the aggregates were diluted with 1 ml PBS for 2 hrs at room temperature. Platelet aggregation was calculated by counting the number of free platelets (< 5 μm) shifted to a bit map representing platelet aggregates (> 5 μm).

Analysis of VWF released from HUVEC cells. Human umbilical vein endothelial cells (HUVECs) from Clonetics were maintained in EBM medium (Clonetics, MD) at 37℃ in an atmosphere of 95% air and 5% CO_2. Cells were incubated with anthralysin O (AnlO) and culture supernatants of *B. anthracis* delta Ames. After incubation for 15 min (AnlO) and 60 min (culture supernatants), 500 μL of the conditioned media was precipitated with EtOH, and the precipitates were dissolved in 15 μL of native sample buffer. ULVWF multimers were visualized in 1% agarose-SDS-Tris-glycine gel followed by Western blotting on a PVDF membrane with anti-VWF-HRP (1:2000) as described above.

Plasma Preparation from spore-challenged mice. The 9 week old mice (DBA/2 from Jackson Laboratory) were challenged intraperitoneally with 1×10^7 spores of *B. anthracis* non-encapsulated Sterne strain 34F2 [$pXO1^+$, $pXO2^-$] and non-toxigenic delta Sterne strain [$pXO1^-$, $pXO2^-$] obtained from the Colorado Serum Company (Boulder, CO). The 50% lethal dose of 3×10^6 spores (LD_{50}) by the inraperitoneal (i.p.) route was established earlier. At 24 h time points, blood was drown into 0.38% sodium citrate, and was centrifuged at 900 g for 15 min to obtain platelet-poor plasma (PPP). For the ELISA assay of VWF antigen (VWF:Ag), plasma from each mice (10 μg) was diluted in 100 μl of phosphate buffered saline (PBS) and used to coat wells of the Nunc Maxisorp™ plates (eBiosciences) overnight at 4℃. After incubation, the plates were washed 3 times with 100 μl per well of PBS, 0.1% Tween-20 and blocked for 1 h at 4℃ with 100 μl per well of PBS plus 5% BSA (Sigma). Plates were incubated in 100 μl per well of fresh blocking solution plus 1:2000 dilution of HRP-conjugated anti-human VWF antibody 226 (Dako) for 1 h at room temperature, washed 7 times

with 200 µl per well of PBS, 0.1% Tween-20, and then developed using tetramethyl benzidine reagent (Beckman Coulter) added to all wells and incubated at room temperature for 30 min. Absorbance was detected at 450/570 nm using µQuant plate reader (Bio-Tek Instruments). The average absorbance calculated for each treatment group was corrected for the average absorbance of the control wells without plasma, and the results were presented as a percent change relative to the untreated control group.

Cell culture reagents and antibodies were from Cellgro (Herndon, VA). Antibodies against total and phosphorylated forms of following proteins used for reverse phase protein microarrays and Western blots were from Cell Signaling Technology (Beverly, MA). Antibodies were used at dilution: 1:20 for p70 S6 Kinase (Thr389); 1:50 for c-Abl (Thr 735), Stat5 (Tyr694), 4E-BP1 (Ser65); 1:100 for Akt (Ser473), MEK1/2 (Ser 217/221), pIKBa (Ser32/Ser36), Bad (Ser112, 155 and 136), 4E-BP1 (Thr70), GSK-3α/β (Ser21/9), CREB (Ser 133), Stat3 (Ser727, Tyr705), Jak1 (Tyr1022/1023), FAK (Tyr576/577), Etk (Tyr 40), Elk-1 (Ser383), MARCKS (Ser152/156); 1:200 for mTOR (Ser2448), eNOS (Ser1177), Pyk2 (Tyr402), FADD (Ser194), Stat6 (Tyr641), Bcl-2 Ser70; 1:250 for p38 (Thr180/Tyr182), IL-1β-cleaved (Asp116); 1:400 for p90RSK (Ser380);1:500 for PKC-δ (Thr505), Src (Tyr 527), PKC-α/β (Thr638/641), PKC-θ (Thr538), caspase-7-cleaved (Asp198), caspase-9-cleaved (Asp330), caspase-3-cleaved (Asp175), ERK 1/2 (Thr202/Tyr204), pPKC-z (Thr410/403), Src (Tyr527), Stat1 (Tyr701), Bax; 1:1000 for 4E-BP1 (Thr37/46), Bcl-xL; 1:2000 for eIF4G (Ser1108). Recombinant protective antigen (PA), lethal factor (LF) and edema factor (EF) were from List Biological Laboratories (Campbell, CA).

Challenge of lung epithelial cells with spores. HSAECs were grown up in Ham's F12 media supplemented with non-essential aminoacids, pyruvate, β-mercaptoethanol and 10% FCS. Confluent HSAECs (10^6 /well in 12-well plates) were starved in serum-free media plus 1% FCS for 16 h before challenge with spores, supernatant was removed, and cells were lysed and immediatly boiled for 10 min in 100 µl of 1:1 mixture of T-PER Reagent (Pierce, Rockford, IL) and 2x Tris–glycine SDS

sample buffer (Novex/Invitrogen) in presence of 2.5% β-mercaptoethanol and protease inhibitors. Lysed samples were stored at -80^{o}C before arraying.

Slide printing and staining. Three nl of each sample were arrayed by a pin and ring GMSE 417 Arrayer (Affymetrix, Santa Clara, CA) onto nitrocellulose slides (Whatman, MA). Samples were printed in duplicate and in five-point dilution curves to ensure the linear detection range for the antibody concentrations used. Slides were kept at -20^{o}C before analysis with antibodies.

To estimate the total protein amount, selected slides were stained with Sypro Ruby Protein Blot Stain (Molecula Probes, Eugene, OR) and visualized on a Fluorchemk imaging system (Alpha Innotech, San Leandro, CA). Slides were stained with specific antibodies on an automated slide stainer (Dako, Carpinteria, CA) using a biotin-linked peroxidase catalyzed signal amplification. The arrayed slides were placed into 1X Re-Blot solution (Chemicon, Temecula, CA) for 15 min, washed two times for 5 min each in PBS, placed into I-Block solution (Applied Biosystems, Foster City, CA) in PBS/0.1% Tween-20 for at least 2 h, and then immunostained using an automatic slide stainer (Autostainer, Dako Cytomation, Carpinteria, CA) using manufacturer-supplied reagents. Briefly, the slides were incubated for 5 min with hydrogen peroxide, rinsed with high-salt Tris-buffered saline (CSA Buffer, Dako) supplemented with 0.1% Tween-20, blocked with avidin block solution for 10 min, rinsed with CSA buffer, and then incubated with biotin block solution for 10 min. After another CSA buffer rinse, a 5 min incubation with Protein Block solution was followed with air-drying. The slides were then incubated with either a specific primary antibody diluted in Dako Antibody Diluent or, as a control, with only DAKO Antibody Diluent for 30 min. The slides were then washed with CSA buffer and incubated with a secondary biotinylated goat anti-rabbit IgG H+L antibody (1:5000) (Vector Labs, Burlingame, CA) for 15 min. For amplification purposes, the slides were washed with CSA buffer and incubated with streptavidin-horseradish peroxidase (HRP) for 15 min, followed by a CSA buffer rinse. Slides were then incubated in diaminobenzidine (DAB) chromogen diluted in Dako DAB diluent for 5 min, washed in deionized water and imaged using a UMAX PowerLook III scanner (UMAX, Dallas, TX) at 600 dpi. The images were analyzed with

software AlphaEase FC (Alpha Innotech, San Leandro, CA). For each antibody, the average pixel intensity value for negative control (staining with only second antibody) was subtracted from the average pixel intensity value for specific antibody and was divided by the corresponding value of the Sypro-stained total potein slide. To confirm the reverse phase protein microarray data, 20 ul of cell lysates were used for Western blots, which were stained with 1:1000-diluted primary antibodies and 1:7500-diluted secondary antibody. Primary and secondary antibodies were the same as in the reverse phase protein microarray. Reverse-phase protein microarray and Western blot data were presented as average of two independent experiments. For reverse-phase protein microarray each sample was printed in duplicate.

Animal pharmacological protection experiments. Male 6 to 8 week old DBA/2 mice (Jackson Labs) received food and water *ad libitum*, and were challenged with anthrax spores ($1x10^7$ spores, i.p.) on day 0. Survival of animals was monitored for 15 days. Ciprofloxacin (Sigma, St Louis, MO) treatment (50 mg/kg, once daily, i.p.) was initiated at day +1 simultaneously with the administration of inhibitors, and continued for 10 days. Two doses (2.5 mg/kg and 12.5 mg/kg) of YVAD (acetyl−tyrosyl-valyl-alanyl-aspartyl−chloromethylketone from Bachem Bioscience, PA) and 3 doses (0.05, 0.15 and 0.3 mg/kg) of Cl-IB-MECA (1-[2-Chloro-6-[[(3-iodophenyl) methyl]amino]-9H-purin-9-yl]-1-deoxy-N-methyl-β-D- ribofuranuronamide from Sigma, St Louis, MO) were chosen for this study. Animals received YVAD on days +1 to +4, and Cl-IB-MECA on days +1 to +10 once daily, s.c. Survival was monitored daily.

The George Mason University Institutional Animal Care and Use Committee and the BIOCON, Incorporated Animal Care and Use Committee/Institutional Review Board have approved all protocols prior to animal experiments.

Plasmid curing, strain selection, and typing. Bacillus anthracis Sterne strain ($pXO1^+$, $pXO2^-$) was used in this study. This strain was cured of the pXO1 plasmid by growth for 6 days in LB media at 42.5℃. To detect the presence of pXO1, the gene for protective antigen (PA), found only the

plasmid, was PCR-amplified. Colonies were checked *via* PCR, and a colony negative for the PA gene was picked and designated *Bacillus anthracis* delta Sterne. Spores were generated by growth for 4 days on LB plates, followed by re-suspension in water and pelleting by centrifugation from two to four times. Spores were stored in water at 4℃. During the course of this study, PCR was used to control for the absence of the pXO1. Additionally, multi locus sequence typing (MLST) was done using the method and primers of Helgason et. al. (2004), which helped ensure that major genomic changes had not occurred during curing. MLST results showed the cured and the parental strains to be identical for all variable sequences tested. Growth curves for both *B. anthracis* Sterne and *B. anthracis* delta Sterne were identical in both serum-free, and 1% fetal bovine serum (FBS) cell culture media, with 4 h corresponding to the mid point of the exponential phase of growth.

THP-1 cell cultures, growth and viability measurement. THP-1 was obtained from ATCC (Manassas, VA) and grown in complete medium (RPMI 1640 with glutamine, 25mM HEPES, 4.5 g/l glucose, and 10% FBS) for propagation, until 24 h before challenge with either *B. anthracis* Sterne, or *B. anthracis delta* Sterne, at which point THP-1 cells were washed and re-suspended for 24 h in serum-free (low protein) Cellgro media (Media Tech, Herndon, Va.) at a concentration of 1.0×10^6 cells/ml. Cell cultures were challenged for 2 h or 4 h at a cell to spore multiplicity of infection (MOI) of either 1 to 1 or 1 to 10 for microarray experiments. The timepoints are similar to previously reported transcriptional analyses, with the 4 h timepoint also representing the midpoint for the mid-logarithmic phase of growth. Viability was measured by a standard trypan blue assay counted on a hemocytometer. Infection of THP-1 monocytes by both strains at both tested MOIs did not result in a loss of viability at 2 and 4 h time points.

Microarrays and ANOVA analysis. The microarray platform was developed, printed, hybridized and analyzed at Avalon Pharmaceuticals, Inc.(Germantown, MD). Arrays consist of proprietary 80-mer long, spotted oligonucleotides representing 2,000 human genes. Each chip contains 4 replicates of each gene (8,000 total/chip) with 64 perfect match and 64 mismatch

controls. Arrays were hybridized using standard Cy3/Cy5 sample/reference labeling and analyzed using a Scanarray reader (Perkin-Elmer, Wellesly, MA). To determine whether genes were differentially expressed between two experimental states, an ANOVA (analysis of variance) was performed on the log-transformed expression ratios. The following model was used for this analysis: $y_{ijkl}=E_i + M_j + T_k + (EMT)_{ijkl} + \varepsilon_{ijkl}$ where y_{ijkl} denotes the $\log_2$ expression ratio measured for experimental state *i*, MOI *j*, time state *k*, replicate *l,* with $1 \le i \le 3$, $1 \le j \le 2$, $1 \le k \le 2$, and $1 \le l \le 6$. The term E_i measures the effect of the infection; M_j measures the effect of the MOI; T_k measures the effect of the time state, and the term $(EMT)_{ijkl}$ measures the interaction effect of all three variables. An ANOVA was performed on each gene using the linear model above. Twelve contrasts were based on pair-wise differences between each experimental condition and the control state, as well as the experimental state which differed in the MOIs only. The R package limma was used for ANOVA methods (www.bioconductor.org/repository/devel/vignette/affy.pdf.). A multiple testing correction controlled the false discovery rate, which is the expected proportion of false positives in the rejected hypotheses. Genes with adjusted F-statistic *p*-values < 0.05 were inspected further.

Real-Time PCR. To confirm microarray data, realtime PCR was performed using the iQ SYBR Green kit from BIO-RAD (Hercules, CA) using the manufacturers specifications. Primers chosen for realtime analysis were as follows: The human 18-S ribosomal gene (18S) consisting of the sense strand 5'AGGAATTCCCAGTAAGTGCG 3', and the anti-sense strand 5' GCCTCACTAAACCATCCAA 3'; Tumor necrosis factor-α (TNF superfamily, member 2; TNF-α), consisting of the sense strand 5' TGTCTCAACCCCGCATCG 3' and the anti-sense strand 5' AGGAACAGCCACCAATAAGC 3'; consisting of the sense strand 5' ras-related C3 botulinum toxin substrate 2 (rho family, small GTP-binding protein Rac2; RAC2), consisting of the sense strand 5' CCTCATCATCCAGTCCAACG 3', and the anti-sense strand 5' GGCGAACTCCTGCTCCTC 3'; Ribosomal protein S6 kinase (90kDa, polypeptide 1;RPS6KA1), consisting of the sense strand 5' ACAGGATTGACAGATTGATAGC 3', and the anti-sense strand 5' ATGCCAGAGTCTCGTTCG 3'; Angiotensinogen proteinase inhibitor (clade A; alpha-1 antiproteinase, antitrypsin, member 8; AGT),

consisting of the sense strand 5' CAGGGACCTCTCTCTAATCAG3', and the anti-sense strand 5' TGCTACAACATGGGCTACAG 3'; Plasminogen activator/urokinase receptor (PLAUR), consisting of the sense strand 5' CTGGCTTTCAACACCTACG 3' and the anti-sense strand 5' TTGTCCACCCAGAACTCC 3'; and CASP8/FADD-like apoptosis regulator (CFLAR), consisting of the sense strand 5' AGATCACCAGCCTTACCG 3', and the anti-sense strand 5' GATGAGCCACAGGAAATGC 3'. T_ms used in realtime cyclers consisted of 54.3℃ for TNF-α, AGT, CFLAR, and 18-S genes; 52.9℃ for RAC and RPS6KA1 g enes; and 63.2℃ for the PLAUR gene.

Representation of biological response modules. Values for genes from each of three replicate chips for each treatment were summed and averaged, and genes corresponding to specific gene ontology (GO) profiles were evaluated. These GO profiles represent modules of genes involved in specific biological responses or tasks. The GO profiles which we used were developed by the Gene Ontology Consortium (http://www.godatabase.org). GO ID numbers for the GO modules represented in this study can be found by searching the GO descriptions found within this article on the described website. Data were processed using '*Cluster*' (http://rana.lbl.gov/EisenSoftware.htm) without additional filtering or adjustment. Hierarchical clustering was done on genes using an uncentered correlation, followed by complete linkage clustering, and the generated map used.

Sandwich Thrombin-anti-thrombin (TAT) complex ELISA. Wells of a 96-mictotiter (NUNC MaxiSorp) plate was coated with 100 µL of anti-AT antibody (1 µg/ml in coating buffer.) Plates were incubated overnight at 4℃. The plates were washed 3 times with PBST and 200 µL of PBS/10% FCS was added to each well as a blocking step for 1 hour. Added 50 □L of standard or 4-fold diluted plasma samples in PBST/FCS (1%) for 1 h on a shaker. The plate is washed 3 times with PBST then incubated with 100µL of AT antibody (0.5 µg/ml) in PBST/1% FCS for 1 hour. Washed 3 times with PBST and incubated with 100□L HRP-antibody (mouse IgG) in PBST. Then washed 3 times with PBST and developed with 100□L of TMB solution. Added 50µL of 2N H_2SO_4 to stop the reaction and read at OD_{450nm}.

Western Blot. 20μg of plasma from normal control and spore-challenged mice was boiled in SDS sample buffer with 30mM DTT. The samples were loaded onto a NuPAGE 4-12% Bis Tris Gel (Invitrogen) and transferred onto a PVDF membrane. The membrane was blocked with 5% milk, incubated with primary antibody and HRP-conjugated secondary antibody sequentially. The membranes were developed using an ECL Western blotting detection kit and Kodak BioMax light film.

Reverse-transcriptase (RT) polymerase chain reaction (PCR). For determination of expression of syndecan-4 and AT mRNA: total RNA was prepared from frozen liver sections and was immediately frozen in liquid nitrogen, and stored frozen at −80 C. Oligo(dT)-primed cDNA was prepared from 5 μg of total RNA by use of Platinum PCR Supermix® (Invitrogen). Specific primers were designed for: ***Antithrombin*** (5'- ATG GTA CAT TCC TCA CCC TGC G-3' [sense] and 5'- AGC ACC ACT GCT CCC ACA ATG A-3' [antisense] ***Syndecan-4*** (5'- AAC CAC ATC CCT GAG AAT GC-3' [sense] and 5'- AGG AAA ACG GCA AAG AGG AT-3' [antisense] After amplification, PCR products were separated on a 1.7% agarose gel and stained with ethidium bromide. Photographs were scanned and analyzed by densitometry.

Immunodepletion Assay. AnlO treated culture supernatant (30 μL) was incubated with anti-syndecan 1 (2 μL) and anti-syndecan 4 (2 μL) antibody for 2 hours at 4^{o}C with gentle shaking. The control is without antibody. Protein A/G-agarose beads (10 μL) was added into the solution and incubated at 4^{o}C overnight with gentle shaking. Centrifuge and save supernatants. AT assay: % of supernatant was used in the AT inactivation assay (5 μL Supernatant and 5 μL AT-elastase = 50%.)

AT inactivation Assay (with Immunodepleted Supernatant).

2 μM AT in 20 mM Tris-HCl, 150 mM NaCl, pH 7.5 in the presence or absence of heparin (100 ng/ml) and shed syndecan (CS, AnlO-treated NMuMG culture supernatants) was added into 5 nM elastase, and then incubated at 37℃ for 15 min. After diluting to 1:20 in stop solution (50 mM Tris-HCl, 150 mM NaCl, pH 8.4 cont'g 1 mg/ml a1-proteinase inhibitor), the resulting solution (80 μL) was subjected to chromogenic heparin cofactor assay containing 20 μL thrombin (1 U/ml) and 40 μL substrate (Tos-Gly-Pro-Arg-pNA, 1.5 mM). After incubation at 37℃ for 30 min, the reaction was stopped by adding 60 μL concentrate acetic acid, and then OD was read at 405 nm.

Overlay Assay

2 μg of AT was ran on an SDS-PAGE gel (4-12%). The gel was transferred to nitrocellulose membrane using the iBlot Gel Transfer System©. The membrane was incubated overnight at 4^{o}C in

PBST (PBS + 0.05% Tween 20), and then washed three times with PBST. The paper was overlaid with 1) elastase (50 nM, 1 ml), 2) AnlO-treated NMuMG culture supernatant (150 μL) and 3) α_1-antitrypsin (5 μg) in 5 ml PBST for 1.5 hours at room temperature. The membrane was washed and detected with corresponding antibodies.

KEY RESEARCH ACCOMPLISHMENTS

Task 1

This task is completed. Key accomplishments on this task have been reported in the year 2004.

Task 2

- Two anthrax proteases, namely M4 elastase and M6 immune inhibitor, have been further characterized including:

  Syndecan cleavage site sequences involved in shedding;

  Catalytic activity parameters of secreted proteases.

- It has been shown that secreted proteases of *B. anthracis*, and other factors such as pore-forming hemolysin AnlO, can cause hemostatic abnormalities in endothelial cells, namely:

  Npr599 and InhA cleave synthetic VWF substrate FRET-VWF73, and InhA degrades native VWF;

  Npr599 and InhA abolish VWF's collagen-binding activity;

  Npr599 and InhA bind to VWF;

  InhA inhibits ristocetin-induced platelet aggregation;

  Anthrax proteases induce and then degrade VWF multimers from HUVEC cells;

  VWF is induced but functionally inactive in plasma of spore-challenged mice.

- Experiments with lung endothelial cells exposed to toxigenic and non-toxigenic strains of *B. anthracis* identified cell signaling pathways associated with virulence. Experiments with

pharmacological inhibitors directed against several of the pathways involved in survival of challenged animals confirmed the pro-survival function of these pathways, and allowed explain previously observed effects of the central nervous system on anthrax toxicity.

- The results in cell culture model suggested a therapeutic intervention targeting cAMP-mediated signaling, along with the inhibition of caspase-1. Post-exposure treatment of *B. anthracis* (Sterne) spore-challenged mice with a combination of A3AR agonist, caspase 1/4 inhibitor YVAD, and ciprofloxacin resulted in up to 90% synergistic protection while antibiotic alone protected only 30% of mice.
- The results implicate EdTx/cAMP signaling in the PI3K/AKT pathway as an important contributor to anthrax mortality and demonstrate a new therapeutic modality adjunct to antibiotic treatment, which can confer a high level of protection by targeting the pathogenic host response to infection without a direct inhibition of anthrax toxins.

Task 3

- *B. anthracis* exoproducts in the absence of proteases are capable of stimulating production of TNF-α in RAW264.7 cells through TLR2. LB culture supernatants containing secreted proteases abrogate LPS- and Pam_3CSk- mediated TNF-α production.
- Our results do not support the initial hypothesis that TLR-4 plays a pathogenic role in anthrax infection.
- The TLR-2 signaling anthrax proteins have been fractionated, isolated and partially characterized. The most plausible candidates are the heat shock protein BaSHP60 and the S-layer protein Sap precursor.
- Toxigenic spore challenge of HBMEC cells in culture induces mainly bacterial chaperonin BaHSP60, while the atoxigenic delta Sterne spores predominantly induce an endogenous HSP60 from HBMEC cells.

- BaHSP60 can tightly bind bacterial LPS, and that both compounds synergistically activate TLR-2. It remains to be studies if TLR-2-stimulating activity of BaHSP60 is relevant to anthrax infection.
- Stimulation of host cells with HSP60 induces apoptosis and a pro-inflammatory response, including TNF-α, IL-6, GM-CSF, IL-8, IFN-γ, and COX-2 independently of LPS. BaHSP60 down-regulates phosphorylation of ERK, p38 and JNK, and up-regulates AKT. Inhibitors for PI3K, MEK1/2 and p38 decrease IL8-production in HBMEC cells.
- CD91 (LDL receptor-related protein; LRP1) was identified as a receptor for BaHSP60.
- The THP-1 cells display significant innate response of host macrophage-like cells to both virulent and avirulent infection.

    The early responses are preferentially suppressed by the toxigenic strain. This supports a hypothesis that in anthrax the suppression of apoptosis in macrophage-like cells may contribute to disease virulence, and that apoptosis itself may represent a protective response to infection.

    The experiments did not reveal a TLR gene upregulation upon anthrax infection in THP cells, and support the notion that anthrax apoptosis may take place in the absence of toxins.

    The production of CFLAR during the toxigenic infection may partially protect cells against TNF-α induced caspase-8-dependent apoptosis thus allowing for more successful bacterial survival and dissemination resulting in systemic disease.

Two manuscripts have been published in 2006:

Myung-Chul Chung, Taissia G. Popova, Bryan A. Millis, Dhritiman V. Mukherjee, Weidong Zhou, Lance A. Liotta, Emanuel F. Petricoin, Vikas Chandhoke, Charles Bailey, and Serguei G. Popov. 2006. Secreted neutral metalloproteases of *Bacillus anthracis* as candidate pathogenic factors. *J. Biol. Chem.* 281: 31408 - 31418

T.G. Popova, B. Millis, C. Bradburne, S. Nazarenko, V. Chandhoke, C. Bailey, S.G. Popov. 2006. Acceleration of epithelial cell syndecan-1 shedding by anthrax hemolytic virulence factors. *BMC Microbiol.* 6:8

Two manuscripts have been submitted for publication.

Different parts of this work have been presented at several conferences:

American Society for Microbiology Biodefense Research Conference, Baltimore, MD, 2006 - two posters presented;

AMS conference in Toronto - 2 posters presented;

Mid-Atlantic Regional Conference in Wintergreen, VA - 2 posters presented;

International Conference on Anthrax, Oslo, Norway - 2 posters presented and oral presentation given.

Reportable outcomes

Task 1. Synergistic Anti-Toxin/Antibiotic Treatment of Anthrax

a. Perform a synthesis of alkylamino derivatives and test them in *in vitro* and *in vivo* experiments.

b. Based on the findings of the apoptotic activity of lethal toxin (LT), evaluate various caspase inhibitors for their ability to inhibit toxin using a murine animal model with various doses and administration schedule.

c. Perform further studies to determine the efficacy of inhibitors combined with immunostimulators that were found to be active against LT in *in vitro* experiments with macrophages.

Task 2. Anthrax Protease Inhibitors for Therapy of Late-Stage Inhalational Anthrax

a. Identify proteases produced by *B. anthracis* that are typical of numerous pathogenic organisms using bioinformatics analyses. Choose representative proteases for further study based on their amino acid sequence homology, common structural elements, and shared catalytic groups.

b. Amplify selected protease genes from *B. anthracis* genomic DNA using PCR with specific primers. Perform recombinant expression in E.coli and purification of selected proteases. Characterize purified recombinant proteases for their enzymatic activity and substrate specificity.

c. Study the role of *B. anthracis* secreted proteins from culture supernatants as virulence factors *in vivo*. Determine whether *B. anthracis* proteins are toxic to mice, cause severe hemorrhage or/and increase vascular permeability upon injection into mice. Use cell culture lines as an alternative *in vitro* model system to determine if secreted factors are capable of disrupting the integrity of cell monolayers. In control experiments use *B. anthracis* spores and lethal toxin.

d. Study if activity of secreted factors results in the proteolytic removal (shedding) of cell surface molecules (ectodomain), cell death, and changes in cell-to-cell signaling. Using immunological and biochemical tools investigate specific biological nature of shed molecules, and carry out experiments to identify signaling pathways involved in cell response to shedding.

e. Test inhibition of shedding in cultured cells using available protease and/or signaling pathway inhibitors. Analyze if correlation exists between shedding inhibition and protective efficacy of inhibitors in mouse challenge model.

f. Perform assays to evaluate the systemic level of ectodomain shedding, such as the amount of circulated soluble syndecans, in the mouse spore-challenge model of anthrax infection.

g. Undertake separation of secreted *B. anthracis* proteins from culture supernatants. Characterize hemorrhagic and vascular permeability-enhancing and other potential pathogenic activities of isolated proteins. Wherever possible, identify substrate specificities of isolated proteins, as well as susceptibility of cells in culture. In control experiments use relevant bacterial proteins from other bacterial species.

h. Evaluate protective efficacy of inhibitors, selected from the analysis of the experimental data on the other bacterial proteases, against *B. anthracis* proteases *in vitro*. Based on the results of

the *in vitro* experiments, test the ability of protease inhibitors to protect mice from challenges with purified proteases or *B. anthracis* spores.

k. Generate polyclonal antibodies against recombinant proteases. Characterize specificity of antibodies towards proteases *in vitro*. Use antibodies as immunological detection tools in the analyses of individual proteases among secreted proteins produced by *B. anthracis*.

l. Evaluate efficacy of antibodies, generated against purified bacterial proteases, in neutralization of *B. anthracis* proteases activity *in vitro*. Based on the results of the *in vitro* experiments, test the ability of protease inhibitors to protect mice from challenges with purified proteases or *B. anthracis* spores.

Task 3. Toll-like Receptor (TLR) Neutralizing Antibodies and Soluble TLRs as Specific and Broad-Spectrum Protection against Biological Weapons

a. Assess commercially available anti-TLR antibodies as specific and broad-spectrum protection against biological weapons. Use TLR-neutralizing antibodies *in vitro* to test their effect on internalization, germination of anthrax spores and intracellular proliferation of vegetative bacilli in macrophages. If neutralizing antibodies block germination of spores and increase viability of macrophages, carry out the experiments on the protective efficacy of antibodies against anthrax infection in mice.

b. Use genetic constructs capable of expressing TLRs to evaluate the possible role of TLRs in the infectious process caused by vaccinia virus in cell culture. Test if TLR-neutralizing antibodies can interfere with the vaccinia infections.

c. Generate recombinant constructs for the expression of soluble TLR-2 and -4 in *E. coli* cells. Evaluate the possibility of isolation and purification of recombinant soluble TLRs from *E. coli*. If isolation of soluble TLRs is successful, assess the protective effect of soluble TLRs as potential therapeutic products against biological weapons. Test if administration of soluble TLRs will block interaction between the membrane-bound TLR and the pathogen spore, LT or vaccinia virus.

Determine if soluble TLR administration will decrease internalization of the invading anthrax spores, block the effect of LT and enhance survival of infected macrophages.

d. Test the *in vivo* role of selected TLRs or TLR adaptors (e.g., MyD88 and TRIF) in the vaccinia virus (TLR2, TLR3 and TLR4) or *B. anthracis* infections (TLR2 and TLR4) using commercially available mice deficient in these TLRs or adaptors.

e. Investigate the role of selected TLRs in the induction of pro-inflammatory cytokines/chemokines. In case the TLR-modulating antibodies are available, test if they are able of enhancing the function of immunocompetent cells and elimination the infected agents, such as vaccinia virus or *B. anthracis*.

f. Test if secreted proteolytic factors produced by atoxigenic strain of *B. anthracis* exhibit signaling through TLR-2 and TLR-4 proteins. Evaluate possible effect of anthrax pathogenic factors, such as lethal toxin, protective antigen, and hemolysins on TLR signaling.

g. In case, the TLR signaling effect is identified, test if protease inhibitors targeting major signaling pathways or specific anti-protease antisera are effective in the inhibition of TLR signaling.

h. Using *in virto* signaling system, evaluate a hypothesis that soluble ectodomain molecules shed from host cells could cause a pathologic condition similar to systemic inflammatory response, by activation of TLRs and consequent release of cytokines/ chemokines.

Conclusions

In 2006-2007, our research further confirmed that secreted virulence factors, in addition to lethal toxin, play important role in anthrax and may be considered as candidate targets for post-exposure therapies. Our experiments revealed several pathogenic mechanisms of these factors. The data generated using epithelial and endothelial cells in culture challenged with *B. anthracis* spores allow conclude that the activities of proteolytic proteins and hemolysins lead to profound pathological changes in the function of host cells. We found that hemostatic abnormalities during infection are manifested in the degradation of von Willebrand factor, release of this factor in

response to *B. anthracis* proteins, and degradation of the ADAMTS13 protease. The results favor a hypothesis that an anticoagulant activity of secreted pathogenic factors along with the disruption of barrier permeability could be considered as a major cause of hemorrhage during infection.

In the current report we characterized the response of primary lung epithelial cells to the pathogenic factors secreted by *B. anthracis* using the phosphoproteomics approach. The ability to broadly measure the phosphorylation-mediated activation of cell signaling pathways using the novel proteomic platform and the matched pair of isogenic non-toxigenic and toxigenic *B. anthracis* strains helped us expand available information on specific signaling pathways altered by the infection. Previous studies did not utilize this comparative approach and typically reported results using only virulent strains or toxins. Consequently, silencing of host responses may not have always been detected and recognized as a pathogenic process. Our major finding is that, in addition to the inhibition of MAPK signaling, the exposure of epithelial cells to the toxigenic *B. anthracis* causes dampening of the cell survival signaling in the PI3K/AKT pathway. This effect is consistent with the mechanism in which downregulation of AKT phosphorylation upstream of GSK3β and CREB is mediated by the elevated levels of intracellular cAMP resulting from the activity of either EdTx or cellular AC.

The fundamental importance of MAPK and AKT in the cell behavior suggested us to explore correlation between the lung epithelial cell signaling and the most important direct biological outcome of anthrax exposure: mortality. The information from the *in vitro* cell model provided a rationale for a highly effective post-exposure treatment strategy that targets host response through specific pro-survival pathways. The inhibitors we tested demonstrate a synergistic effect on survival in combination with a low dose of the current state-of-care antibiotic, ciprofloxacin. Instead of blocking the enzymatic activity of anthrax toxins, both the caspase inhibitor and the A3AR agonist are expected to modulate host cell inflammatory and apoptotic signaling. Although the specific mechanisms of animal protection and the predictive power of our *in vitro* model are far from being completely understood and warrant further analyses, we can conclude that in mice the interference with host cell response represents an important part of anthrax pathogenic strategy. Extending our

results to other animal models is necessary to confirm relevance of this conclusion to human exposure.

A paradigm where infectious disease pathogenesis is controlled by modulating host response represents an exciting approach to combating pathogenic organisms, including weaponized versions where agents such as anthrax are purposefully engineered to resist conventional anti-microbial therapies. Based on these findings, it seems intriguing to expand the application of the phosphoproteomic approach for signal pathway and molecular network analyses used here to other infectious agents.

Investigation of the TLR contribution in anthrax allowed identify the candidate bacterial agonist HSP60 capable of inducing a pro-inflammatory response, but overall the results of our experiments do not support the hypothesis that TLR stimulation plays a major role during anthrax infectious process.

References

[1] Pezard, C., Berche, P., and Mock, M. (1991) *Infect. Immun.* **59,** 3472-3477.
[2] Guidi-Rontani, C., Levy, M., Ohayon, H., and Mock, M. (2001) *Mol. Microbiol.* **42**, 931-938.
[3] Pellizzari, R., Guidi-Rontani, C., Vitale, G., Mock, M., and Montecucco, C. (1999) *FEBS Lett.* **462**, 199-204.
[4] Agrawal A., Lingappa, J., Leppla, S. H., Agrawa,l S., Jabbar, A., Quinn, C., and Pulendran, B. (2003) *Nature* **424**, 329-334.
[5] Pickering, A. K., Osorio, M., Lee, G. M., Grippe, V. K., Bray, M., and Merkel, T. J. (2004) *Infect. Immun.* **72**, 6382-6389.
[6] Popov, S. G., Popova, T. G., Grene, E., Klotz, F., Cardwell, J., Bradburne, C., Jama, Y., Maland, M., Wells, J., Nalca, A., Voss, T., Bailey, C., and Alibek, K. (2004) *Cell. Microbiol*. **6**, 225-233.
[7] Shoop, W.L., Xiong, Y., Wiltsie, J., Woods, A., Guo, J., Pivnichny, J. V., Felcetto, T., Michael, B. F., Bansal, A., Cummings, R. T., Cunningham, B. R., Friedlander, A. M., Douglas, C. M., Patel, S. B., Wisniewski, D., Scapin, G., Salowe, S. P., Zaller, D. M., Chapman, K. T., Scolnick, E. M., Schmatz, D. M., Bartizal, K., MacCoss, M., and Hermes, J. D. (2005) *Proc. Natl. Acad. Sci. USA* **102**, 7958-63.
[8] Turk, B. E., Wong, T.Y., Schwarzenbacher, R., Jarrell, E. T., Leppla, S. H., Collier, R. J., Liddington, R. C., and Cantley, L. C. (2004) *Nat. Struct. Mol. Biol.* **11**, 60-66.
[9] Jernigan, D. B., Raghunathan, P. L., Bell, B. P., Brechner, R., Bresnitz, E. A., Butler, J. C., Cetron, M., Cohen, M., Doyle, T., Fischer, M., Greene, C., Griffith, K. S., Guarner, J., Hadler, J. L., Hayslett, J. A., Meyer, R., Petersen, L. R., Phillips, M., Pinner, R., Popovic, T., Quinn, C. P., Reefhuis, J., Reissman, D., Rosenstein, N., Schuchat, A., Shieh, W. J., Siegal, L., Swerdlow, D. L., Tenover, F. C., Traeger, M., Ward, J. W., Weisfuse, I., Wiersma, S., Yeskey, K., Zaki, S., Ashford, D. A., Perkins, B. A., Ostroff, S., Hughes, J., Fleming, D., Koplan, J. P., and Gerberding, J. L. (2002) *Emerg. Infect. Dis*. **8**, 1019-1028.
[10] Popov, S. G., Popova, T. G., Hopkins, S., Weinstein, R. S., MacAfee, R., Fryxell, K. J., Chandhoke, V., Bailey, C., and Alibek, K. (2005) *BMC Infect. Dis*. **5**, 25-38.
[11] Harrington, D. J. (1996) *Infect. Immun*. **64**, 1885-1891.
[12] Miyoshi, S., and Shinoda, S. (2000) *Microbes Infect*. **2**, 91-98.
[13] Dinwiddie, R. (2000) *Respiration* **67**, 3-8.
[14] Lahteenmaki, K., Edelman, S., and Korhonen, T. K. (2005) *Trends Microbiol*. **13**, 79-85.
[15] Lahteenmaki, K., Virkola, R., Pouttu, R., Kuusela, P., Kukkonen, M., and Korhonen, T. K. (1995) *Infect. Immun*. **63**, 3659-3664.
[16] Park, P. W., Pier, G. B., Hinkes, M. T., and Bernfield, M. (2001) *Nature* **411**, 98-102.
[17] Park, P. W., Pier, G. B., Preston, M. J., Goldberger, O., Fitzgerald, M. L., and Bernfield, M. (2000) *J. Biol. Chem*. **275**, 3057-3064.
[18] Haynes, A. 3rd, Ruda, F., Oliver, J., Hamood, A. N., Griswold, J. A., Park, P. W., and Rumbaugh, K. P. (2005) *Infect. Immun*. **73**, 7914-7921.
[19] Marshall, L. J., Ramdin, L. S., Brooks, T., DPhil, P. C., and Shute, J. K. (2003) *J. Immunol*. **171**, 2057-2065.
[20] Elenius, V., Gotte, M., Reizes, O., Elenius, K., and Bernfield, M. (2004) *J. Biol. Chem.* **279**, 41928-4135.
[21] Wetmore, D. R., Wong, S. -L., and Roche, R. S. (1992) *Mol. Microbiol*. **6**, 1593-1604.
[22] Narasaki, R., Kuribayashi, H., Shimizu, K., Imamura, D., Sato, T., and Hasumi, K. (2005) *J. Biol. Chem.* **280**, 14278-14287.
[23] Bonventre, P. F., and Eckert, N. J. (1963) *J. Bacteriol*. **85**, 490-501.
[24] Abramova, F. A., Grinberg, L. M., Yampolskaya, O. V., and Walker, D. H. (1993) *Proc. Natl. Acad. Sci. USA* **90**, 2291-2294
[25] Chitlaru, T., Gat, O., Gozlan, Y., Ariel, N., and Shafferman, A. (2006) *J. Bacteriol*. **188**, 3551-3571.
[26] Read, T. D., Peterson, S. N., Tourasse, N., Baillie, L. W., Paulsen, I. T., Nelson, K. E., Tettelin, H., Fouts, D. E., Eisen, J. A., Gill, S. R., Holtzapple, E. K., Okstad, O. A., Helgason, E., Rilstone, J., Wu, M., Kolonay, J. F., Beanan, M. J., Dodson, R. J., Brinkac, L. M., Gwinn, M., DeBoy, R. T., Madpu, R., Daugherty, S. C., Durkin, A. S., Haft, D. H., Nelson, W. C., Peterson, J. D., Pop, M., Khouri, H. M., Radune, D., Benton, J. L., Mahamoud, Y., Jiang, L., Hance, I. R., Weidman, J. F., Berry, K. J., Plaut, R. D., Wolf, A. M., Watkins, K. L., Nierman, W. C., Hazen, A., Cline, R., Redmond, C., Thwaite, J. E., White, O., Salzberg, S. L., Thomason, B., Friedlander, A. M., Koehler, T. M., Hanna, P. C., Kolsto, A. B., and Fraser, C. M. (2003) *Nature* 423, 81-86.
[27] Charlton, S., Moir, A. J., Baillie, L., and Moir, A. (1999) *J. Appl. Microbiol.* **87**, 241-245.
[28] Cook, L., and Ternai, B. (1988) *Biochem Int*. **17**, 637-646.
[29] Hooper, N. M. (1994) *FEBS Lett*. **354**, 1-6.
[30] Barrett, A. J. (2004) *Curr. Opin. Drug Discov. Devel.* **7**, 334-341.
[31] Travis, J., Potempa, J., and Maeda, H. (1995) *Trends Microbiol*. **3**, 405-407.

[32] Borth, W. (1992*) FASEB J.* **6**, 3345-3353.
[33] Bernfield, M., Gotte, M., Park, P. W., Reizes, O., Fitzgerald, M. L., Lincecum, J., and Zako, M. (1999) *Annu. Rev. Biochem*. **68**, 729-777.
[34] Park, P. W., Foster, T. J., Nishi, E., Duncan, S. J., Klagsbrun, M., and Chen, Y. (2004) *J. Biol. Chem*. **279**, 251-258
[35] Arribas, J., and Borroto, A. (2002) *Chem. Rev.* **102**, 4627-4638
[36] Ralevic, V., and Burnstock, G. (1998) *Pharmacol. Rev*. **50**, 413-492.
[37] Zhang, Y. L., Keng, Y. F., Zhao, Y., Wu, L., and Zhang, Z. Y. (1998) *J. Biol. Chem*. **273**, 12281-12287.
[38] Stoker, A. W. (2005) *J. Endocrinol.* **185**, 19-33.
[39] McCain, D. F., Wu, L., Nickel, P., Kassack, M. U., Kreimeyer, A., Gagliardi, A., Collins, D. C., Zhang, Z. Y. (2004) *J. Biol. Chem*. **279**, 14713-14725.
[40] Subramanian, S. V., Fitzgerald, M. L., and Bernfield, M. (1997) *J. Biol. Chem*. **272**, 14713-14720.
[41] Zhang, L., David, G., and Esko, J. D. (1995) *J. Biol. Chem.* **270**, 27127-27135.
[42] Lamonica, J. M., Wagner, M., Eschenbrenner, M., Williams, L. E., Miller, T. L., Patra, G., and DelVecchio, V. G. (2005) *Infect. Immun*. **73**, 3646-58.
[43] Antelmann, H., Williams, R. C., Miethke, M., Wipat, A., Albrecht, D., Harwood, C. R., and Hecker, M. (2005) *Proteomics* **5**, 3684-3695.
[44] Aronson, A. I., Bell, C., and Fulroth, B. (2005) *J. Bacteriol.* **187**, 3133-3138.
[45] Guarner, J., Jernigan, J. A., Shieh, W. J., Tatti, K., Flannagan, L. M., Stephens, D. S., Popovic, T., Ashford, D. A., Perkins, B. A., and Zaki, S. R. (2003) *Am. J. Pathol.* **163**, 701-709.
[46] Warfel, J. M., Steele, A. D., and D'Agnillo, F. (2005) *Am. J. Pathol.* **166**, 1871-1881.
[47] Supuran, C. T., Casini, A., and Scozzafava, A. (2003) *Med. Res. Rev*. **23**, 535-558.
[48] Grinberg, L. M., Abramova, F. A., Yampolskaya, O. V., Walker, D. H., and Smith, J. H. (2001) *Mod. Pathol*. **14**, 482-495.
[49] Loy, J. A., Lin, X., Schenone, M., Castellino, F. J., Zhang, X. C., Tang, J. (2001) *Biochemistry* **40**, 14686-14695.
[50] Sun, H., Ringdahl, U., Homeister, J. W., Fay, W. P., Engleberg, N. C., Yang, A. Y., Rozek, L. S., Wang, X., Sjobring, U., and Ginsburg, D. (2004) *Science* **305**, 1283-1286.
[51] Li, Q., Park, P. W., Wilson, C. L., and Parks, W. C. (2002) *Cell* **111**, 635-646.
[52] Andrian, E., Grenier, D., and Rouabhia, M. (2006) *Oral Microbiol. Immunol*. **21**, 123-128.
[53] Wang, Z., Gotte, M., Bernfield,. M, and Reizes, O. (2005) *Biochemistry* **44**, 12355-12361.
[54] Schmidt, A., Echtermeyer, F., Alozie, A., Brands, K., and Buddecke, E. (2005) *J. Biol. Chem*. **280**, 34441-34446.
[55] Kainulainen, V., Wang, H., Schick, C., and Bernfield, M. (1998) *J. Biol. Chem*. **273**, 11563-11569.
[56] Schmidt A, Echtermeyer F, Alozie A, Brands K, Buddecke E. Plasmin- and thrombin-accelerated shedding of syndecan-4 ectodomain generates cleavage sites at Lys(114)-Arg(115) and Lys(129)-Val(130) bonds. J Biol Chem. 2005;280(41):34441-6.
[57] Ihrcke NS, Platt JL. Shedding of heparan sulfate proteoglycan by stimulated endothelial cells: evidence for proteolysis of cell-surface molecules. J Cell Physiol. 1996;168(3):625-37.
[58] Subramanian SV, Fitzgerald ML, Bernfield M. Regulated shedding of syndecan-1 and -4 ectodomains by thrombin and growth factor receptor activation. J Biol Chem. 1997;272(23):14713-20.
[59] Li L, Couse TL, Deleon H, Xu CP, Wilcox JN, Chaikof EL. Regulation of syndecan-4 expression with mechanical stress during the development of angioplasty-induced intimal thickening. J Vasc Surg. 2002;36(2):361-70.

[60] Xiao Z, Theroux P. Platelet activation with unfractionated heparin at therapeutic concentrations and comparisons with a low-molecular-weight heparin and with a direct thrombin inhibitor. Circulation. 1998; 97(3):251-6.
[61] Maita N, Nishio K, Nishimoto E, Matsui T, Shikamoto Y, Morita T, Sadler JE, Mizuno H. Crystal structure of von Willebrand factor A1 domain complexed with snake venom, bitiscetin: insight into glycoprotein Ibalpha binding mechanism induced by snake venom proteins. J Biol Chem. 2003;278(39):37777-81.
[62] Sporn LA, Shi RJ, Lawrence SO, Silverman DJ, Marder VJ. Rickettsia rickettsii infection of cultured endothelial cells induces release of large von Willebrand factor multimers from Weibel-Palade bodies. Blood. 1991; 78(10):2595-602.
[63] Teysseire N, Arnoux D, George F, Sampol J, Raoult D. von Willebrand factor release and thrombomodulin and tissue factor expression in Rickettsia conorii-infected endothelial cells. Infect Immun. 1992;60(10):4388-93.
[64] George F, Brouqui P, Boffa MC, Mutin M, Drancourt M, Brisson C, Raoult D, Sampol J. Demonstration of Rickettsia conorii-induced endothelial injury in vivo by measuring circulating endothelial cells, thrombomodulin, and von Willebrand factor in patients with Mediterranean spotted fever. Blood. 1993; 82(7):2109-16.
[65] Rao AK, Schapira M, Clements ML, Niewiarowski S, Budzynski AZ, Schmaier AH, Harpel PC, Blackwelder WC, Scherrer JR, Sobel E, et al. A prospective study of platelets and plasma proteolytic systems during the early stages of Rocky Mountain spotted fever. N Engl J Med. 1988;318(16):1021-8.

[66] Rahbar A, Soderberg-Naucler C. Human cytomegalovirus infection of endothelial cells triggers platelet adhesion and aggregation. J Virol. 2005;79(4):2211-20.
[67] Visser MR, Tracy PB, Vercellotti GM, Goodman JL, White JG, Jacob HS Enhanced thrombin generation and platelet binding on herpes simplex virus-infected endothelium. Proc Natl Acad Sci U S A. 1988; 85(21): 8227-30.
[68] Etingin OR, Silverstein RL, Hajjar DP. von Willebrand factor mediates platelet adhesion to virally infected endothelial cells. Proc Natl Acad Sci U S A. 1993; 90(11):5153-6.
[69] Franchini M. Thrombotic thrombocytopenic purpura: proposal of a new pathogenic mechanism involving Helicobacter pylori infection. Med Hypotheses. 2005;65(6):1128-31.
[70] Crawley TB, Lam JK, Rnce JB, Mollica LR, O'Donnel JS, and Lane DA. Proteolytic inactivation of ADAMTS13 by thrombin and plasmin. Blood. 2005; 105:1085-1093.
[71] Ono T, Mimuro J, Madoiwa S, Soejima K, Kashiwakura Y, Ishiwata A, Takano K, Ohmori T, Sakata Y. Severe secondary deficiency of von Willebrand factor-cleaving protease (ADAMTS13) in patients with sepsis-induced disseminated intravascular coagulation: its correlation with development of renal failure. Blood. 2006;107(2):528-34.
[72] Hunt BJ, Lammle B, Nevard CH, Haycock GB, Furlan M. von Willebrand factor-cleaving protease in childhood diarrhoea-associated haemolytic uraemic syndrome. Thromb Haemost. 2001; 85(6):975-8.
[73] Stearns-Kurosawa, D. J., Lupu, F., Taylor, F. B. Jr., Kinasewitz, G., and Kurosawa, S. 2006. *Am. J. Pathol.* 169, 433-444.
[74] Mina, B., Dym, J. P., Kuepper, F., Tso, R., Arrastia, C., Kaplounova, I., Faraj, H., Kwapniewski, A., Krol, C. M., Grosser, M., Glick, J., Fochios, S., Remolina, A., Vasovic, L., Moses, J., Robin, T., DeVita, M., and Tapper, M. L. 2002. *JAMA* 287, 858-862.
[75] Denis, C., Methia, N., Frenette, P. S., Rayburn, H., Ullman-Cullere, M., Hynes, R. O., and Wagner, D. D. 1998. *Proc. Natl. Acad. Sci. USA* **95**, 9524-9529.
[76] Banno, F., Kokame, K., Okuda, T., Honda, S., Miyata, S., Kato, H., Tomiyama, Y., and Miyata, T. 2006. *Blood* 107, 3161-3166.
[77] Tsai HM. Current concepts in thrombotic thrombocytopenic purpura. Annu Rev Med. 2006;57:419-36.
[78] Ono, T., Mimuro, J., Madoiwa, S., Soejima, K., Kashiwakura, Y., Ishiwata, A., Takano, K., Ohmori, T., and Sakata, Y. 2006. *Blood* 107, 528-534
[79] Culley, N. C., Pinson, D. M., Chakrabarty, A., Mayo, M. S., and Levine, S. M. 2005. *Infect. Immun.* 73, 7006-7010.
[80] Tsai, H. M. 1996. *Blood* 87, 4235-4244
[81] Ono, T., Mimuro, J., Madoiwa, S., Soejima, K., Kashiwakura, Y., Ishiwata, A., Takano, K., Ohmori, T., and Sakata, Y. 2006. *Blood* 107, 528-534
[82] Crawley, J. T., Lam, J. K., Rance, J. B., Mollica, L. R., O'Donnell, J. S., and Lane, D. A. 2005. *Blood* 105, 1085-1093.
[83] Denis, C., Methia, N., Frenette, P. S., Rayburn, H., Ullman-Cullere, M., Hynes, R. O., and Wagner, D. D. 1998. *Proc. Natl. Acad. Sci. USA* 95, 9524-9529.
[84] Galbusera, M., Benigni, A., Paris, S., Ruggenenti, P., Zoja, C., Rossi, C., and Remuzzi, G. 1999. *J. Am. Soc. Nephrol.* 10, 1234-1241.
[85] Bergmeier, W., Piffath, C. L., Goerge, T., Cifuni, S. M., Ruggeri, Z. M., Ware, J., and Wagner, D. D. 2006. *Proc. Natl. Acad. Sci. USA* 103, 16900-16905.
[86] Yang, H., Reheman, A., Chen, P., Zhu, G., Hynes, R. O., Freedman, J., Wagner, D. D., and Ni, H. 2006. *J. Thromb. Haemost.* 4, 2230-2237.
[87] Ni, H., Denis, C. V., Subbarao, S., Degen, J. L., Sato, T. N., Hynes, R. O., and Wagner, D. D. 2000. *J. Clin. Invest.* 106, 385-392.
[88] Aird W: Vascular bed specific hemostasis: role of endothelium in sepsis. *Crit Care Med* 2001, 29:S28-S24.
[89] Hack C, Zeerleder S: The endothelium in sepsis: source of and a target for inflammation. *Crit Care Med* 2001 29:S21-S27.
[90] Mavrommatis A, Theodoridis, T., Economou, M., Kotanidou, A., Ali, M., Christopoulou-Kokkinou, V., et al.: Activation of the fibrinolytic system and utilization of the coagulation inhibitors in sepsis: comparison with severe sepsis and septic shock. *Intensive Care Med* 2001(27):1853-1859.
[91] Riewald M, Ruf W: Role of coagulation protease cascades in sepsis. *Crit Care Med* 2003, 7(2):123-129.
[92] Roemisch J GE, Hoffmann JN, Wiedermann CJ.: Antithrombin: a new look at the actions of a serine protease inhibitor. *Blood Coagul Fibrinolysis* 2002, 13(8):657-670.
[93] Ten C: Thrombocytopenia: one of the markers of disseminated intravascular coagulation. *Pathophysiol Haemost Thromb* 2003, 33(5):413-416.
[94] Abramova F, Grinberg L, Yampolskaya O, Walker D: Pathology of inhalational anthrax in 42 cases from the Sverdlovsk outbreak of 1979. *Proc Natl Acad Sci* 1993, 90:2291-2294.

[95] Asakura H OM, Ontachi Y, Mizutani T, Omote M, Yoshida T, Kaneda M, Yamazaki M, Morishita E, Takami A, Miyamoto K, Nakao S.: Antithrombotic role of nitric oxide in rats under physiological conditions. *Thromb Haemost* 2004, 91(1):71-75.
[96] Schrecengost JE LR, Boyd JC, Moons KG, Gonias SL, Rose CE Jr, Bruns DE.: Comparison of diagnostic accuracies in outpatients and hospitalized patients of D-dimer testing for the evaluation of suspected pulmonary embolism. *Clin Chem* 2003, 49(9):1483-1490.
[97] Wiman B, Collen D: On the mechanism of the reaction between human alpha 2-antiplasmin and plasmin. *J Biol Chem* 1979, 254(18):9291-9297.
[98] Wiman B, Lijnen H, Collen D: On the specific interaction between the lysine-binding sites in plasmin and complementary sites in alpha2-antiplasmin and in fibrinogen. *Biochim Biophys Acta* 1979, 579(1):142-154.
[99] Blasi F, Vassalli J, Dano K: Urokinase-type plasminogen activator: proenzyme, receptor, and inhibitors. *J Cell Biol* 1987, 104(4):801-804.
[100] Paul R, Winkler F, Bayerlein I, Popp B, Pfister H, Koedel U: Urokinase-type plasminogen activator receptor regulates leukocyte recruitment during experimental pneumococcal meningitis. *J Infect Dis* 2005, 191(5):776-782.
[101] Robbie L, Dummer S, Booth N, Adey G, Bennett B: Plasminogen activator inhibitor 2 and urokinase-type plasminogen activator in plasma and leucocytes in patients with severe sepsis. *Br J Haematol* 2000, 109(2):342-348.
[102] Janciauskiene S, Nita I, Stevens T: Alpha1-antitrypsin, old dog, new tricks. Alpha1-antitrypsin exerts in vitro anti-inflammatory activity in human monocytes by elevating cAMP. *J Biol Chem* 2007, 282(12):8573-8582.
[103] Gettins PG OS: Use of fluorescence resonance energy transfer to study serpin-proteinase interactions. *Methods* 2004, 32(2):110-119.
[104] Mahadeva R, Stewart S, Bilton D, Lomas D: Alpha-1 antitrypsin deficiency alleles and severe cystic fibrosis lung disease. *Thorax* 1998, 53(12):1022-1024.
[105] Montes R, Paramo J, Angles-Cano E: Development and clinical application of a new ELISA assay to determine plasmin-alpha2-antiplasmin complexes in plasma. *Br J Haematol* 1996, 92:979-985.
[106] Lijnen H, De Cock F, Van Hoef B: Characterization of the interaction between plasminogen and staphylokinase. *Eur J Biochem* 1994, 224:143-149.
[107] Matsuno H, Ishisaki A, Nakajima K, Okada K, Ueshima S, Matsou O, Kozawa O: Lack of alpha2-antiplasmin promotes re-endothelialization via over-release of VEGF after vascular injury in mice. *Blood* 2003, 102(10):3621-3627.
[108] Zeerleder S, Schroeder V, Hack C, Kohler H, Wuillemin W: TAFI and PAI-1 levels in human sepsis. *Thromb Res* 2006, 118(2):205-212.
[109] Carmeliet P, Collen D: Gene manipulation and transfer of the plasminogen and coagulation system in mice. *Semin Thromb Hemost* 1996, 22:525-542.
[110] Bayes-Genis A, Guindo J, Oliver A: Elevated levels of plasmin-alpha2-antiplasmin complexes in unstable angina. *Thromb Haemost* 1999, 81:865-868.
[111] Bick R, Strauss J, Frenkel E: Thrombosis and hemorrhage in oncology patients. *Hematol Oncol Clin North Am* 1996, 10(4):875-907.
[112] Spero J, Lewis J, Hasiba U: Disseminated intravascular coagulation. Findings in 346 patients. *Thromb Haemost* 1980, 43(1):28-33.
[113] Jordan R, Kilpatrick J, Nelson R: Heparin promotes the inactivation of AT by neutrophil elastase. *Science* 1987, 14(237):777-779.
[114] Park P, Pier G, Hinkes M, Bernfield M: Exploitation of syndecan-1 shedding by Pseudomonas aeruginosa enhances virulence. *Nature* 2001, 411(6833):98-102.
[115] Park P, Foster T, Nishi E, Duncan S, Klagsbrun M, Chen Y: Activation of syndecan-1 ectodomain shedding by Staphylococcus aureus alpha-toxin and beta-toxin. *J Biol Chem* 2004, 279(1):251-258.
[116] Wiessmann G, Smolen J, Korchak H: Release of inflammatory mediators from stimulated neutrophils. *N Engl J Med* 1980 303:27-34.
[117] Fouret P, duBois R, Bernaudin J, Takahashi H, Ferrans V, Crystal R: Expression of the neutrophil elastase gene during hjman bone marrow cell differentiation. *J Exp Med* 1989, 169:833-845.
[118] Roemisch J GE, Hoffmann JN, Wiedermann CJ.: Antithrombin: a new look at the actions of a serine protease inhibitor. *Blood Coagul Fibrinolysis* 2002, 13(8):657-670.
[119] Holty JE, Bravata DM, Liu H, Olshen RA, McDonald KM, Owens DK. Systematic review: a century of inhalational anthrax cases from 1900 to 2005. Ann Intern Med. 2006 Feb 21;144(4):270-80.
[120] Inglesby TV, O'Toole T, Henderson DA, Bartlett JG, Ascher MS, Eitzen E, Friedlander AM, Gerberding J, Hauer J, Hughes J, McDade J, Osterholm MT, Parker G, Perl TM, Russell PK, Tonat K. Anthrax as a biological weapon, 2002: updated recommendations for management. JAMA. 2002 May 1;287(17):2236-52.
[121] Moayeri M, Leppla SH. The roles of anthrax toxin in pathogenesis. Curr Opin Microbiol. 2004 Feb;7(1):19-24.

[122] Shoop WL, Xiong Y, Wiltsie J, Woods A, Guo J, Pivnichny JV, Felcetto T, Michael BF, Bansal A, Cummings RT, Cunningham BR, Friedlander AM, Douglas CM, Patel SB, Wisniewski D, Scapin G, Salowe SP, Zaller DM, Chapman KT, Scolnick EM, Schmatz DM, Bartizal K, MacCoss M, Hermes JD. Anthrax lethal factor inhibition. Proc Natl Acad Sci U S A. 2005 May 31;102(22):7958-63.
[123] Popov SG, Popova TG, Hopkins S, Weinstein RS, MacAfee R, Fryxell KJ, Chandhoke V, Bailey C, Alibek K. Effective antiprotease-antibiotic treatment of experimental anthrax. BMC Infect Dis. 2005 Apr 8;5(1):25.
[124] Vancurik J. Causes of the failure of antibiotic prophylaxis of inhalation anthrax and clearance of the spores from the lungs. Folia Microbial (Praha). 1966; 11(6): 459-64.
[125] Wulfkuhle JD, Edmiston KH, Liotta LA, Petricoin EF 3rd. Technology Insight: pharmacoproteomics for cancer--promises of patient-tailored medicine using protein microarrays. Nat Clin Pract Oncol. 2006 May;3(5):256-68.
[126] Tucker AE, Salles II, Voth DE, Ortiz-Leduc W, Wang H, Dozmorov I, Centola M, Ballard JD. Decreased glycogen synthase kinase 3-beta levels and related physiological changes in Bacillus anthracis lethal toxin-treated macrophages. Cell Microbiol. 2003 Aug;5(8):523-32.
[127] Bergman NH, Passalacqua KD, Gaspard R, Shetron-Rama LM, Quackenbush J, Hanna PC. Murine macrophage transcriptional responses to Bacillus anthracis infection and intoxication. Infect Immun. 2005 Feb;73(2):1069-80.
[128] Comer JE, Galindo CL, Zhang F, Wenglikowski AM, Bush KL, Garner HR, Peterson JW, Chopra AK. Murine macrophage transcriptional and functional responses to Bacillus anthracis edema toxin. Microb Pathog. 2006 Jul 15; [Epub ahead of print]
[129] Comer JE, Chopra AK, Peterson JW, Konig R. Direct inhibition of T-lymphocyte activation by anthrax toxins in vivo. Infect Immun. 2005 Dec;73(12):8275-81.
[130] Comer JE, Galindo CL, Chopra AK, Peterson JW. GeneChip analyses of global transcriptional responses of murine macrophages to the lethal toxin of Bacillus anthracis. Infect Immun. 2005 Mar;73(3):1879-85.
[131] Brazil DP, Park J, Hemmings BA. Getting in on the Akt Cell. 2002 Nov 1;111(3):293-303.
[132] Datta SR, Brunet A, Greenberg ME. Cellular survival: a play in three Akts. Genes Dev. 1999 Nov 15;13(22):2905-27.
[133] Wesche DE, Lomas-Neira JL, Perl M, Chung CS, Ayala A. Leukocyte apoptosis and its significance in sepsis and shock. J Leukoc Biol. 2005 Aug;78(2):325-37.
[134] Franke TF, Hornik CP, Segev L, Shostak GA, Sugimoto C. PI3K/Akt and apoptosis: size matters. Oncogene. 2003 Dec 8;22(56):8983-98.
[135] Duesbery NS, Vande Woude GF. Anthrax lethal factor causes proteolytic inactivation of mitogen-activated protein kinase kinase. J Appl Microbiol. 1999 Aug;87(2):289-93.
[136] Pellizzari R, Guidi-Rontani C, Vitale G, Mock M, Montecucco C. Lethal factor of Bacillus anthracis cleaves the N-terminus of MAPKKs: analysis of the intracellular consequences in macrophages.Int J Med Microbiol. 2000 Oct;290(4-5):421-7.
[137] Popov SG, Villasmil R, Bernardi J, Grene E, Cardwell J, Wu A, Alibek D, Bailey C, Alibek K. Lethal toxin of Bacillus anthracis causes apoptosis of macrophages. Biochem Biophys Res Commun. 2002 Apr 26;293(1):349-55.
[138] Park JM, Greten FR, Li ZW, Karin M. Science. 2002 Sep 20;297(5589):2048-51. Macrophage apoptosis by anthrax lethal factor through p38 MAP kinase inhibition.
[139] Wang L, Liu F, Adamo ML. Cyclic AMP inhibits extracellular signal-regulated kinase and phosphatidylinositol 3-kinase/Akt pathways by inhibiting Rap1. J Biol Chem. 2001 Oct 5;276(40):37242-9.
[140] Liu L, Xie Y, Lou L. Cyclic AMP inhibition of proliferation of hepatocellular carcinoma cells is mediated by Akt. Cancer Biol Ther. 2005 Nov;4(11):1240-7.
[141] Singh K, Xiao L, Remondino A, Sawyer DB, Colucci WS. Adrenergic regulation of cardiac myocyte apoptosis. J Cell Physiol. 2001 Dec;189(3):257-65.
[142] Williams RP, Hill HR, Hawkins D, Chao K-C, Neuenschwander J, Lipscomb HS. Epinephrinelike activity of culture filtrate from Bacillus anthracis. Fed Proc. 1967; 26(5):1545-48.
[143] Smith H, Keppie J, Stanley JL. The chemical basis of the virulence of Bacillus anthracis. V. The specific toxin produced by B. anthracis in vivo. Br J Exp Pathol. 1955 Oct;36(5):460-72.
[144] Popov SG, Popova TG, Grene E, Klotz F, Cardwell J, Bradburne C, Jama Y, Maland M, Wells J, Nalca A, Voss T, Bailey C, Alibek K. Systemic cytokine response in murine anthrax. Cell Microbiol. 2004 Mar;6(3):225-33.
[145] Monack D, Falkow S. Apoptosis as a common bacterial virulence strategy. Int J Med Microbiol. 2000 Mar;290(1):7-13.
[146] Restifo NP. Building better vaccines: how apoptotic cell death can induce inflammation and activate innate and adaptive immunity. Curr Opin Immunol. 2000 Oct;12(5):597-603.
[147] Park SS, Zhao H, Jang Y, Mueller RA, Xu Z. N6-(3-Iodobenzyl)-adenosine-5'-N-methylcarboxamide confers cardioprotection at reperfusion by inhibiting mitochondrial permeability transition pore opening via glycogen synthase kinase 3beta. J Pharmacol Exp Ther. 2006 Jul;318(1):124-31.

[148] Matot I, Weiniger CF, Zeira E, Galun E, Joshi BV, Jacobson KA. A3 adenosine receptors and mitogen-activated protein kinases in lung injury following in vivo reperfusion. Crit Care. 2006 Apr 19;10(2):R65 [Epub ahead of print].
[149] Panjehpour M, Karami-Tehrani F. An adenosine analog (IB-MECA) inhibits anchorage-dependent cell growth of various human breast cancer cell lines. Int J Biochem Cell Biol. 2004 Aug;36(8):1502-9.
[150] Hasko G, Nemeth ZH, Vizi ES, Salzman AL and Szabo C. An agonist of adenosine A3 receptors decreases interleukin-12 and interferon-gamma production and prevents lethality in endotoxemic mice. Eur J Pharmacol. 1998;358:261-68.
[151] Mabley J, Soriano F, Pacher P, Hasko G, Marton A, Wallace R, Salzman A and Szabo C. The adenosine A3 receptor agonist, N6-(3-iodobenzyl)-adenosine-5'-N-methyluronamide, is protective in two murine models of colitis. Eur J Pharmacol.2003;466: 323-29.
[152] Lee H, Kim M, Joo JD, Gallos G, Chen JF, Emala CW. A3 Adenosine Receptor Activation Decreases Mortality, Renal and Hepatic Injury in Murine Septic Peritonitis. Am J Physiol Regul Integr Comp Physiol. 2006 May 25; [Epub ahead of print]
[153] Comer JE, Chopra AK, Peterson JW, Konig R Infect Immun. Direct inhibition of T-lymphocyte activation by anthrax toxins in vivo. 2005 Dec;73(12):8275-81.
[154] Eckert N, Bonventre P. In vivo effects of Bacillus anthracis culture filtrates
[155] Slein MW, Logan GF Jr. Mechanism of action of the toxin of Bacillus anthracis. I. Effect in vivo on some blood serum components. J Bacteriol. 1960 Jul;80:77-85.
[156] Remmele NS, Klein F, Vick JA, Walker JS, Mahlandt BG, Lincoln RE. Anthrax toxin: primary site of action. J Infect Dis. 1968 Feb;118(1):104-13.
[157] van Nieuw Amerongen GP, van Hinsbergh VW. Targets for pharmacological intervention of endothelial hyperpermeability and barrier function. Vascul Pharmacol. 2002 Nov;39(4-5):257-72.
[158] Zhu WZ, Zheng M, Koch WJ, Lefkowitz RJ, Kobilka BK, Xiao RP. Dual modulation of cell survival and cell death by beta(2)-adrenergic signaling in adult mouse cardiac myocytes. Proc Natl Acad Sci U S A. 2001 Feb 13;98(4):1607-12.
[159] Communal C, Colucci WS, Singh K. p38 mitogen-activated protein kinase pathway protects adult rat ventricular myocytes against beta -adrenergic receptor-stimulated apoptosis. Evidence for Gi-dependent activation. J Biol Chem. 2000 Jun 23;275(25):19395-400.
[160] Ariel N, Zvi A, Makarova KS, Chitlaru T, Elhanany E, Velan B, Cohen S, Friedlander AM, Shafferman A. Genome-based bioinformatic selection of chromosomal Bacillus anthracis putative vaccine candidates coupled with proteomic identification of surface-associated antigens. Infect Immun. 2003 Aug;71(8):4563-79.
[161] Mikshis NI, Korsakova AIu, Bolotnikova MF, Novikova LV, Popov IuA. [Role of the components of the S-layer in immunogenicity of Bacillus anthracis][Article in Russian] Zh Mikrobiol Epidemiol Immunobiol. 2006 Jan-Feb;(1):29-32.
[162] Ohashi K, Burkart V, Flohe S, Kolb H. Cutting edge: heat shock protein 60 is a putative endogenous ligand of the toll-like receptor-4 complex. J Immunol. 2000 Jan 15;164(2):558-61.
[163] Kishimoto M, Yoshimura A, Naito M, Okamoto K, Yamamoto K, Golenbock DT, Hara Y, Nakayama K. Gingipains inactivate a cell surface ligand on Porphyromonas gingivalis that induces TLR2-and TLR4-independent signaling. Microbiol Immunol. 2006;50(4):315-25.
[164] Da Costa CU, Wantia N, Kirschning CJ, Busch DH, Rodriguez N, Wagner H, Miethke T. Heat shock protein 60 from Chlamydia pneumoniae elicits an unusual set of inflammatory responses via Toll-like receptor 2 and 4 in vivo. Eur J Immunol. 2004 Oct;34(10):2874-84.
[165] Argueta JG, Shiota S, Yamaguchi N, Masuhiro Y, Hanazawa S. Induction of Porphyromonas gingivalis GroEL signaling via binding to Toll-like receptors 2 and 4. Oral Microbiol Immunol. 2006 Aug;21(4):245-51.
[166] Park JM, Greten FR, Li ZW, Karin M. Macrophage apoptosis by anthrax lethal factor through p38 MAP kinase inhibition. Science. 2002 Sep 20;297(5589):2048-51.
[167] Park JM, Greten FR, Wong A, Westrick RJ, Arthur JS, Otsu K, Hoffmann A, Montminy M, Karin M. Signaling pathways and genes that inhibit pathogen-induced macrophage apoptosis--CREB and NF-kappaB as key regulators. Immunity. 2005 Sep;23(3):319-29.
[168] Pezard C, Berche P, Mock M. Contribution of individual toxin components to virulence of *Bacillus anthracis*. Infect Immun. 1991 Oct;59(10):3472-7
[169] Vitale G, Pellizzari R, Recchi C, Napolitani G, Mock M, Montecucco C. Anthrax lethal factor cleaves the N-terminus of MAPKKs and induces tyrosine/threonine phosphorylation of MAPKs in cultured macrophages. Biochem Biophys Res Commun. 1998 Jul 30;248(3):706-11
[170] Duesbery NS, Webb CP, Leppla SH, Gordon VM, Klimpel KR, Copeland TD, Ahn NG, Oskarsson MK, Fukasawa K, Paull KD, Vande Woude GF. Proteolytic inactivation of MAP-kinase-kinase by anthrax lethal factor. Science. 1998 May 1;280(5364):734-7
[171] Guidi-Rontani C, Levy M, Ohayon H, Mock M. Fate of germinated *Bacillus anthracis* spores in primary murine macrophages. Mol Microbiol. 2001 Nov;42(4):931-8

[172] Dixon TC, Fadl AA, Koehler TM, Swanson JA, Hanna PC. Early *Bacillus anthracis*-macrophage interactions: intracellular survival survival and escape. Cell Microbiol. 2000 Dec;2(6):453-63
[173] Dixon TC, Meselson M, Guillemin J, Hanna PC. Anthrax. N Engl J Med. 1999 Sep 9;341(11):815-26. Review
[174] Lyons CR, Lovchik J, Hutt J, Lipscomb MF, Wang E, Heninger S, Berliba L, Garrison K. Murine model of pulmonary anthrax: kinetics of dissemination, histopathology, and mouse strain susceptibility. Infect Immun. 2004 Aug;72(8):4801-9
[175] Pickering AK, Osorio M, Lee GM, Grippe VK, Bray M, Merkel TJ. Cytokine response to infection with *Bacillus anthracis* spores. Infect Immun. 2004 Nov;72(11):6382-9
[176] Friedlander, AM. Macrophages are sensitive to anthrax lethal toxin through an acid-dependent process. J Biol Chem 1986; 29: 7123–7126
[177] Welkos SL, Keener TJ, Gibbs PH. Differences in susceptibility of inbred mice to *Bacillus anthracis*. Infect Immun. 1986 Mar;51(3):795-800
[178] Popov SG, Villasmil R, Bernardi J, Grene E, Cardwell J, Wu A, Alibek D, Bailey C, Alibek K. Lethal toxin of *Bacillus anthracis* causes apoptosis of macrophages. Biochem Biophys Res Commun. 2002 Apr 26;293(1):349-55
[179] Popov SG, Villasmil R, Bernardi J, Grene E, Cardwell J, Wu A, Alibek D, Bailey C, Alibek K. Effect of *Bacillus anthracis* lethal toxin on human peripheral blood mononuclear cells. FEBS Letters 2002 527:211-15.

[180] Erwin JL, DaSilva LM, Bavari S, Little SF, Friedlander AM, Chanh TC. Macrophage-derived cell lines do not express proinflammatory cytokines after exposure to *Bacillus anthracis* lethal toxin. Infect Immun. 2001 Feb;69(2):1175-7
[181] Park JK, Chung YM, Kang S, Kim JU, Kim YT, Kim HJ, Kim YH, Kim JS, Yoo YD. c-Myc exerts a protective function through ornithine decarboxylase against cellular insults. Mol Pharmacol. 2002 Dec;62(6):1400-8
[182] Kassam A, Der SD, Mogridge J. Differentiation of human monocytic cell lines confers susceptibility to *Bacillus anthracis* lethal toxin. Cell Microbiol. 2005 Feb;7(2):281-92
[183] Nau GJ, Richmond JF, Schlesinger A, Jennings EG, Lander ES, Young RA. Human macrophage activation programs induced by bacterial pathogens. Proc Natl Acad Sci U S A. 2002 Feb 5;99(3):1503-8
[184] Boldrick JC, Alizadeh AA, Diehn M, Dudoit S, Liu CL, Belcher CE, Botstein D, Staudt LM, Brown PO, Relman DA.Stereotyped and specific gene expression programs in human innate immune responses to bacteria. Proc Natl Acad Sci U S A. 2002 Jan 22;99(2):972-7
[185] Alileche A, Squires RC, Muehlbauer SM, Lisanti MP, Brojatsch J. Mitochondrial Impairment is a Critical Event in Anthrax Lethal Toxin-Induced Cytolysis of Murine Macrophages. Cell Cycle. 2006 Jan;5(1):100-6
[186] Bergman NH, Passalacqua KD, Gaspard R, Shetron-Rama LM, Quackenbush J, Hanna PC. Murine macrophage transcriptional responses to *Bacillus anthracis* infection and intoxication. Infect Immun. 2005 Feb;73(2):1069-80
[187] Tucker AE, Salles II, Voth DE, Ortiz-Leduc W, Wang H, Dozmorov I, Centola M, Ballard JD. Decreased glycogen synthase kinase 3-beta levels and related physiological changes in Bacillus anthracis lethal toxin-treated macrophages. Cell Microbiol. 2003 Aug;5(8):523-32.
[188] Karin M, Lin A. NF-kappaB at the crossroads of life and death. Nat Immunol. 2002 Mar;3(3):221-7
[189] Moayeri M, Haines D, Young HA, Leppla SH. *Bacillus anthracis* lethal toxin induces TNF-alpha-independent hypoxia-mediated toxicity in mice. J Clin Invest. 2003 Sep;112(5):670-82
[190] Hanna PC, Acosta D, Collier RJ. On the role of macrophages in anthrax. Proc Natl Acad Sci U S A. 1993 Nov 1;90(21):10198-201
[191] Brieland, J. K., D. G. Remick, P. T. Freeman, M. C. Hurley, J. C. Fantone, N. C. Engleberg. In vivo regulation of replicative Legionella pneumophila lung infection by endogenous tumor necrosis factor and nitric oxide. Infect. Immun. 1995; 63:3253
[192] Hengartner MO. The biochemistry of apoptosis. Nature. 2000 Oct 12;407(6805):770-6
[193] Kim SO, Jing Q, Hoebe K, Beutler B, Duesbery NS, Han J. Sensitizing anthrax lethal toxin-resistant macrophages to lethal toxin-induced killing by tumor necrosis factor-alpha. J Biol Chem. 2003 Feb 28;278(9):7413-21
[194] Balcewicz-Sablinska MK, Keane J, Kornfeld H, Remold HG. Pathogenic *Mycobacterium tuberculosis* evades apoptosis of host macrophages by release of TNF-R2, resulting in inactivation of TNF-alpha. J Immunol. 1998 Sep 1;161(5):2636-41
[195] Allen HL, Deepe GS Jr. Apoptosis modulates protective immunity to the pathogenic fungus *Histoplasma capsulatum*. J Clin Invest. 2005 Oct;115(10):2875-85
[196] Saez-Lopez C, Ngambe-Tourere E, Rosenzwajg M, Petit JC, Nicolas JC, Gozlan J. Immediate-early antigen expression and modulation of apoptosis after in vitro infection of polymorphonuclear leukocytes by human cytomegalovirus. Microbes Infect. 2005 Jul;7(9-10):1139-49
[197] Matsuzawa A and Ichijo H. Molecular Mechanisms of the Decision between Life and Death: Regulation of Apoptosis by Apoptosis Signal-Regulating Kinase 1. J. Biochem. (Tokyo) 2001; 130: 1 - 8

[198] Popova, T. G., Millis, B., Bradburne, C., Nazarenko, S., Bailey, C., Chandhoke, V., and Popov, S. G. (2006) *BMC Microbiol.* **6**, 8-23.
[199] Shevchenko, A., Jensen, O. N., Podtelejnikov, A. V., Sagliocco, F., Wilm, M., Vorm, O., Mortensen, P., Shevchenko, A., Boucherie, H., and Mann, M. (1996) *Proc. Natl. Acad. Sci. USA* **93**, 14440-14445.
[200] Yates, J. R. 3rd, Eng, J. K., McCormack, A. L., and Schieltz, D. (1995) *Anal. Chem.* **67**, 1426-1436.

Tables and Fifures

Table 1. Effect of protease inhibitors on Npr599 and InhA activity. Protease activity was determined using a fluorescein-labeled casein substrate as described in Materials and Methods. Control protease activity corresponds to 100% activity in the absence of inhibitor. Values represent averages of determinations and standard deviations (±) of three replicates.

Inhibitor	Concentration (mM)	Remaining activity (%) Npr599	InhA	Typical specificity aga type of proteases:
Control	-	100	100	
	10	6 ± 0.3	28 ± 5.0	
EDTA	1	9 ± 0.8	29 ± 1.4	Metallo
	0.1	10 ± 1.1	33 ± 8.0	
	10	0 ± 0.0	0 ± 0.0	
1,10-phenanth	1	3 ± 0.0	0 ± 0.0	Metallo
	0.1	55 ± 4.8	34 ± 13.8	
	5	1 ± 0.2	45 ± 1.5	
Phosphoramidon	0.5	2 ± 0.5	80 ± 0.8	Metallo
	0.05	12 ± 0.6	87 ± 1.6	
	1.28	0 ± 0.0	70 ± 1.5	
Galardin	0.128	12 ± 0.8	104 ± 1.3	Metallo
	0.0128	37 ± 0.8	103 ± 3.2	
	10	88 ± 10.2	111 ± 10.7	
PMSF	1	100 ± 5.4	110 ± 8.5	Serine
	0.1	97 ± 2.3	95 ± 2.2	
	10	95 ± 5.1	75 ± 5.9	
Leupeptin	1	106 ± 3.2	105 ± 2.8	Serine
	0.1	106 ± 2.6	111 ± 3.5	
	5	68 ± 2.2	32 ± 0.9	
Pepstatin A	0.5	75 ± 2.9	86 ± 3.1	Acid (carboxylic)
	0.05	78 ± 0.5	88 ± 4.7	
	5	74 ± 0.5	59 ± 1.8	
E-64	0.5	76 ± 0.1	78 ± 7.5	Thiol (cysteine)
	0.05	80 ± 3.9	84 ± 0.4	
	0.35	21 ± 0.6	15 ± 1.8	
SDS	0.035	87 ± 17.2	78 ± 7.5	Surfactant
	0.0035	243 ± 5.8	84 ± 0.4	
L-Cysteine	10	0 ± 0.0	0 ± 0.0	
	1	108 ± 6.8	100 ± 2.7	Cysteine
	0.1	119 ± 4.1	116 ± 1.1	
β-Mercaptoethanol	10	85 ± 11.8	86 ± 13.3	
	1	133 ± 7.6	106 ± 8.0	Sulfohydryl
	0.1	121 ± 6.6	113 ± 9.4	
Dithiothreitol	10	35 ± 2.7	15 ± 3.5	
	1	84 ± 2.8	65 ± 8.7	Sulfohydryl
	0.1	123 ± 1.2	115 ± 11.3	

Table 2. Effect of divalent ions on Npr599 and InhA activity. Protease activity and value representation were exerted the same as described in Table 1.

Divalent ion	Concentration (mM)	Remaining activity (%) Npr599	InhA
Control		100	100
Ca^{2+}	1	86 ± 1.5	91 ± 5.2
	0.1	97 ± 1.4	94 ± 3.5
Cu^{2+}	1	0 ± 0.0	0 ± 0.0
	0.1	1 ± 1.0	0 ± 0.0
Fe^{2+}	1	0 ± 0.3	0 ± 0.0
	0.1	63 ± 1.8	48 ± 5.2
Mg^{2+}	1	83 ± 2.8	76 ± 6.1
	0.1	97 ± 1.4	97 ± 1.7
Mn^{2+}	1	79 ± 0.2	103 ± 2.5
	0.1	96 ± 4.3	91 ± 5.1
Ni^{2+}	1	46 ± 1.4	45 ± 3.4
	0.1	77 ± 1.4	69 ± 1.3
Zn^{2+}	1	21 ± 0.7	0 ± 0.0
	0.1	78 ± 2.3	51 ± 6.2

Table 3. Kinetic parameters for hydrolysis of synthetic collagenase substrates by Npr599 and InhA.

Substrates	K_m μM	k_{cat} s^{-1}	k_{cat}/K_m $s^{-1}M^{-1}$
Npr599			
Mca-Pro-Leu-Ala-Nva-(DNP)Dpa-Ala-Arg-NH_2 [a]	1.1 ± 0.26	0.2 ± 0.09	0.1 ± 0.04
Mca-Glu-Val-Lys-Met-Asp-Ala-Glu-Phe-(DNP)Lys-OH [a]	0.3 ± 0.02	0.1 ± 0.04	0.4 ± 0.16
Mca-Pro-Leu-Gly-Leu-(DNP)Ala-Ala-Arg-NH_2 [a]	7.0 ± 0.72	1.8 ± 0.66	0.3 ± 0.12
FALGPA[b]	ND[c]	ND[c]	-
DQ-gelatin	0.1 ± 0.02	4.5 ± 0.32	46.6 ± 9.41
InhA			
Mca-Pro-Leu-Ala-Nva-(DNP)Dpa-Ala-Arg-NH_2 [a]	6.7 ± 1.05	54.5 ± 4.41	8.3 ± 1.10
Mca-Glu-Val-Lys-Met-Asp-Ala-Glu-Phe-(DNP)Lys-OH [a]	4.0 ± 0.25	17.5 ± 1.93	4.3 ± 0.38
Mca-Pro-Leu-Gly-Leu-(DNP)Ala-Ala-Arg-NH_2 [a]	11.3 ± 1.28	52.5 ± 6.49	4.6 ± 0.09
FALGPA[b]	ND[c]	ND[c]	-
DQ-gelatin	0.3 ± 0.02	51.2 ± 6.33	190.9 ± 27.91

[a] Mca, 7-methoxycoumarin-4-acetyl; DNP, 2,4-dinitrophenyl; Dpa, L-diaminopropionyl; Nva, L-norvaline.
[b] FALGPA, N-(3-[2-furyl]acryloyl)-Leu-Gly-Pro-Ala.
[c] ND, not detectable.

Table 4. Comparison of kinetic parameters for FRETS-VWF73 proteolysis by Npr599, InhA and ADAMTS13.

Protease	K_m μM	k_{cat} min^{-1}	k_{cat}/K_m μM^{-1} min^{-1}	Ref.
Npr599	1.4 ± 0.5	18.8 ± 4.9	13.6 ± 1.4	This study
InhA	3.9 ± 0.4	1057.4 ± 103.2	274.5 ± 1.9	This study
ADAMTS13	3.2 ± 1.1	~ 58	18	*JBC* **281**, 850 (2006)

Table 5. Identification of Proteins by mass spectrometry

Proteins identified from band **1**

	Protein	Probability	MW	Peptide Hits
1	SLAP1_BACAN S-layer protein sap precursor (Surface l	7.33E-14	86567.9	25
2	Q81S57_BACAN N-acetylmuramoyl-L-alanine amidase, fami	7.57E-05	45323.6	1
3	Q81KY5_BACAN DNA polymerase III, alpha subunit.	6.91E-04	126641.8	1
4	Q81KR1_BACAN Catabolite control protein A.	9.32E-04	36861.9	1

Proteins identified from band **2**

	Protein	Probability	MW	Peptide Hits
1	CH60_BACAN 60 kDa chaperonin (Protein Cpn60) (groEL	4.43E-11	57396.2	8
2	SLAP1_BACAN S-layer protein sap precursor (Surface l	1.34E-07	86567.9	6
3	SLAP2_BACAN S-layer protein EA1 precursor.	1.05E-04	91306.7	1
4	Q81M66_BACAN Leucine dehydrogenase.	3.08E-04	39826.2	1

Proteins identified from band **3**

	Protein	Probability	MW	Peptide Hits
1	SLAP1_BACAN S-layer protein sap precursor (Surface l	1.46E-07	86567.9	7
2	CH60_BACAN 60 kDa chaperonin (Protein Cpn60) (groEL	2.91E-04	57396.2	1
3	Q81M66_BACAN Leucine dehydrogenase.	3.27E-04	39826.2	1

Proteins identified from band **4**

	Protein	Probability	MW	Peptide Hits
1	Q81L19_BACAN Peptidase, M42 family.	1.11E-14	39556.4	3
2	Q81M66_BACAN Leucine dehydrogenase.	2.00E-14	39826.2	14
3	Q81UH5_BACAN Peptidase, family M20/M25/M40 protein.	1.05E-13	38839.6	8
4	Q81KW3_BACAN Alanine dehydrogenase.	3.26E-10	40083.9	4
5	Q81KP6_BACAN Peptidase, M42 family.	2.55E-07	39130.0	1
6	SLAP2_BACAN S-layer protein EA1 precursor.	5.17E-06	91306.7	1
7	SLAP1_BACAN S-layer protein sap precursor (Surface l	1.70E-05	86567.9	2
8	CH60_BACAN 60 kDa chaperonin (Protein Cpn60) (groEL	2.16E-05	57396.2	3
9	Q81Y22_BACAN N-acetylmuramoyl-L-alanine amidase, fami	1.82E-04	64005.1	1

Table 6. Hemostatic parameters of Sterne spore challenged mouse plasma

	Control	Day 1	Day 2	Day 3
D-dimer	100.0 ± 35.3	1261.9 ± 397.1	1411.1 ± 474.0	830.1 ± 613.6
α1-PI	100.0 ± 30.88	142.67 ± 16.64	108.63 ± 54.84	70.77 ± 15.33
PAI-1	100.0 ± 39.26	299.08 ± 55.36	328.70 ± 212.82	300.18 ± 92.66
PAI-2	100.0 ± 36.42	125.63 ± 18.49	156.87 ± 26.16	181.12 ± 36.59
tPA	100.0 ± 22.75	106.66 ± 8.82	114.67 ± 8.79	95.64 ± 28.85
uPA	100.0 ± 21.0	96.9 ± 6.2	129.9 ± 64.8	91.2 ± 18.8
TAT	100.0 ± 74.71	65.72 ± 45.68	121.12 ± 49.85	231.56 ± 108.73
PAP	100.0 ± 14.5	111.55 ± 38.60	101.17 ± 19.58	138.82 ± 70.16
α_2-PI	100.0 ± 1.6	92.9 ± 1.7	89.6 ± 1.7	91.3 ± 5.1

Values are % to control.

Table 7. Hemostatic parameters of □-Sterne spore challenged mouse plasma

	Control	Day 1	Day 2	Day 3
D-dimer	100.0 ± 35.3	1001.5 ± 431.5	1187.3 ± 470.5	985.7 ± 179.3
α1-PI	100.0 ± 30.88	151.01 ± 26.62	66.82 ± 33.06	111.71 ± 44.93
PAI-1	100.0 ± 39.26	151.0 ± 25.58	350.27 ± 141.68	180.25 ± 34.94
PAI-2	100.0 ± 36.42	112.12 ± 55.25	114.56 ± 15.3	150.5 ± 49.7
tPA	100.0 ± 22.75	92.64 ± 14.08	110.92 ± 39.55	148.98 ± 72.62
uPA	100.0 ± 21.0	100.5 ± 7.8	92.3 ± 12.9	85.9 ± 38.9
TAT	100.0 ± 74.71	116.46 ± 104.96	70.89 ± 24.26	203.20 ± 57.86
PAP	100.0 ± 14.5	82.76 ± 29.37	126.0 ± 54.99	168.39 ± 40.93
α_2-PI	100.0 ± 1.6	95.0 ± 2.5	95.1 ± 0.7	92.7 ± 1.5

Values are % to control.

ELISA values are calculated as a percent to control. D-dimer products (D-dimer): Alpha1-protease inhibitor (α_1-PI); plasminogen activator inhibitor-1 and -2 (PAI-1 and 2); tissue-type plasminogen activator (t-PA); urokinase-type plasminogen activator (uPA); thrombin-antithrombin complex (TAT); plasmin-antiplasmin complex (PAP); anti-plasmin (AP).

Table 8. ANOVA comparison of genes induced in THP-1 monocytes by different strains under the same MOI and timepoint conditions.

A. Apoptotic genes

Accession	Name	Description	2 h 1:1 MOI	2 h 1:10 MOI	4 h 1:1 MOI	4 h 1:10 MOI
XM_034567	CCND2	cyclin D2	0.1833	0.3083	0.5300	0.2267
NM_033379	CDC2	cell division cycle 2, G1 to S and G2 to M	0.0250	0.1783	0.4483	0.5400
NM_002357	MAD	MAX dimerization protein 1	0.0150	-0.0433	-0.8050	-0.7250
XM_037657	MYC	v-myc myelocytomatosis viral oncogene homolog (avian)	0.1233	0.1783	0.6903	0.5983
NM_004725	BUB3	BUB3 budding uninhibited by benzimidazoles 3 homolog (yeast)	-0.0500	0.1467	0.4910	0.5767
XM_034725	NRP1	neuropilin 1	-0.0317	0.1583	0.2967	0.5467
XM_008679	TP53	tumor protein p53	0.6183	0.2167	0.6810	-0.1967
NM_005620	S100A11	S100 calcium binding protein A11 (calgizzarin)	0.1667	0.2750	0.4893	0.2567
NM_004705	PRKRIR	protein-kinase, interferon-inducible double stranded RNA dependent inhibitor, (P58 repressor)	0.0033	-0.0567	0.0303	0.0817

B. Cell cycle genes

Accession	Name	Description	2 h 1:1 MOI	2 h 1:10 MOI	4 h 1:1 MOI	4 h 1:10 MOI
NM_004040	ARHB	ras homolog gene family, B	-0.1783	0.0233	-1.7523	-1.5083
NM_002089	CXCL2	chemokine (C-X-C motif) ligand 2	-0.2850	-0.9700	-2.3083	-1.7517
NM_001416	EIF4A1	eukaryotic translation initiation factor 4A, isoform 1	0.1067	0.3233	0.5113	0.5733
NM_005239	ETS2	v-ets erythroblastosis virus E26 oncogene homolog 2 (avian)	-0.0417	-0.1317	-0.7237	-0.6167
NM_006597	HSPA8	heat shock 70kDa protein 8	-0.3167	-0.3550	-0.5897	-0.2633
XM_058230	JUND	jun D proto-oncogene	-0.0883	-0.0133	-0.9497	-0.7983
NM_005566	LDHA	lactate dehydrogenase A	-0.0150	0.6150	0.8707	1.1967
XM_031818	LYN	v-yes-1 Yamaguchi sarcoma viral related oncogene homolog	0.0417	-0.2733	-0.6830	-1.0617
XM_008855	NR2F6	nuclear receptor subfamily 2, group F, member 6	0.0183	0.1483	0.3897	0.4650
XM_007258	TNFAIP2	tumor necrosis factor, alpha-induced protein 2	-0.0383	-0.2517	-1.0440	-1.5067
XM_002762	TNFAIP6	tumor necrosis factor, alpha-induced protein 6	-0.0350	-0.1517	-1.5390	-1.0600
NM_003295	TPT1	tumor protein, translationally-controlled 1	-0.4950	-0.5100	-0.3893	-0.4267

Table 8. Continued

C. Stress-response genes

Accession	Name	Description	2 h 1:1 MOI	2 h 1:10 MOI	4 h 1:1 MOI	4 h 1:10 MOI
NM_001196	BID	BH3 interacting domain death agonist	-0.0317	-0.0750	-0.6127	-0.5717
NM_015675	GADD45B	growth arrest and DNA-damage-inducible, beta	-0.0800	-0.5800	-2.0967	-2.0000
XM_046543	MKPX	mitogen-activated protein kinase phosphatase x	0.1183	0.5667	0.8563	0.8250
XM_010767	NCKAP1	NCK-associated protein 1	0.1750	0.2333	0.4737	0.2750
NM_006107	OA48-18	acid-inducible phosphoprotein	0.0433	0.0333	0.5737	0.7933
NM_004180	TANK	TRAF family member-associated NFKB activator	0.2383	-0.2633	-0.7193	-0.6650
NM_003879	CFLAR	CASP8 and FADD-like apoptosis regulator	-0.0583	-0.1283	-0.7720	-1.1250
XM_028204	NFKB1	nuclear factor of kappa light polypeptide gene enhancer in B-cells 1 (p105)	-0.1467	0.0283	-0.7677	-1.3933
XM_041847	TNF	tumor necrosis factor (TNF superfamily, member 2)	-0.1683	-0.7250	-2.4107	-1.3967
XM_012894	ZNF14	zinc finger protein 14 (KOX 6)	0.3217	0.2067	0.2593	0.1017
NM_014977	ACINUS	apoptotic chromatin condensation inducer in the nucleus	0.2867	0.5983	0.0723	-0.5367

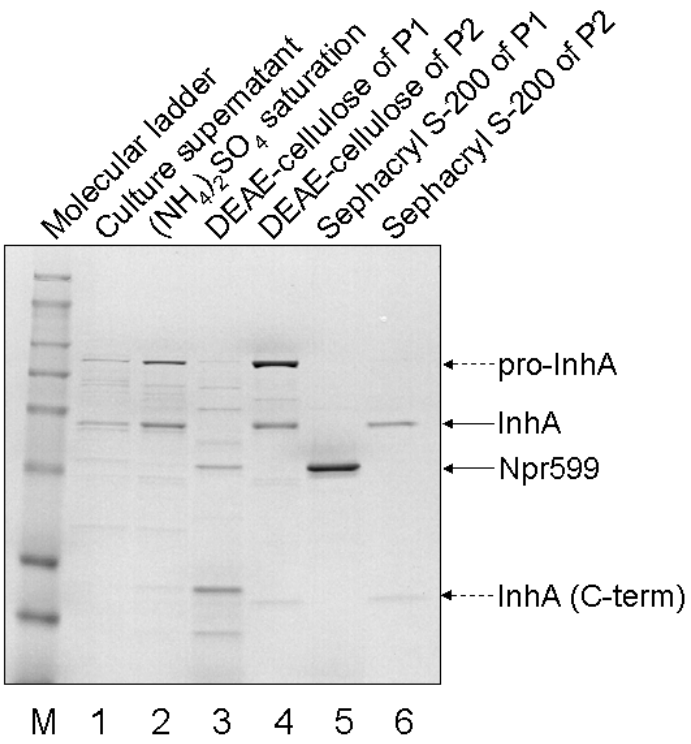

Fig. 1. Purification and identification of Npr599 and InhA. Two proteases were purified from a culture of *B. anthracis* delta Ames through ammonium sulfate saturation, DEAE-cellulose, and sephacryl S-200 column chromatography. M, prestained molecular markers (from top to bottom, 250, 148, 98, 64, 50, 36, 22, and 16 kDa); *lane 1*, culture supernatant; *lane 2*, ammonium sulfate saturation; *lane 3*, DEAE-cellulose of P1; *lane 4*, DEAE-cellulose of P2; *lane 5*, sephacryl S-200 of P1; and *lane 6*, sephacryl S-200 of P2.

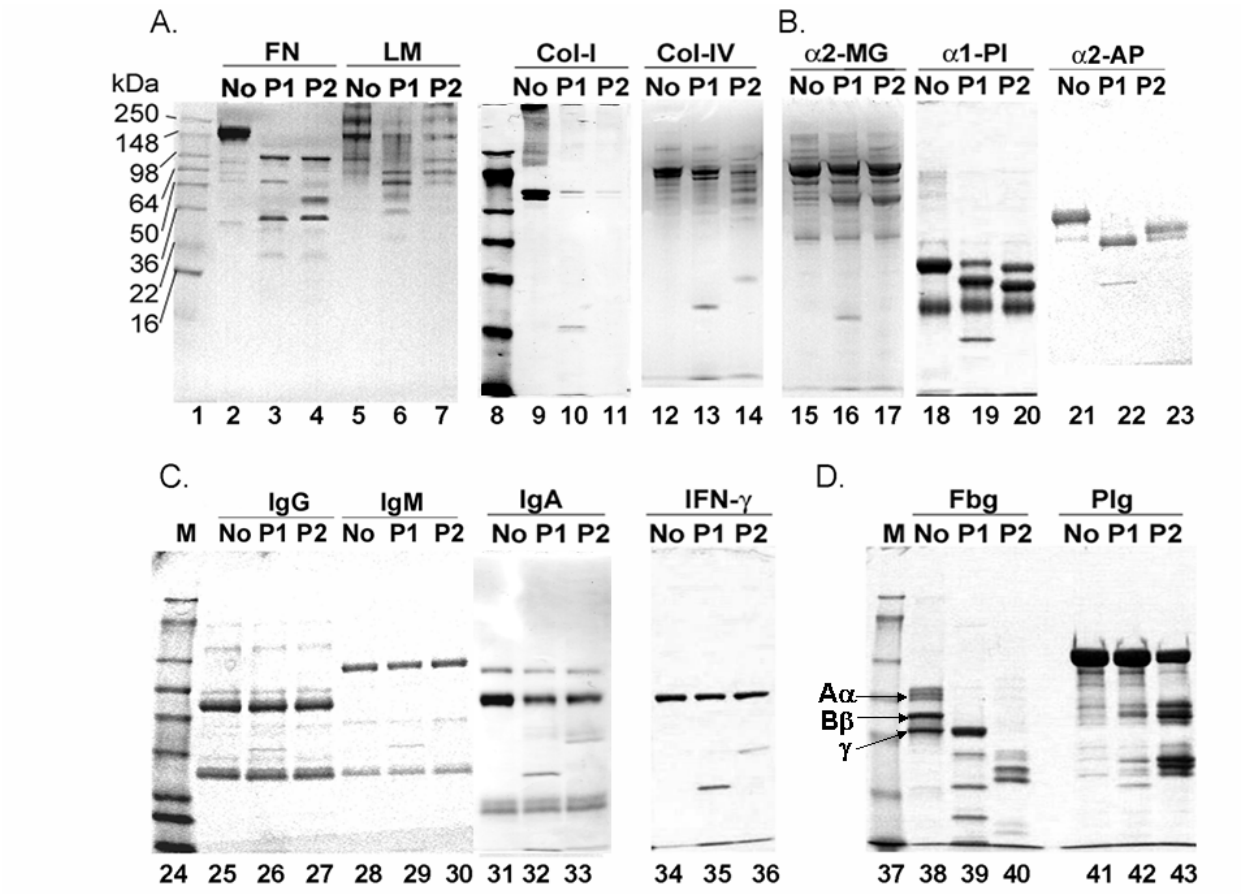

Fig. 2. Potential substrates for Npr599 and InhA. Biologically important substrates were digested with 0.2 □g of Npr599 (P1), InhA (P2) and without protease (No) in each reaction for 4 h at 37 ºC. Boiled samples were separated by SDS-PAGE and stained with Coomassie blue. *A*. Digestion of extracellular matrix proteins (ECMs) was analyzed in 14% gel for fibrinectin (FN, *lanes 2-4*) and laminin (LN, *lanes 5-7*), and in 10% gel for collagen type I (Col-I, *lanes 9-11*) and collagen type IV (Col-IV, *lanes 12-14*). *B*. Digestion of endogenous serum protease inhibitors was analyzed in 10% gel for □$_2$-macroglobulin (□$_2$-MG, *lanes 25-27*), □$_1$-proteinase inhibitor (PI, *lanes 18-19*), and in 4-20% gel for □$_2$-antiplasmin (□2-AP, *lanes 21-23*). *C*. Digestion of immune response proteins was analyzed in 4-20% gel for IgG (*lanes 25-27*), IgM (*lanes 28-30*), and in 10% gel for IgA (*lanes 31-33*), and interferon-□ (IFN-□, *lanes 34-36*). *D*, digestion of blood coagulation or tissue damage related response proteins was analyzed in 10% gel for fibrinogen (Fbg, *lanes 38-40*) and plasminogen (Plg, *lanes 41-43*). *Lanes 1, 8, 24, and 37* represent molecular weight markers.

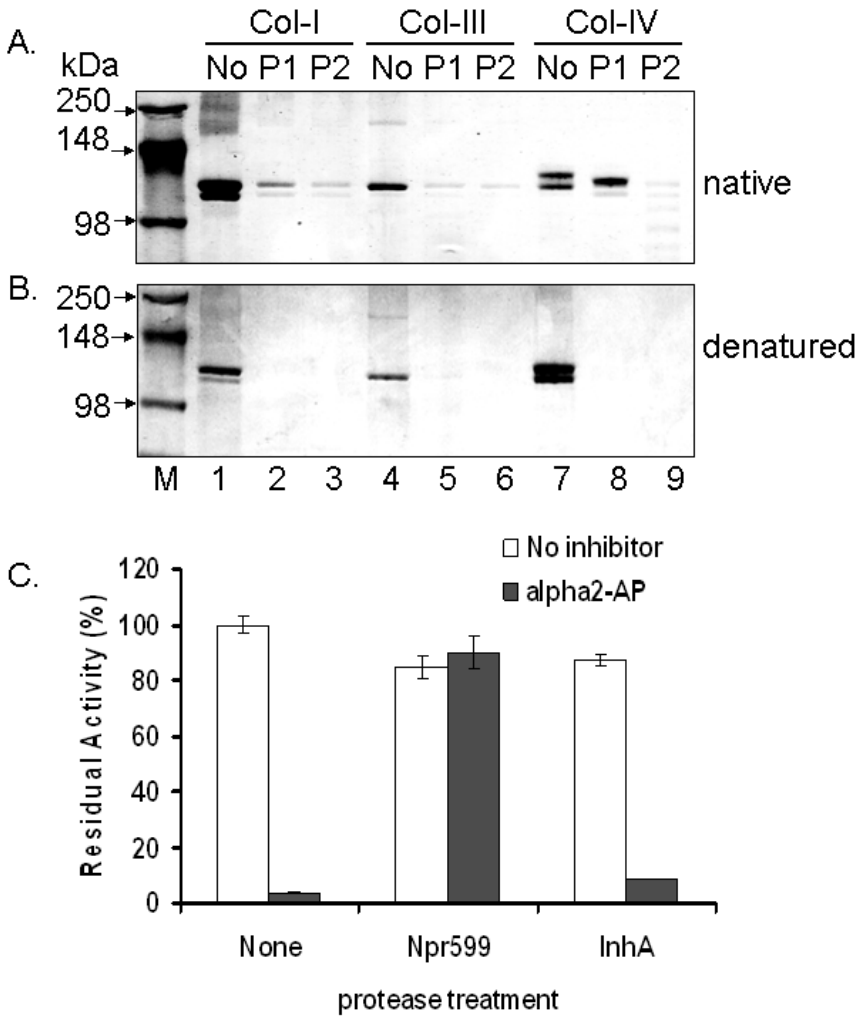

Fig. 3. Collagen proteolysis (*A* and *B*) and □$_2$-antiplasmin inactivation (*C*) by proteases. Native (*A*) and denatured at 95℃ for 2 min (*B*) human collagens of type I (*lanes 1-3*), III (*lanes 4-6*) and IV (*lanes 7-9*) (2 □g each) were digested with 0.2 □g of either Npr599 or InhA, and without protease (No) for 4 h at 37 ºC. Digested fragments were analyzed in 10% gel and visualized with Coomassie brilliant blue staining. □$_2$-Antiplasmin preincubated with proteases at 37^{o}C for 4 h was subjected to plasmin assay as detailed in Experimental Procedures. Residual plasmin activity is expressed relative to untreated control without inhibitor after subtraction of background activity. Error bars show aritmetic means ± SDs; *n* = 3.

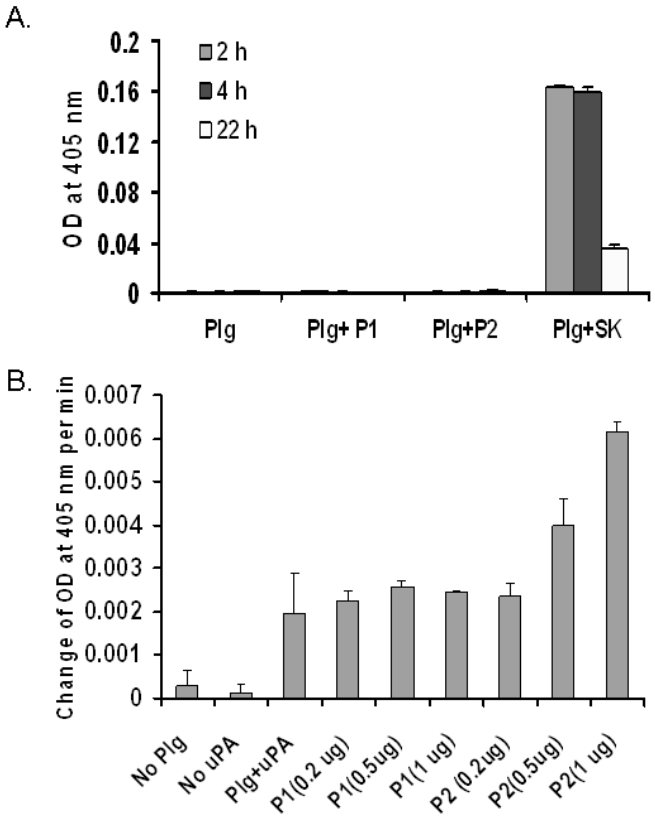

Fig. 4. Acceleration of urokinase-dependent plasminogen (Plg) activation by InhA. *A*. Npr599 (P1) and InhA (P2) are not a bacterial plasminogen activator. Human plasminogen (8.3 □g) was incubated at 37 °C with either 2 □g of the protease or streptokinase (SK). The 20-fold diluted resulting reactions were added to 100 □M Val-Leu-Lys-*p*NA in the presence of fibrin and the release of *p*NA was monitored during the incubation. *B*. Urokinase-type plasminogen activator (uPA)-catalyzed plasminogen activation is accelerated by InhA. The reaction (100 □l) contained 200 U/ml uPA, 0.1 U/ml plasminogen, 100 □M Val-Leu-Lys-*p*NA, and either 2, 5 or 10 □g/ml of the purified proteases. The release of *p*NA from the chromogenic substrate was monitored at 405 nm for 10 min. Error bars represent standard deviations determined from triplicate measurements.

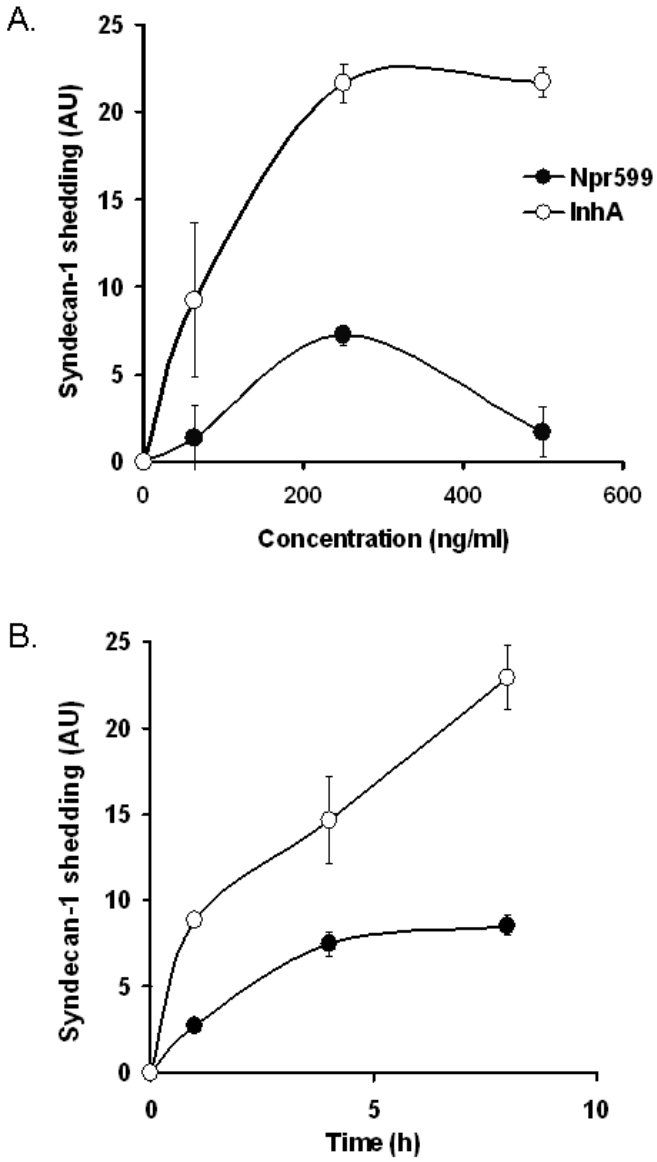

Fig. 5. Enhacement of syndecan-1 shedding by Npr599 and InhA. Confluent NMuMG cells in 96-well plates were incubated at 37 ºC with (*A*) Npr599 (62.5, 250, and 500 ng/ml) and InhA for 4 h, or (*B*) protease (250 ng/ml) for 1, 4 and 8 h. Shed syndecan-1 ectodomain levels were measured by the dot-blot analysis as described in Materials and Methods. Error bars represent standard deviations determined from triplicate measurements.

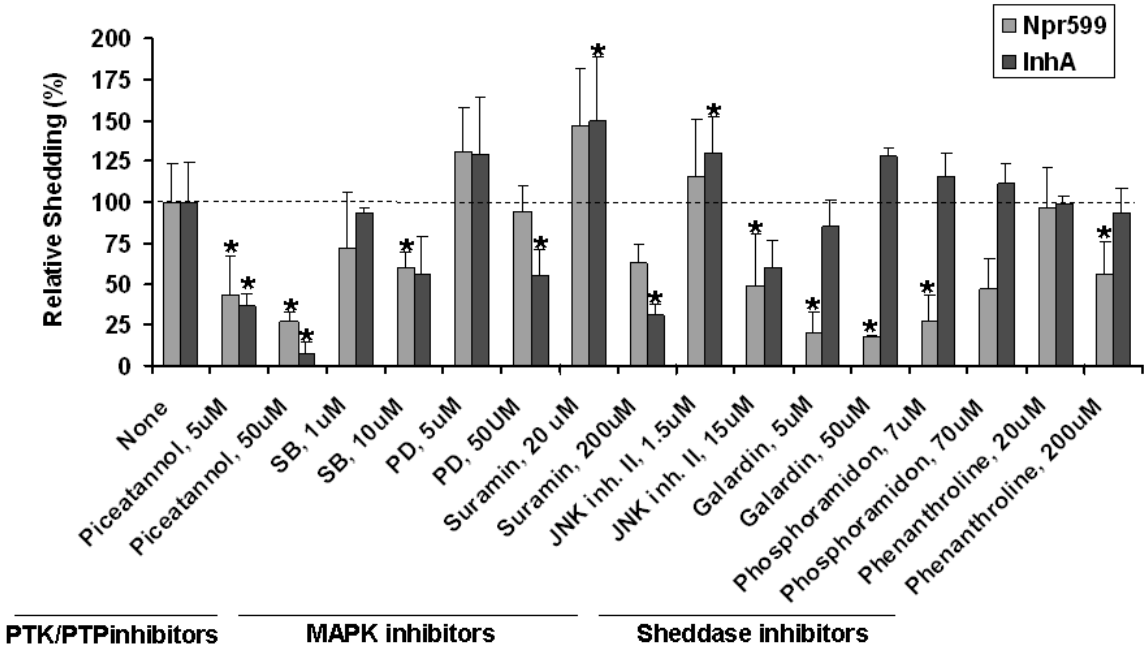

Fig. 6. Effect of inhibitors on syndecan-1 ectodomain shedding from NMuMG cells enhanced by Npr599 and InhA. NMuMG cells in 1% FCS medium were preincubated with the indicated concentrations of inhibitors for 1 h, and then exposed to shedding inducers (250 ng/ml of either Npr599 or InhA) for 24 h. Data are expressed relative to shedding observed without inhibitors in cells either treated or untreated with Npr599 and InhA. Dotted line represents control syndecan-1 ectodomain shedding by Npr599 and InhA in the absence of inhibitors. SB and PD denote SB202190 and PD98059, respectively. Error bars represent SD determined from triplicate measurements. * $p < 0.05$ compared to protease-treated control in the absence of inhibitors by paired Student's t-test.

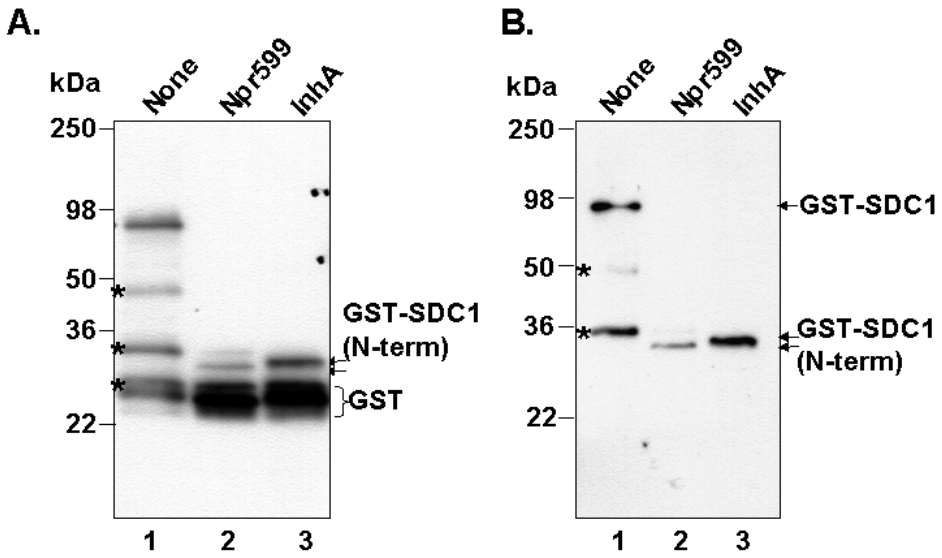

Fig. 7. Direct cleavage of N-terminus of recombinant syndecan-1 by Npr599 and InhA. *A*, partially purified recombinant syndecan-1 core protein tagged with GST (800 ng) was incubated without (*lane 1*) or with 100 ng of Npr599 (*lane 2*) and InhA (*lane 3*) for 4 h at 37 ^{o}C, and analyzed on SDS-4-20% PAGE. After electrophoresis, gel was immunoblotted with antibody against GST. *B*, the immunoblot was incubated with antibody against N-terminus of syndecan-1 epitope. *Lanes 1-3* are the same as legends of *panel A*. GST-SDC1 and GST-SDC1 (N-term) represent GST-fused syndecan-1 and N-terminal fragment of GST-SDC1, respectively.

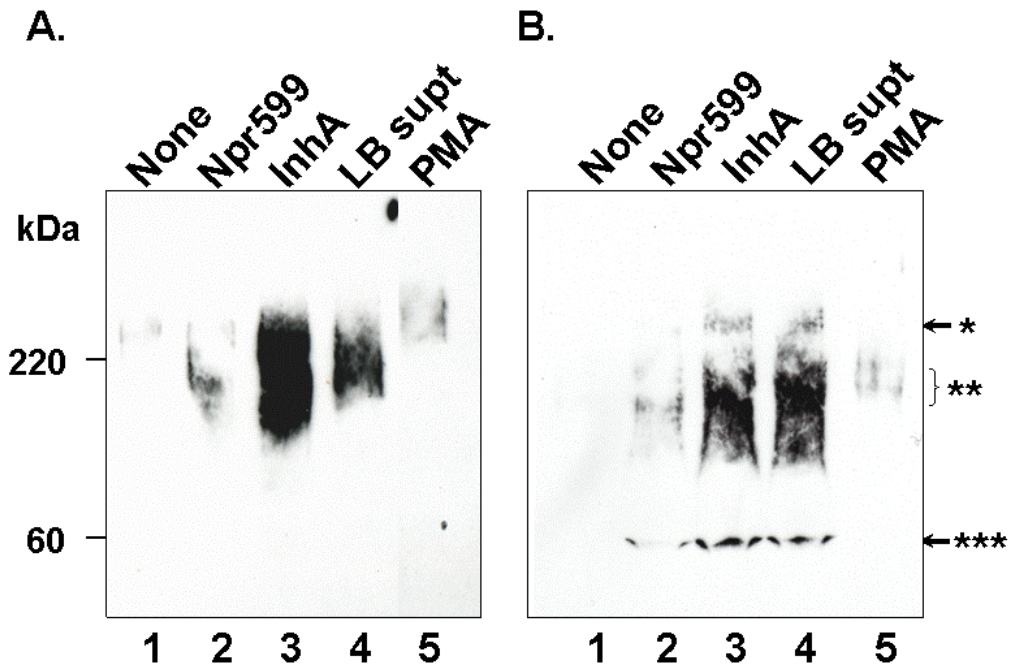

Fig. 8. Western immunoblotting of syndecan-1 ectodomains shed by *B. anthracis* culture supernatant and purified proteases into the culture media of NMuMG cells. The cells were left unstimulated (*lane 1*), or were stimulated with 250 ng/ml of Npr599 (*lane 2*), InhA (*lane 3*), 10% (v/v) *B. anthracis* delta Ames culture supernatant in LB (LB, *lane 4*), or 1 □M PMA (*lane 5*). The shed syndecan-1 was separated in 4-20% SDS-PAGE, the proteins transferred on a cationic nylon membrane and probed with the 281-2 anti-syndecan-1 ectodomain antibody. In *panel A*, intact syndecan-1 ectodomains migrate as smears because of the heterogenous length and the different number of attached HS chains. In *panel B*, samples as in *A* before analysis were additionally digested with 20 mU/ml heparinase II and 20 mU/ml chondroitin sulfate ABC lyase. Asterisks indicate positions of the PMA-shed syndecan-1 before (*) and after removal of HS chains (**) in the region of 80 kDa. The fragments generated by direct proteolysis of syndecan-1 ectodomains by exogenous proteases migrate in the region of 60 kDa (***).

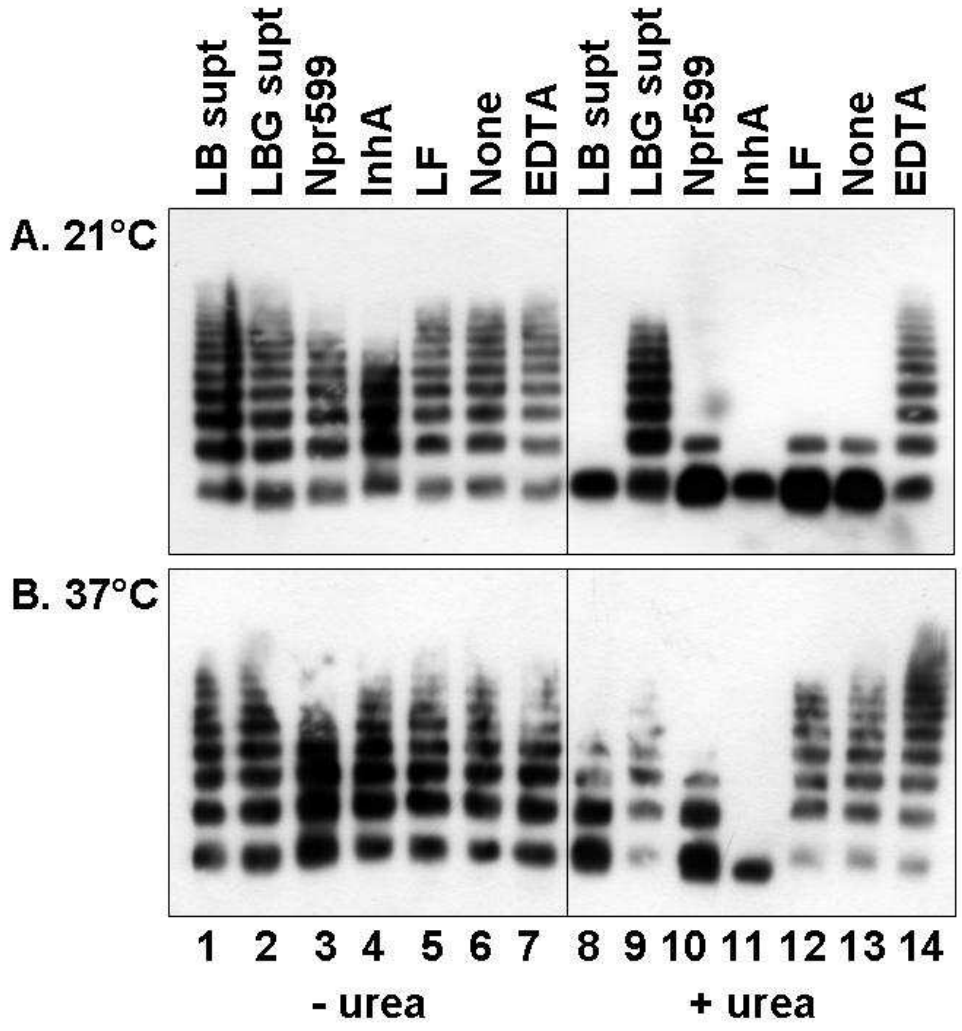
LB supt
LBG supt
Npr599
InhA
LF
None
EDTA
LB supt
LBG supt
Npr599
InhA
LF
None
EDTA
A. 21°C
B. 37°C
1 2 3 4 5 6 7 8 9 10 11 12 13 14
- urea
+ urea

Fig. 9.

A.

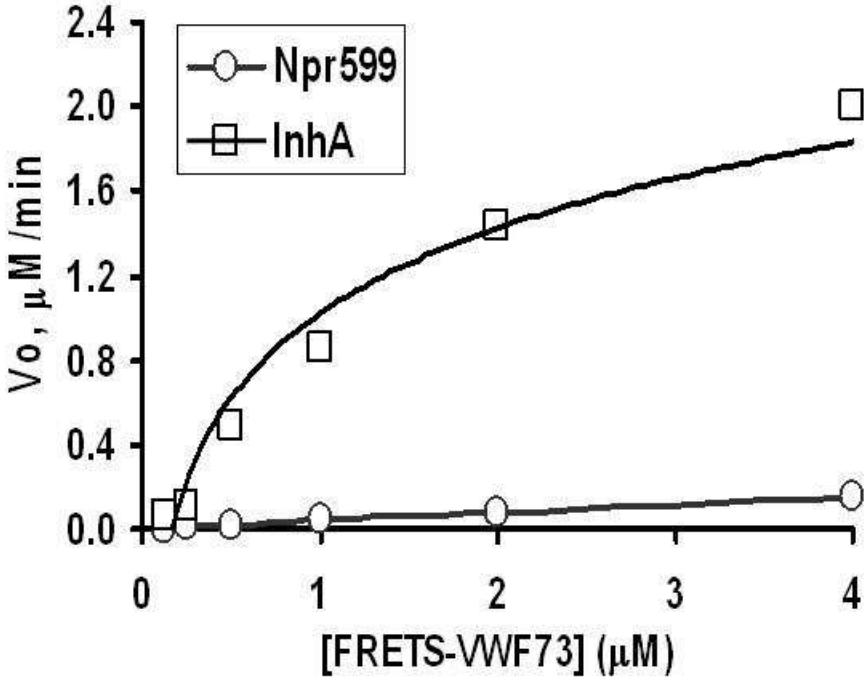

B.

Protease	K_m μM	k_{cat} min^{-1}	k_{cat}/K_m μM^{-1} min^{-1}	Ref.
Npr599	1.4 ± 0.5	18.8 ± 4.9	13.6 ± 1.4	This study
InhA	3.9 ± 0.4	1057.4±103.2	274.5 ± 1.9	This study
ADAMTS13	3.2 ± 1.1	~ 58	18	*JBC* **281**, 850 (2006)

Fig. 10 Kinetic properties of the proteases toward the synthetic VWF substrate

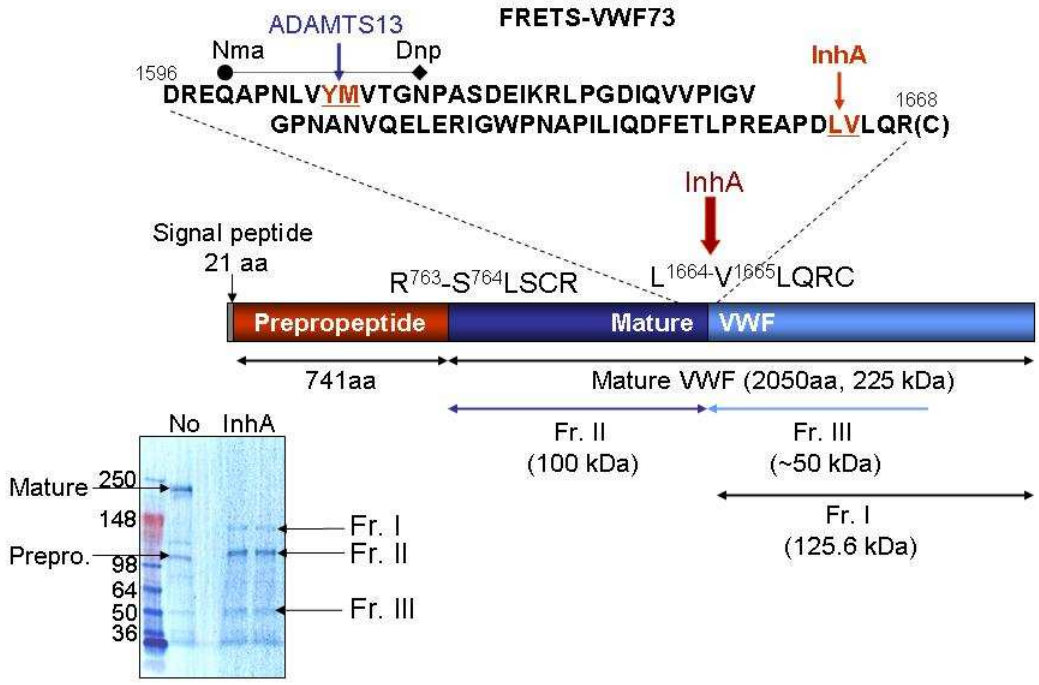

Fig. 11. VWF cleavage site map.

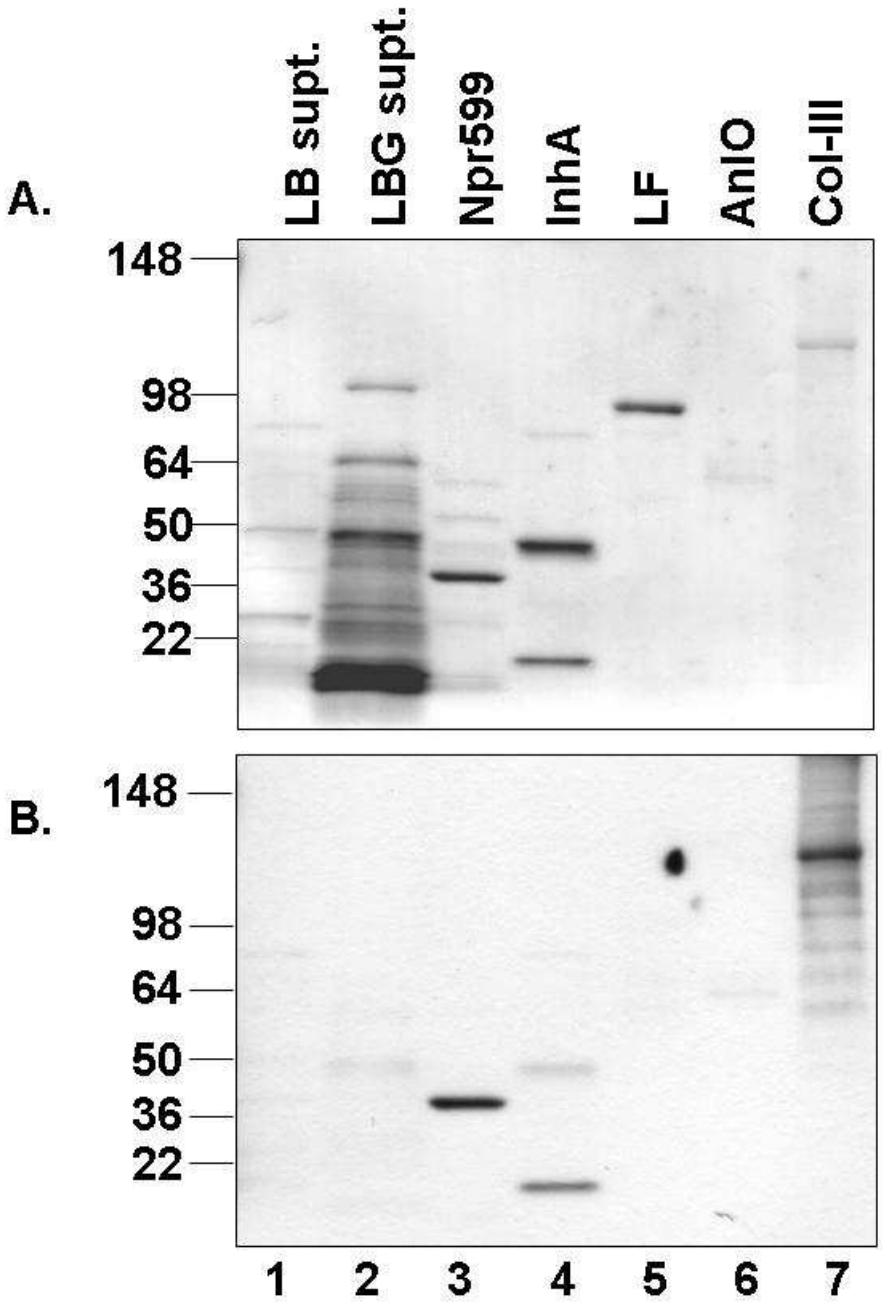

Fig. 12. Protease-transferred PVDF membrane stained with naphthol blue.

Fig. 7

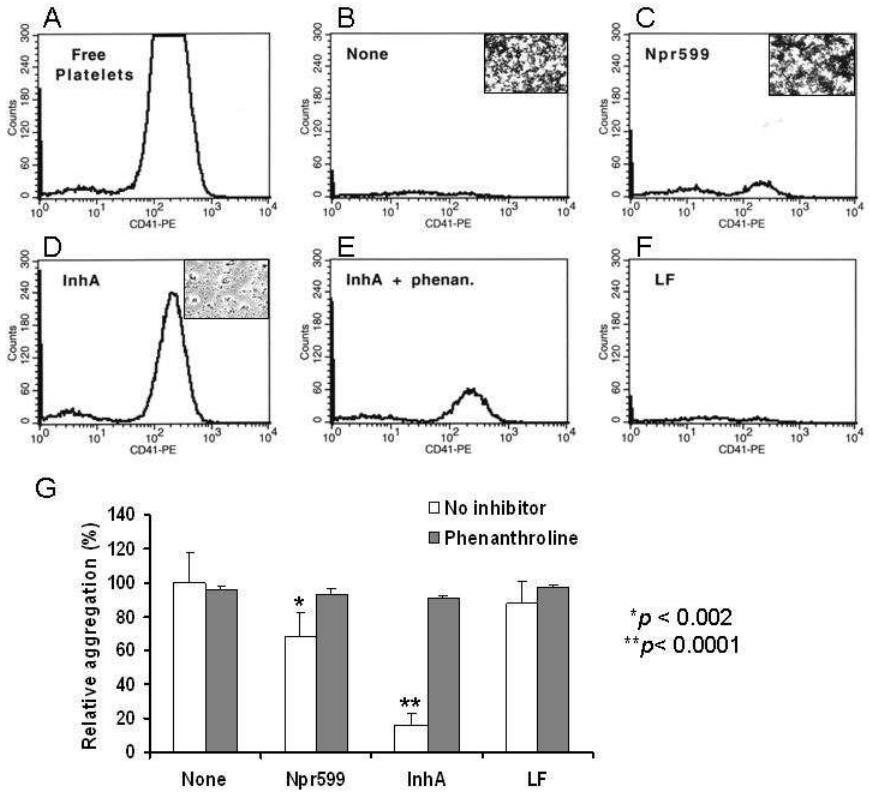

Fig. 13 Rictocetin-induced platelet aggregation (RIPA) at different concentrations of plasma examined under the microscope (inserts) and flow cytometry using anti-CD41 antibody to detect free platelets.

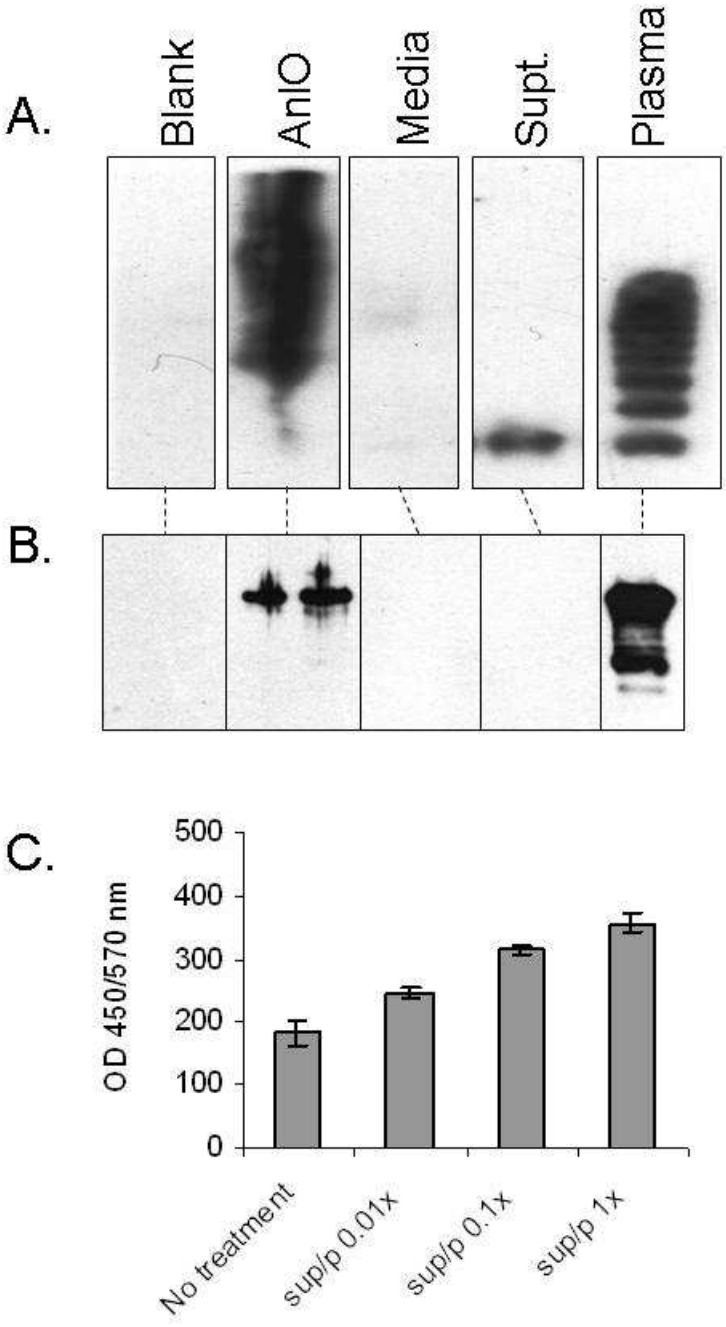

Fig. 14. Anthrax pathogenic factors stimulate secretion of ULVWF multimers in HUVECs.

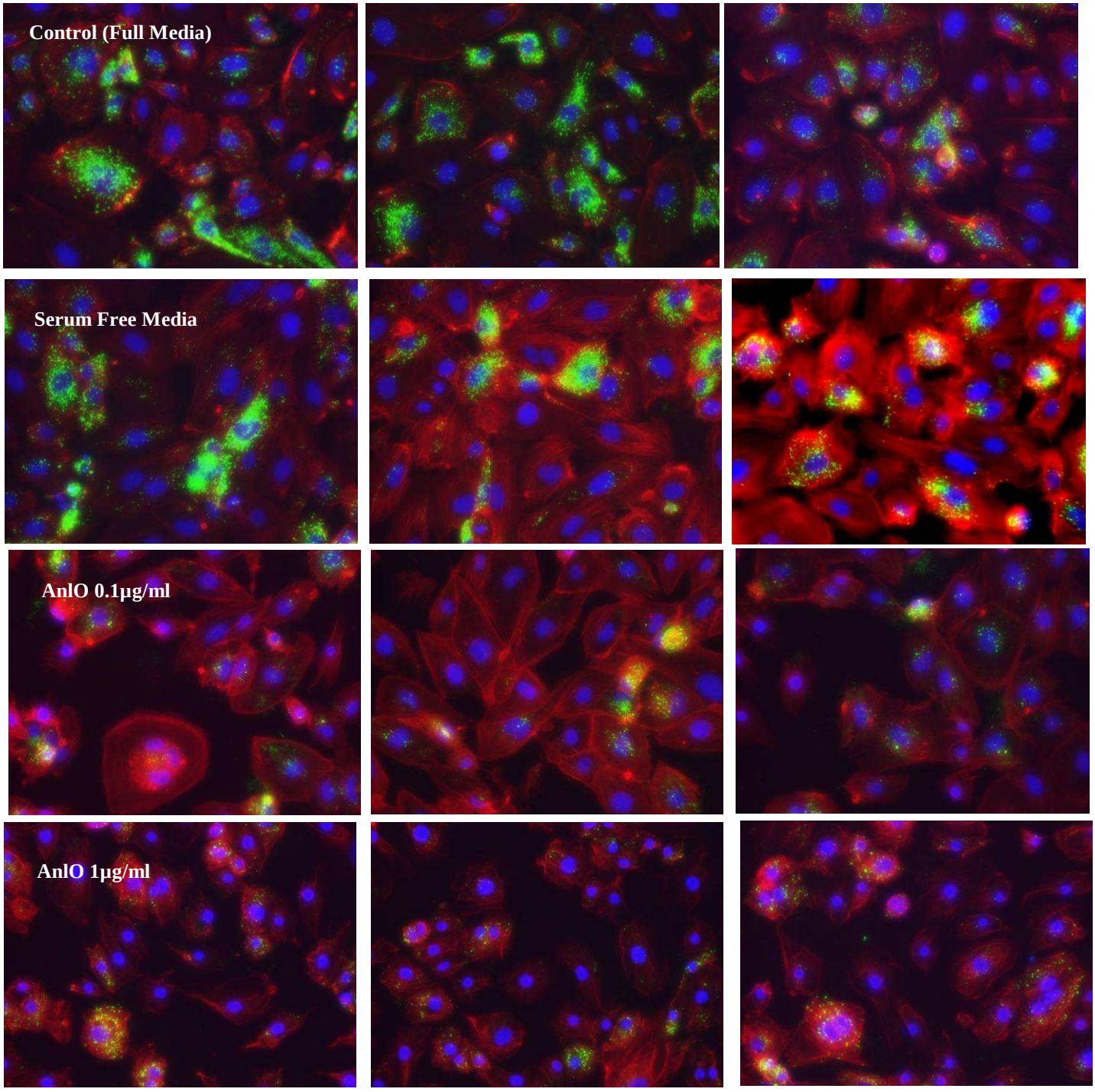

Fig. 15. Release of VWF from HUVECs upon stimulation with AnlO for 4 h, as detected by fluorescence of the stained cells. VWF, green; nuclei, blue, cytoskeleton, red.

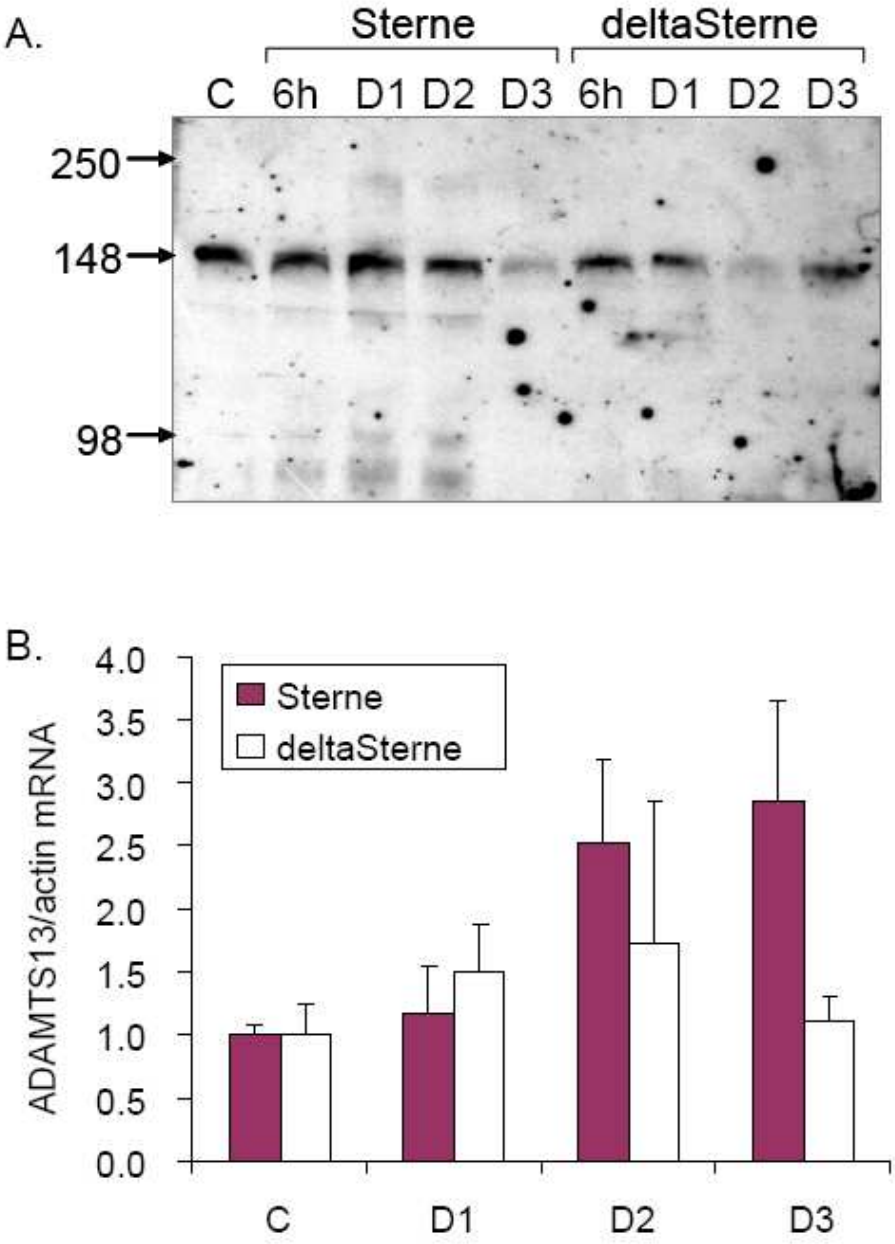

Fig. 16. ADAMTS13 depletion in sera of *B. anthracis* spore-challenged mice. Pooled sera (n = 5) taken from spore-challenged mice at 6 h , day 1, day 2 and day 3 were transferred onto a nitrocellulose membrane, and the membrane was probed with anti-ADAMTS13 antibody (*A*). ADAMTS13 expression in liver was analyzed by RT-PCR with cDNA prepared by a conventional reverse transcription of RNA from livers of spore-challenged mice. Amplified products were estimated by densitometry and normalized by β-actin mRNA levels (*B*) (n = 3, *p < 0.05 to control).

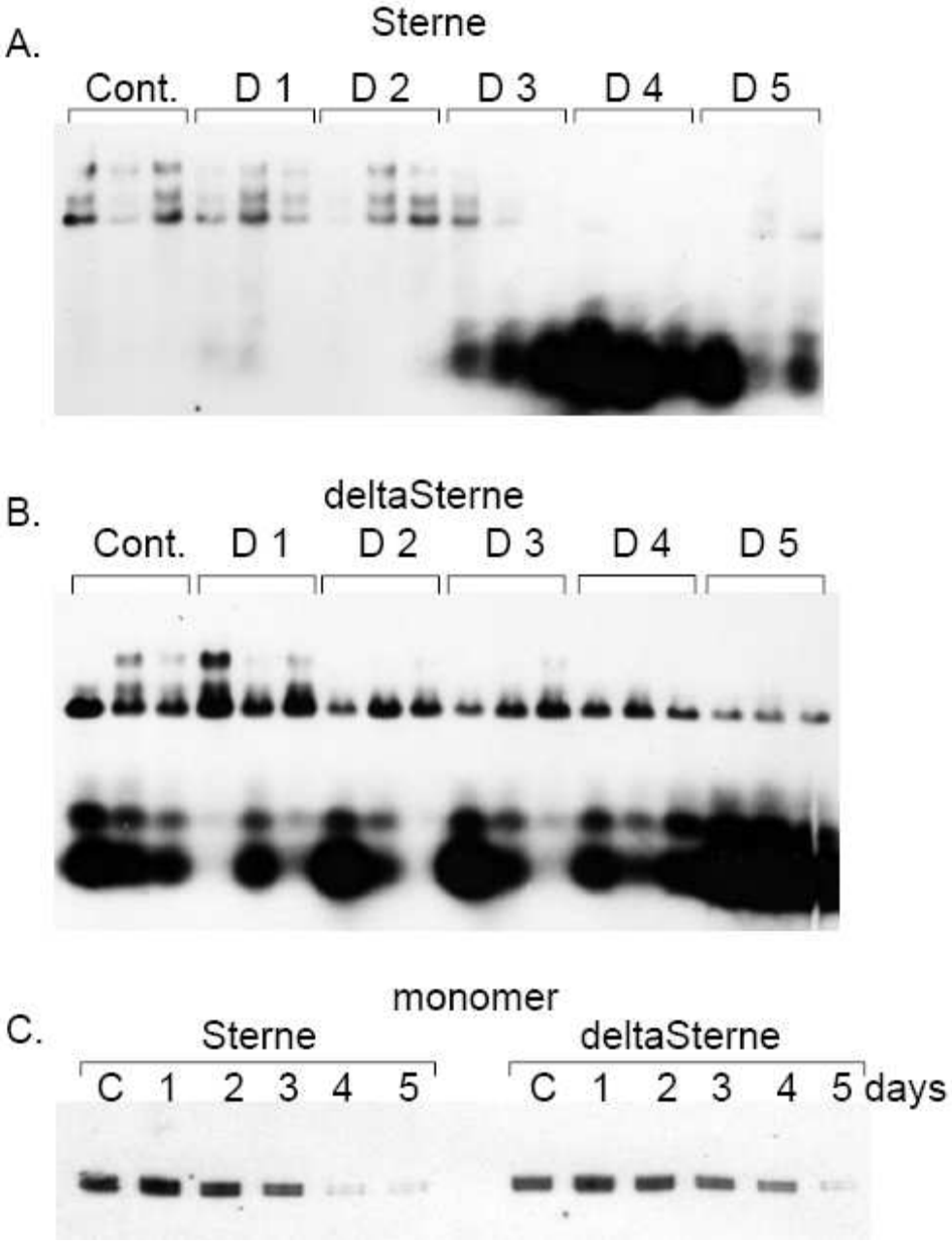

Fig. 17. ULVWF multimers and intact monomers are degraded in plasma of Sterne (A) and delta Sterne (*B*) spore-challenged mice. After incubation at room temperature overnight, plasma taken from spore-challenged mice was subjected to ULVWF analysis in a 1% agarose-SDS gel, as described in Materials and Methods.

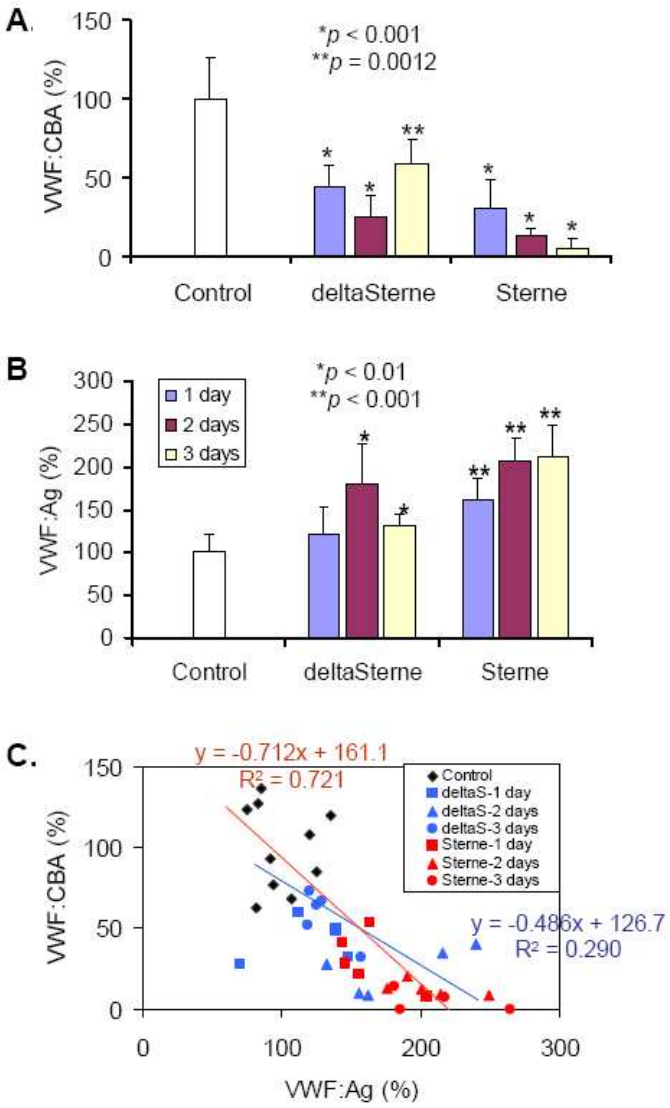

Fig. 18. VWF:CBA is impaired by *B. anthracis* spore challenges. Plasma (10 µg of protein per well) in PBS was added to a collagen-coated Maxisorp microplate for 1 h. After washing the plate with PBS, collagen-bound VWF was detected colorimetrically by probing with HRP-conjugated VWF antibody (*A*). VWF antigen levels were determined by a conventional ELISA. Plasma (10 µg) was coated onto a microplate overnight. Total VWF antigen was determined colorimetrically as above (*B*). Error bars indicate standard deviations (n = 10 for control and n = 5 for spore-challenged samples). Correlation between VWF:CBA and VWF:Ag uses the data presented in panels A and B (*C*). *Open circle, square, triangle* and *diamond* represent control, day 1, day 2, and day 3 post spore challenge, respectively. Black and grey distinguish between Sterne and delta Sterne challenge, respectively. Solid and dotted lines represent best-fit lines of linear regression between VWF:CBA and VWF:Ag for Sterne and delta Sterne challenges, respectively.

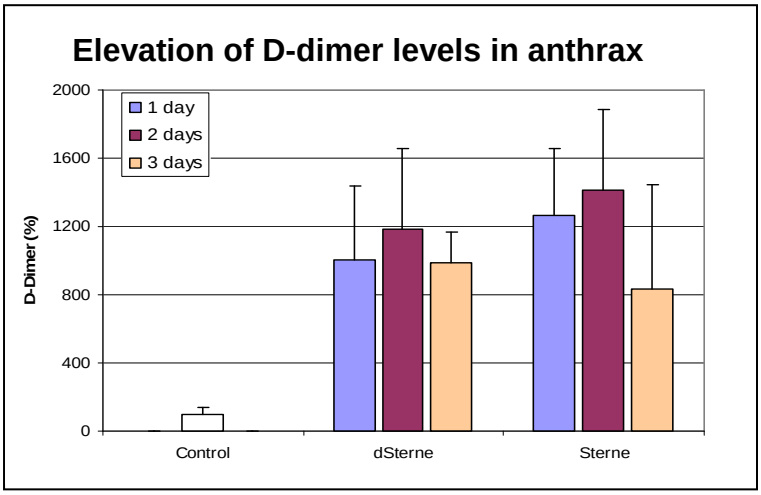

Fig.19. ELISA showing elevation of D-dimers in spore-challenged mouse plasma. This is an early indicator of consumptive coagulopathy which leads to septic shock.

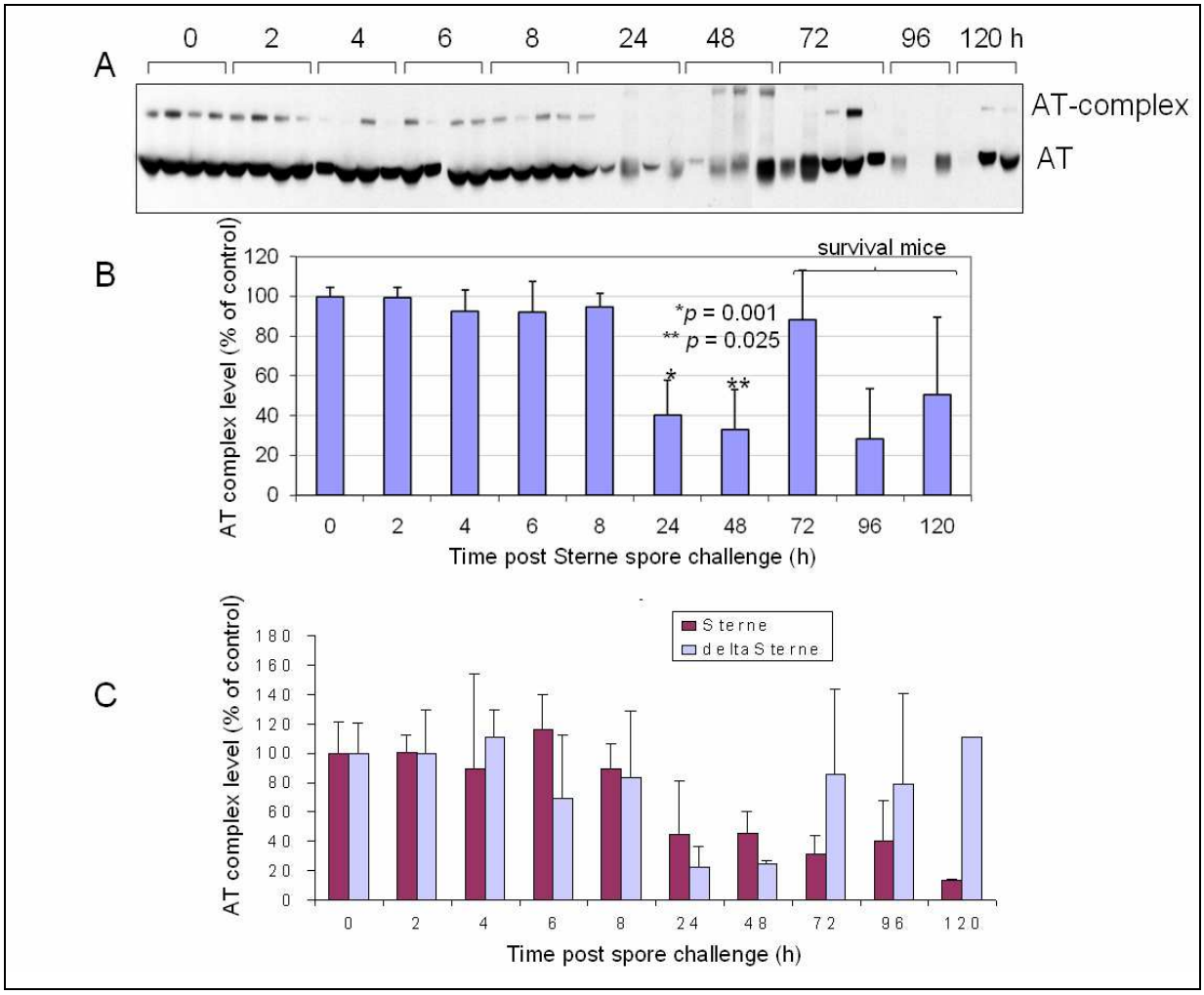

Fig. 20. Western blot (A) showing antithrombin (AT) and AT-complex levels in plasma from Sterne spore-challenged mice. Densitometic analysis of AT in plasma of Sterne-challenged mice (B) and AT complex levels (C) in plasma of Sterne and delta Sterne-challenged mice. Both strains show depletion of AT 24 h post challenge and recovery of Δ-Sterne spore-challenge at 72 h. *, $p < 0.001$ and **, $p < 0.025$ compared with the PBS-treated control mice (paired Student's t test).

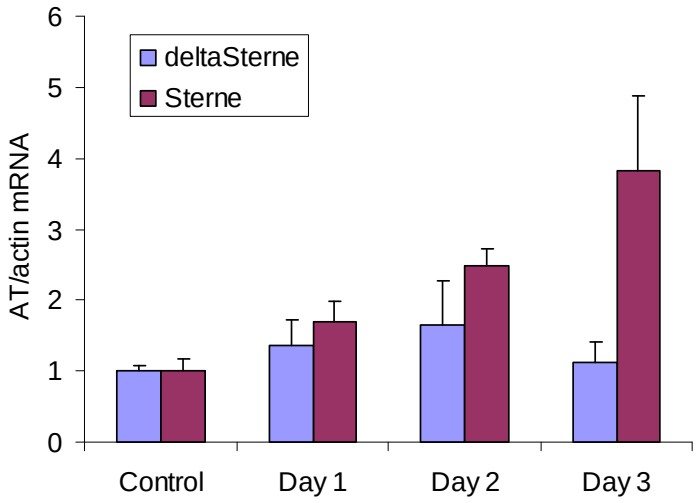

Fig. 21. RT-PCR showing gene expression of antithrombin in the liver of both Sterne and Δ-Sterne spore-challenged mice. Expression steadily increases after Sterne strain challenge. This data shows AT depletion is not caused by suppression of its gene expression in the liver, suggesting AT proteolysis takes place in the plasma.

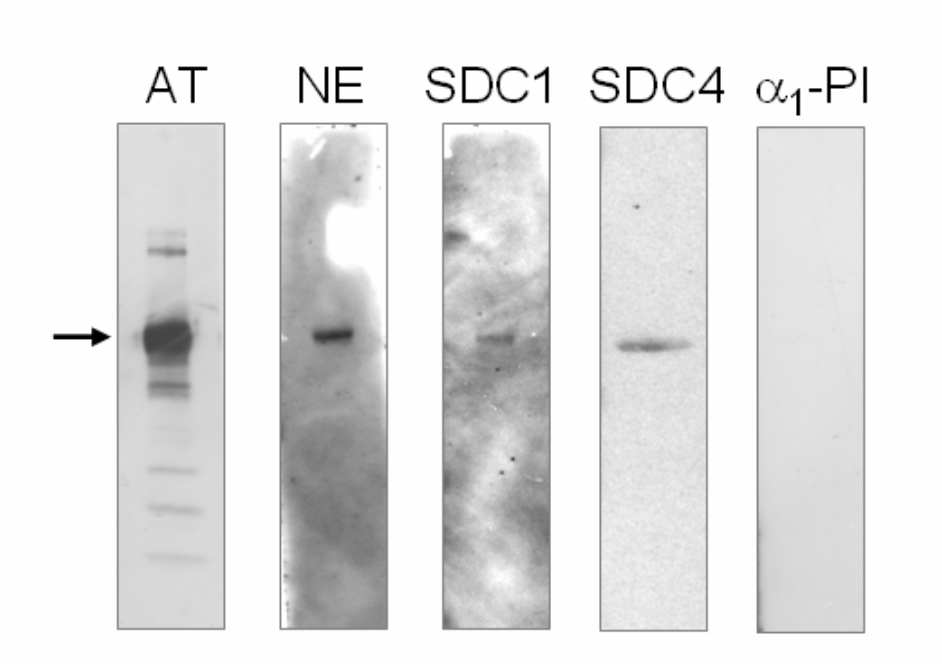

Fig. 22. Overlay assay showing AT interacts with NE, shed syndecan-1(SDC1) and syndecan-4 (SDC4) *in vitro*.

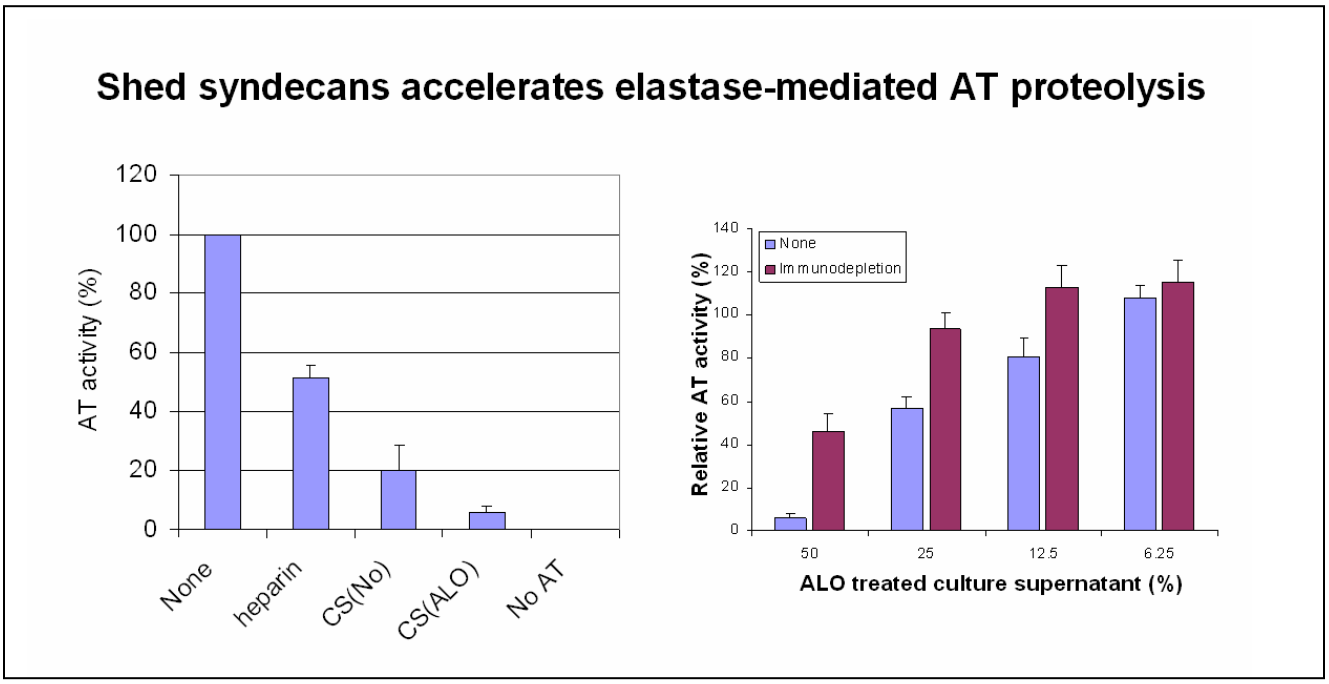

Fig. 23. (A) NE accelerates antithrombin (AT) proteolysis in the presence of anthralysin O (ALO)-treated culture supernatant. (B) Syndecan-1 and syndecan-4 immunodepleted ALO culture supernatants recovered more AT activity than the control (with no antibody depletion) in a concentration-dependent manner. This data suggests that shed syndecan-1 and syndecan-4 accelerate elastase-dependent AT proteolysis in a concentration dependant manner. (50% = 5µl ALO treated culture supernatant and 5µl AT + NE.)

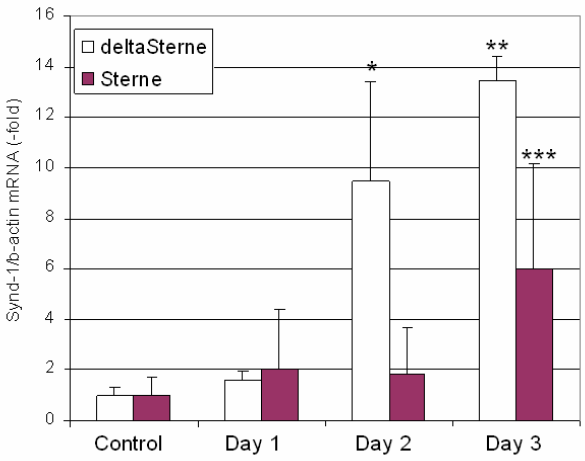

Fig. 24**.** RT-PCR showing gene expression of syndecan-1 in the liver of both Sterne and Δ-Sterne spore-challenged mice. * p = 0.60, ** p = 0.00008, *** p = 0.17 compared with the PBS treated control mice (paired Student's t test).

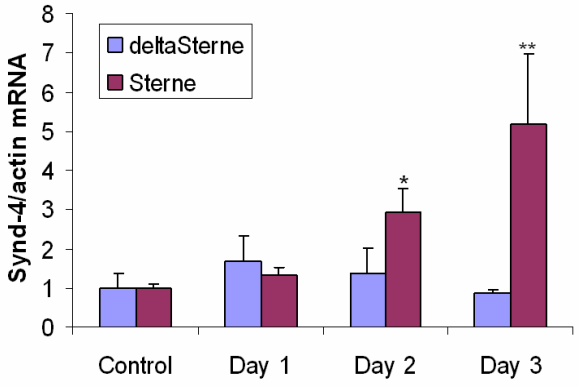

Fig. 25. RT-PCR showing gene expression of syndecan-4 in the liver of both Sterne- and Δ-Sterne spore-challenged mice. Expression is steadily increased after Sterne strain challenge. * p = 0.04 and ** p = 0.06 compared with the PBS treated control mice (paired Student's t test).

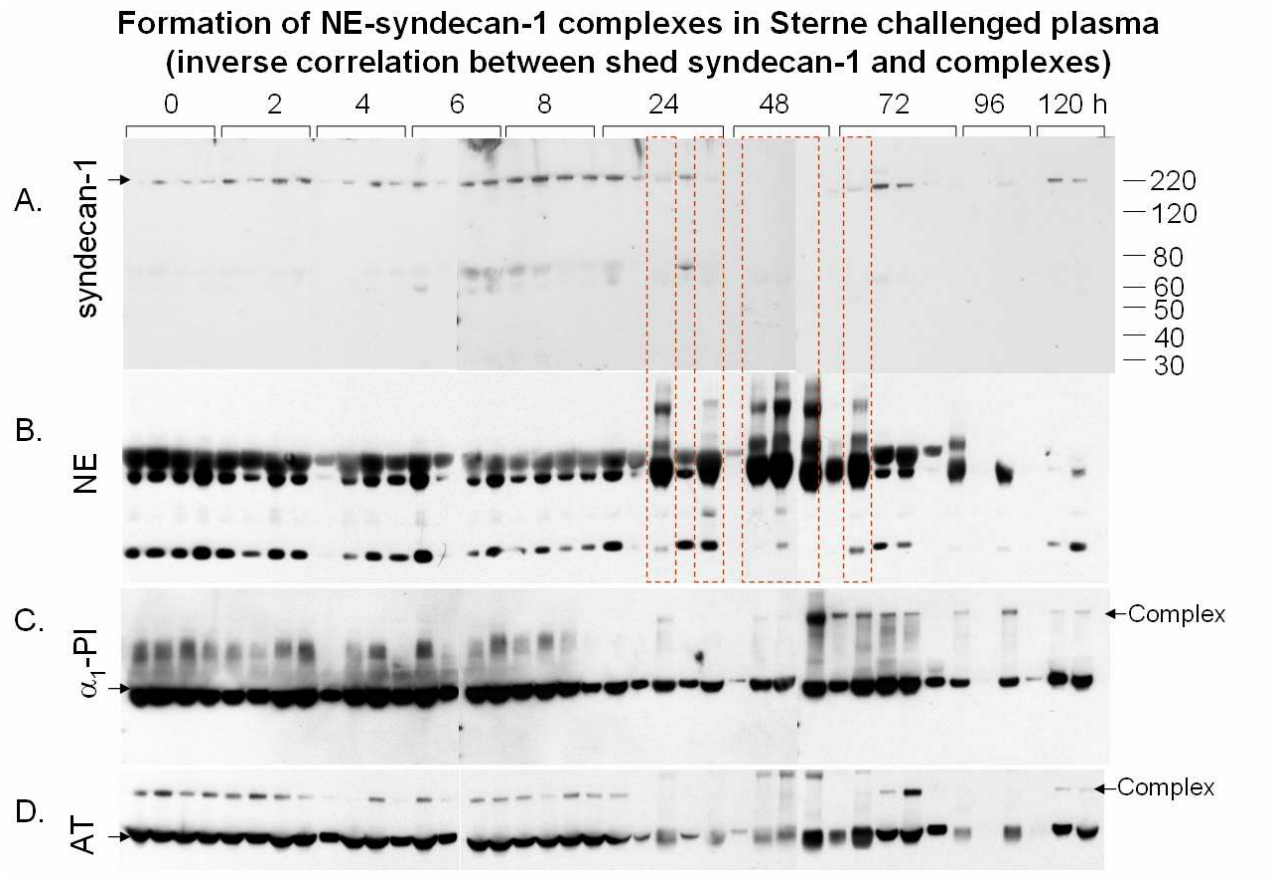

Fig. 26. Western Blot using the same 3 membranes probed with different antibodies namely, (A) syndecan-1, (B) neutrophil elastase, (C) α_1-PI and (D) antithrombin. We suggest that a supramolecular complex visible between 24-48 h post challenge contains NE, syndecan-1 and/or α_1-PI. Mice with NE-complexes show an inverse correlation with levels of free shed syndecan and AT, suggesting a complex formation of shed syndecan and NE accelerates AT degradation during infection.

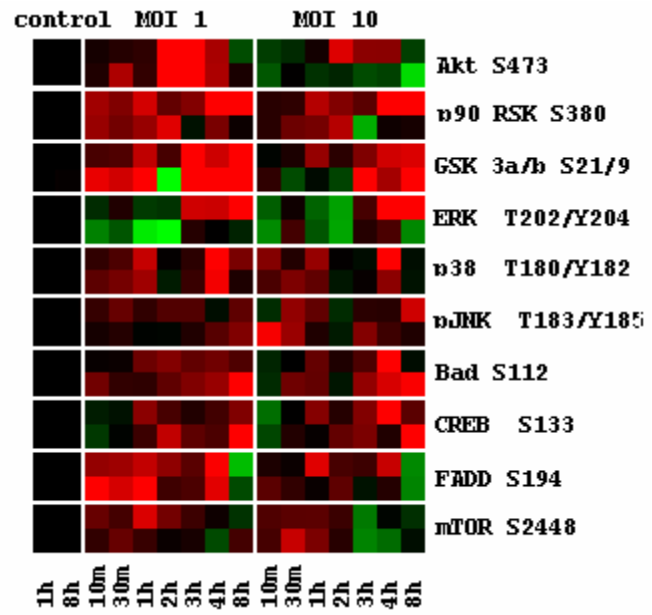

Fig.27. Dynamics of the signaling protein phosphorylation in HSAECs exposed to anthrax spores of the non-pathogenic delta Sterne strain (upper row of each protein panel) in comparison with the toxigenic Sterne strain (lower row) at the multiplicity of infection (MOI) 1 and 10. Specificity of each detection antibody is indicated at the right. Red and green colors correspondingly indicate increase and decrease in the amount of phosphorylated protein relative to untreated cells (black color).

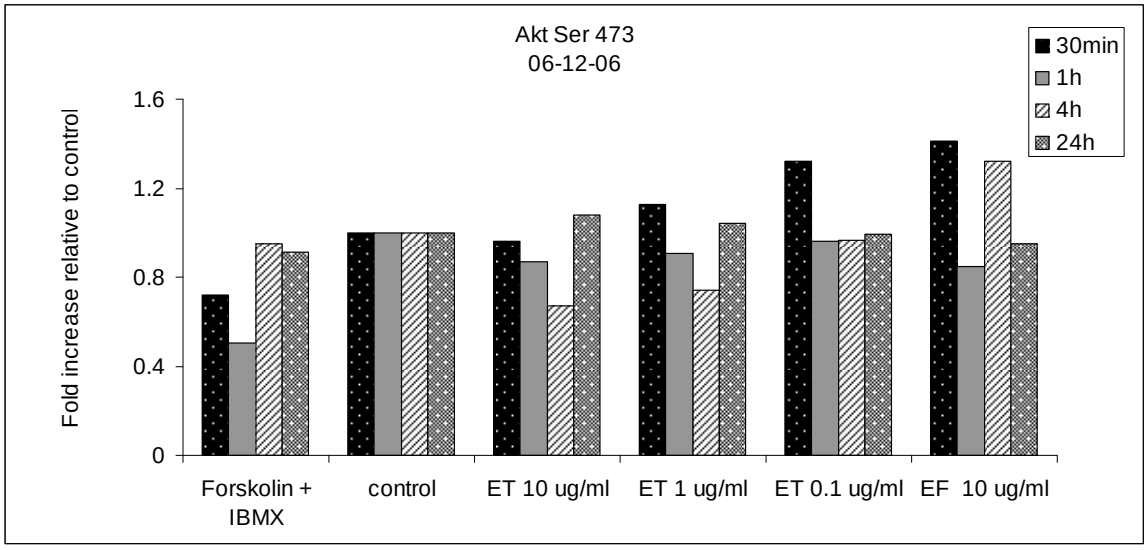

Fig. 28. EdTx modulates AKT phoshphorylation in HSAECs in a time- and concentration-dependent manner. Foskolin, as cAMP inducer, serves as a positive control.

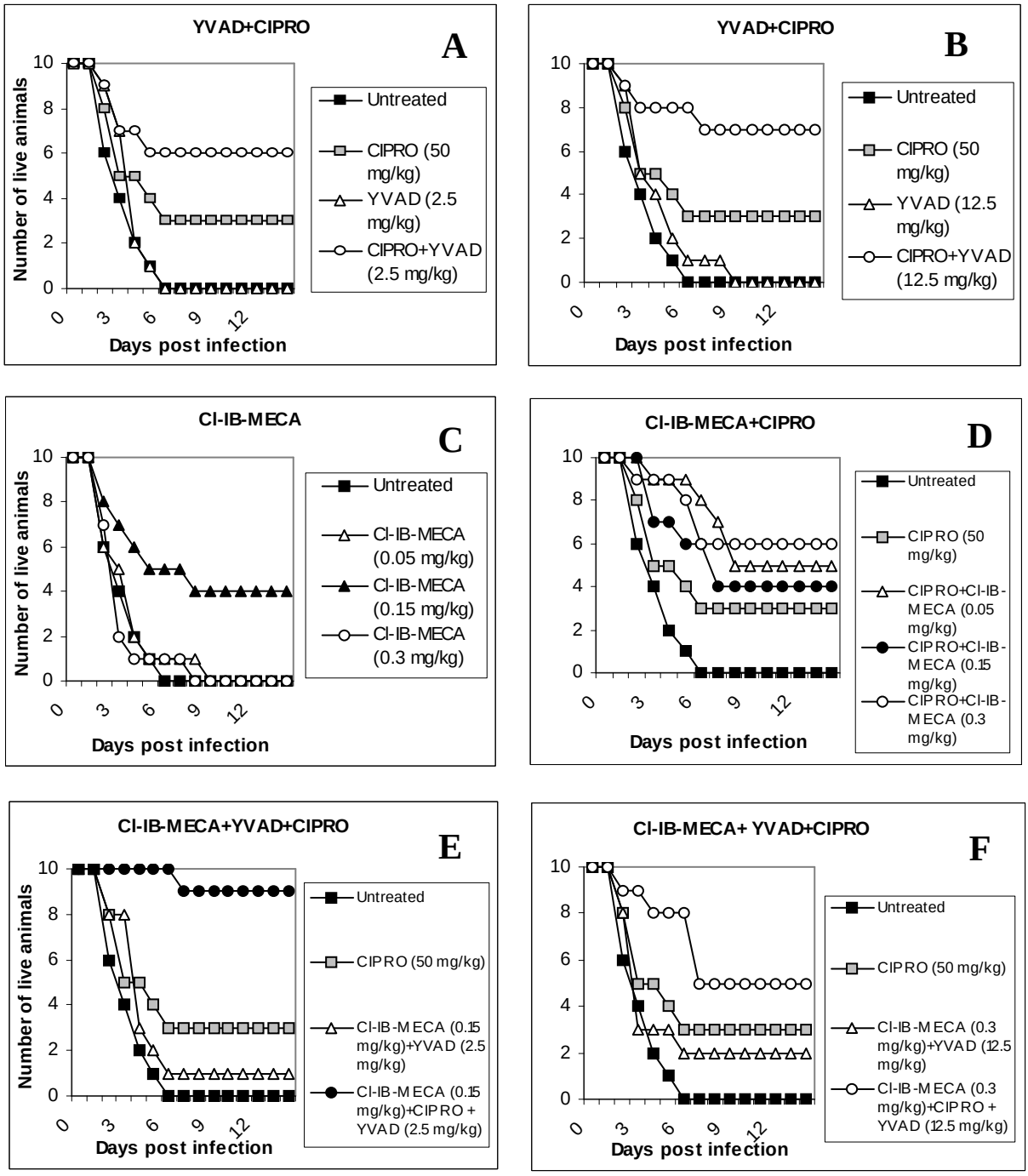

Fig. 29. Survival of DBA/2 mice after treatment: with caspase-1 inhibitor YVAD (A, 2.5 mg/kg; B, 12.5 mg/kg) in combination with ciprofloxacin (B); A3R agonist Cl-IB-MECA alone (C) and in combination with ciprofloxacin (D); triple combination of caspase-1 inhibitor YVAD (2.5 mg/kg, A; 12.5 mg/kg, B), A3R agonist Cl-IB-MECA (0.15 mg/kg, A; 0.3 mg/kg, B) and ciprofloxacin, 50 mg/kg.

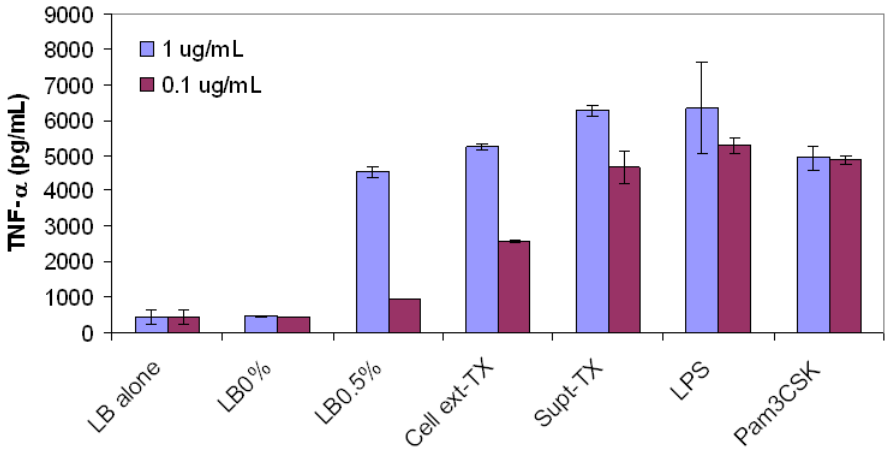

- Bacterial products (μg/mL) in protein level
- RAW264.7 cells (5 x 10^5 cells/mL: 200 μL in 48-well plate) + samples → 24 hrs → TNF-α ELISA

Fig. 30. Effect of bacterial products on TNF-α production.

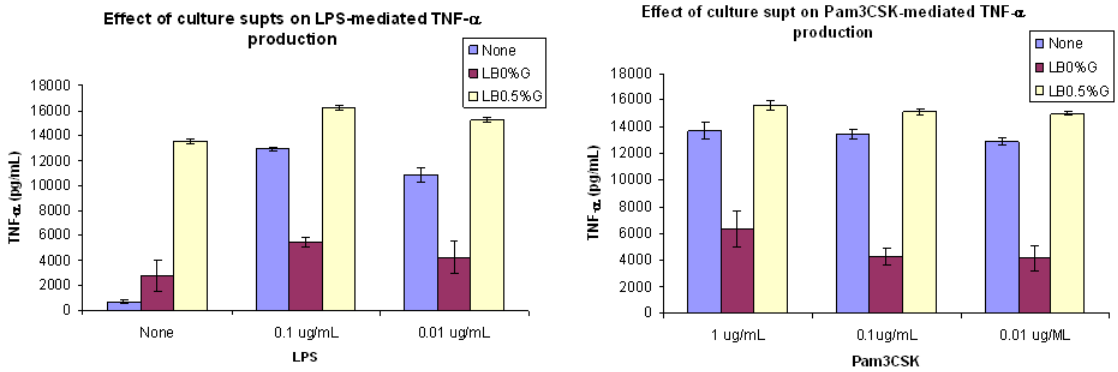

LB0%G, LB0.5%G: 1 μg/mL of protein

Fig. 31. Effect of culture supernatants on LPS- and Pam_3CSK-mediated TNF-α production.

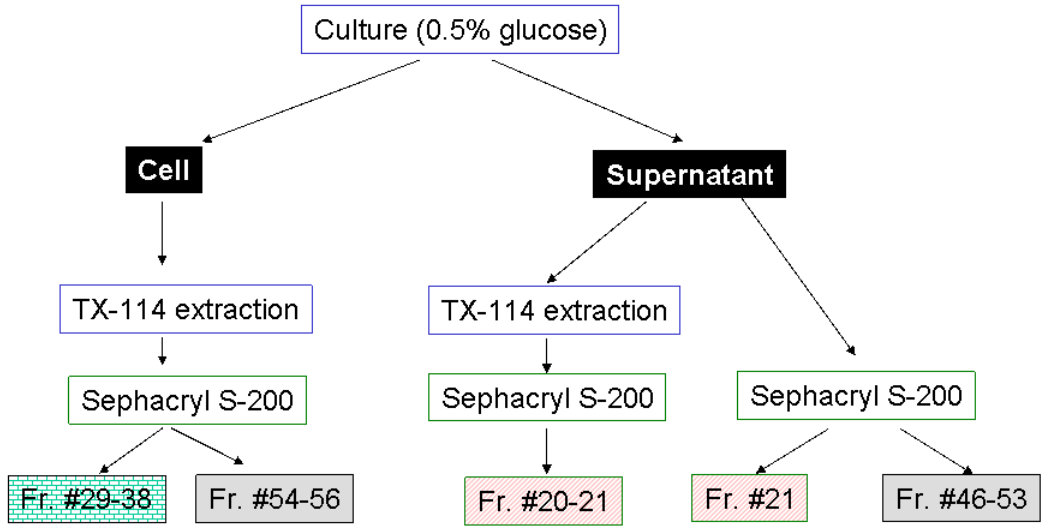

Fig. 32. Fractionation of B. anthracis cultures.

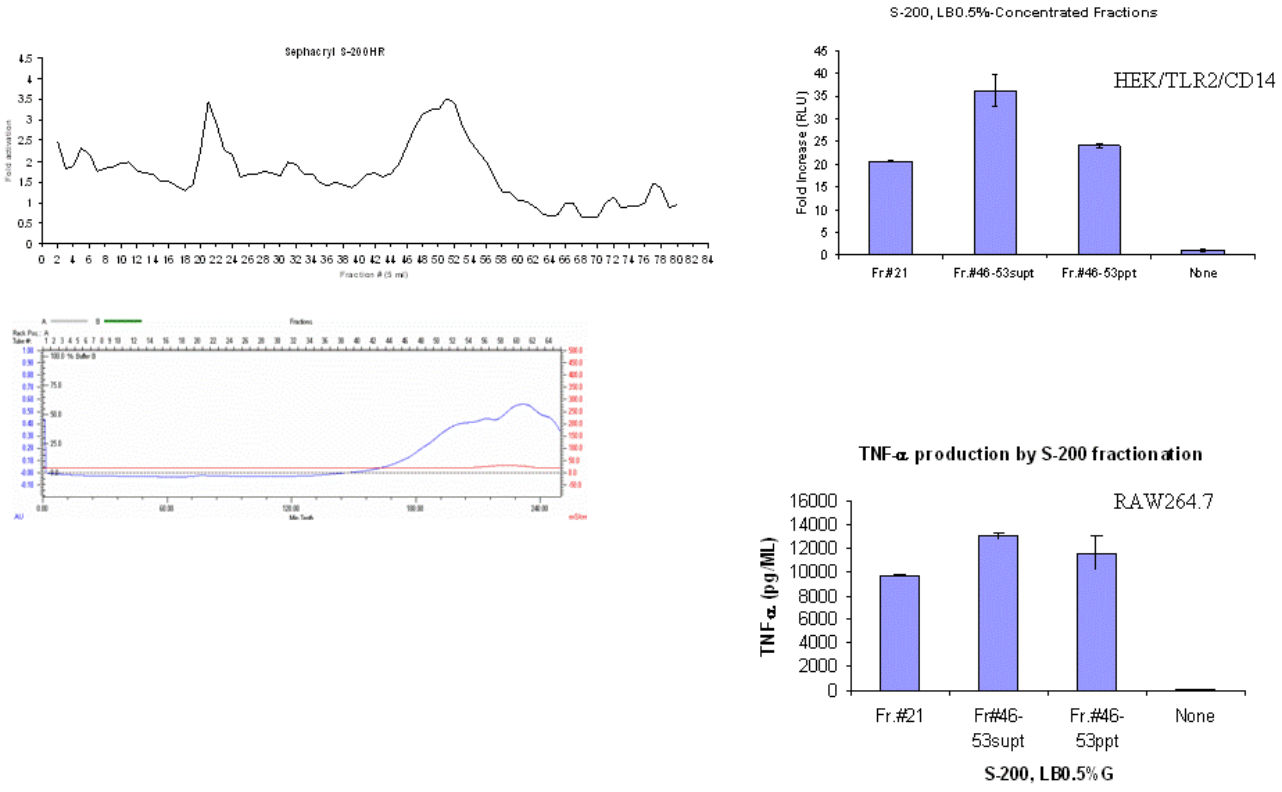

Fig. 33. Fractionation of supernatants (LB 0.5%G) by Sephacryl S-200 chromatography (NF-kB-luciferase, *left top* and chromatogram, *left bottom panel*) of each fraction, and TLR-mediated NF-κB activation (*right top*) and TNF-α production (*right bottom*) of the combined fractions.

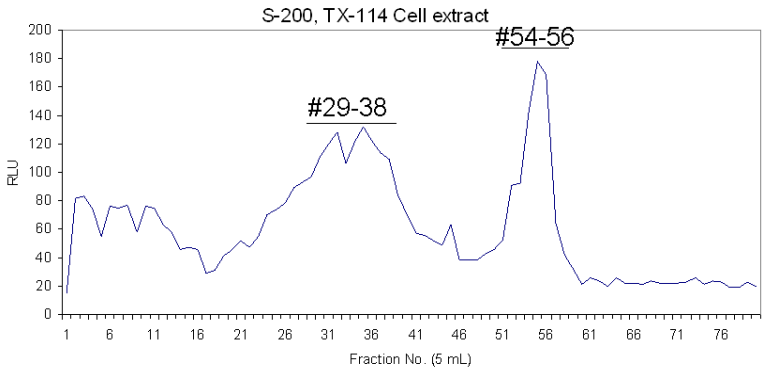

Fig. 34. NF-kB-luciferase activity of Sephacryl S-200 fractions of cell extracts.

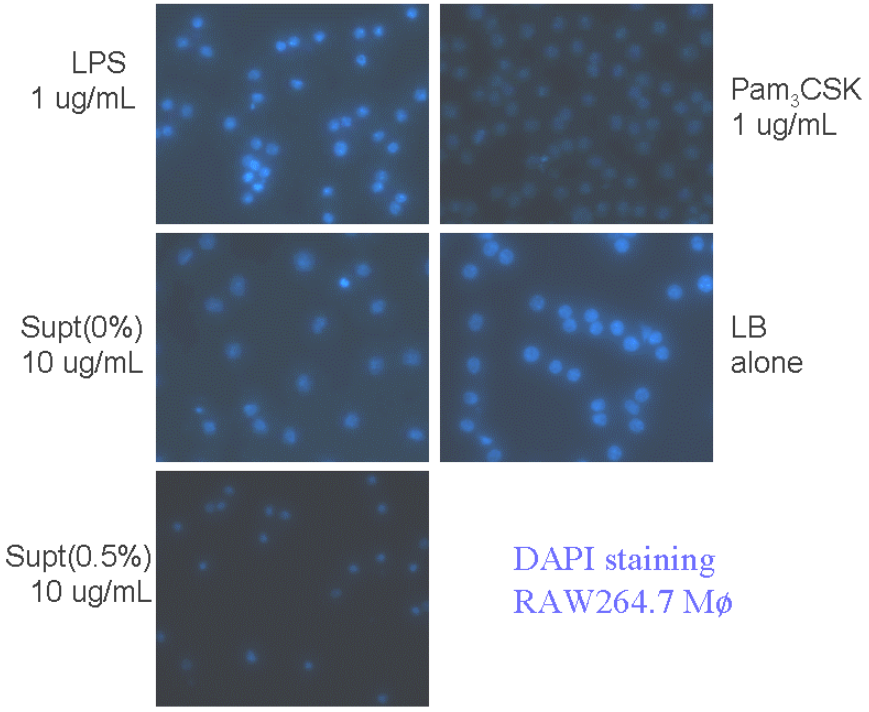

Fig. 35. DAPI staining of RAW264.7 cells after exoproduct treatment.

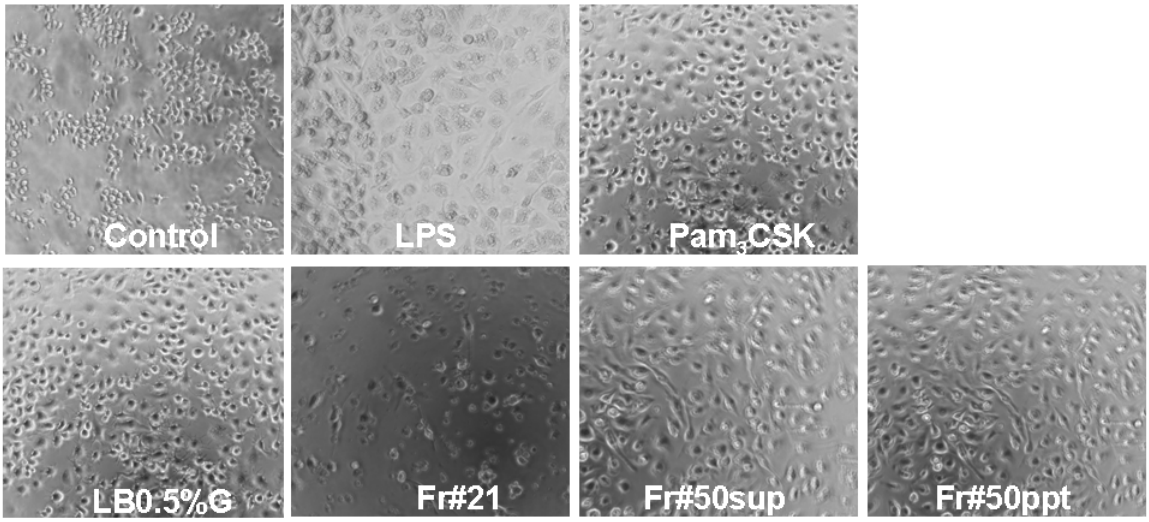

Fig. 36. Apoptosis of RAW264.7 cells by bacterial exoproducts.

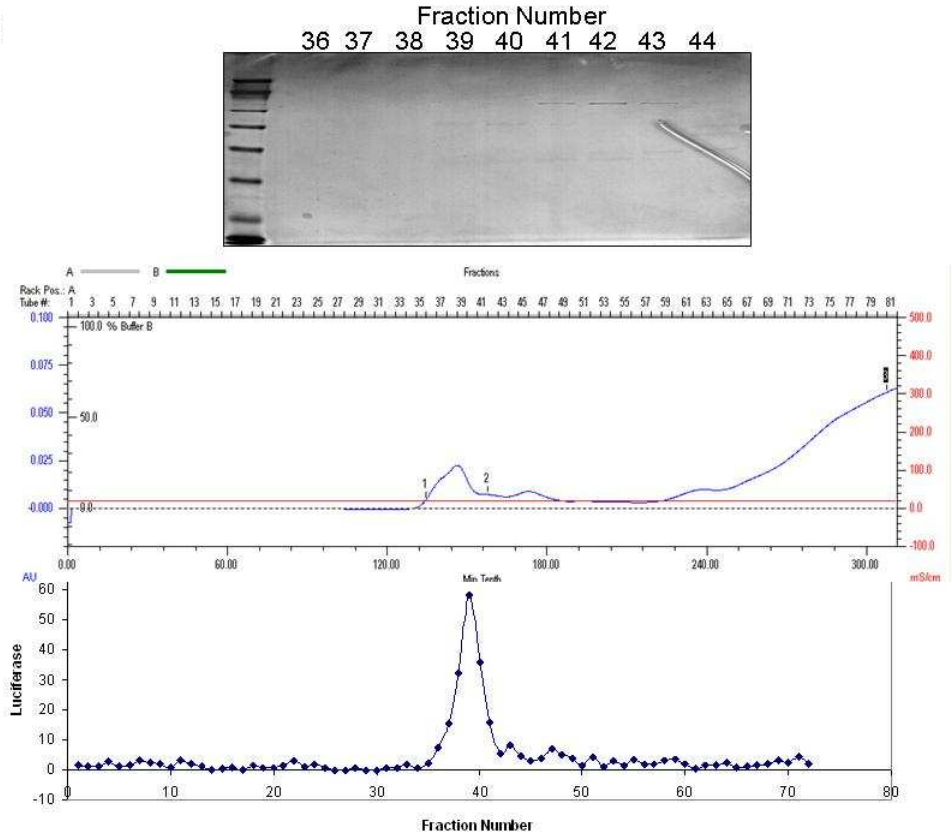

Fig. 37. TLR-2-stimulating activity of supernatant fractions.

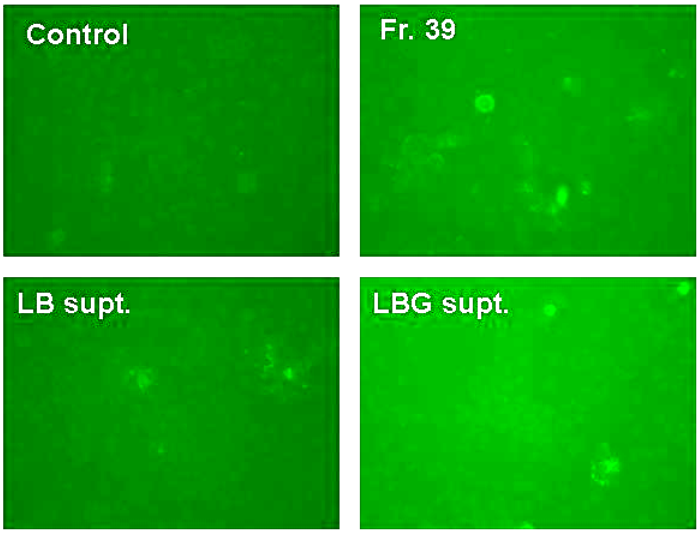

Fig. 38. Annexin V-FITC staining of RAW 267.4 cells after treatment with the fractions of supernatant.

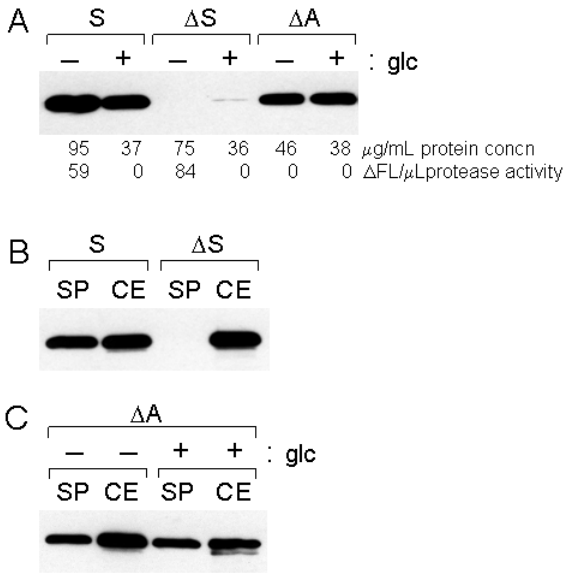

15 μL culture supt/cell extract with lysozyme(3 mg/mL) and 0.1% TX100 in PBS
→anti-GroEL antibody
S, Sterne; ΔS, deltaSterne; ΔA, deltaAmes
SP, culture supernatants; CE, cell extracts

Fig. 39. Western blot of culture supernatants and cell extracts by anti-GroEL antibody. Toxigenic Sterne starin, but not non-toxigenic delta Sterne, secrets HSP60 in LB culture supernatants.

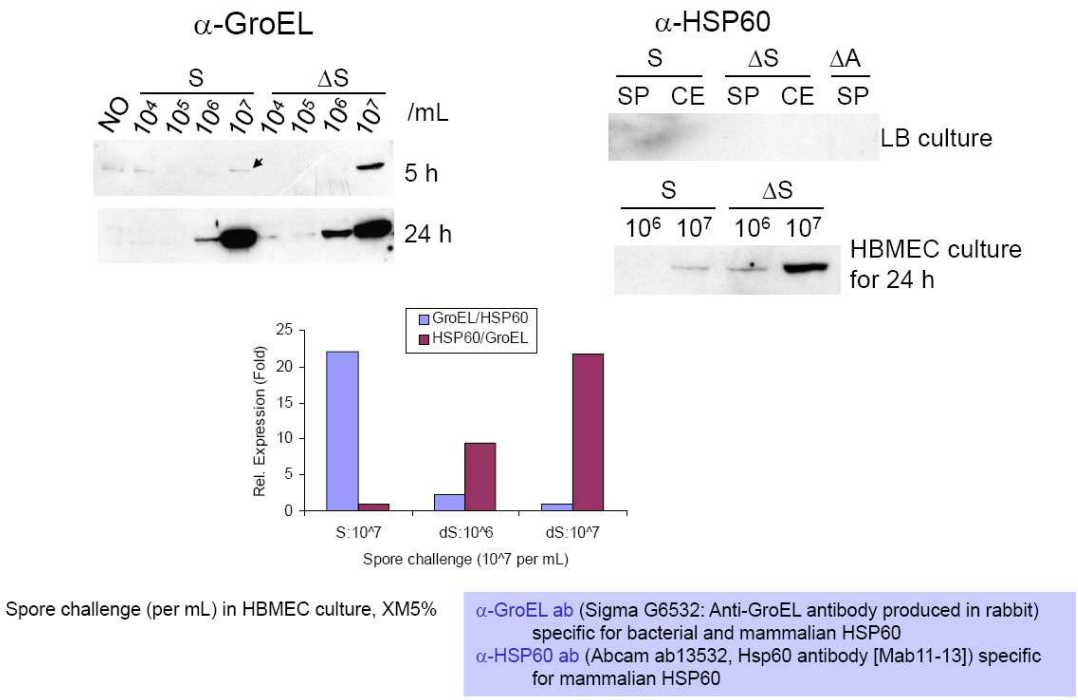

Spore challenge (per mL) in HBMEC culture, XM5%

α-GroEL ab (Sigma G6532: Anti-GroEL antibody produced in rabbit) specific for bacterial and mammalian HSP60
α-HSP60 ab (Abcam ab13532, Hsp60 antibody [Mab11-13]) specific for mammalian HSP60

Fig. 40. Spore challenge of Sterne and deltaSterne to HBMEC. Spore challenge of non-toxigenic strain delta Sterne induces endogenous HSP60 in HBMEC. Left panel, Western blot of LB culture of B. anthracis with anti-GroEL antibody. Right panel, Western blot of LB and HBMEC cells (XM5%) with anti-HSP60 antibody. SP, supernatant; CE, cell extracts.

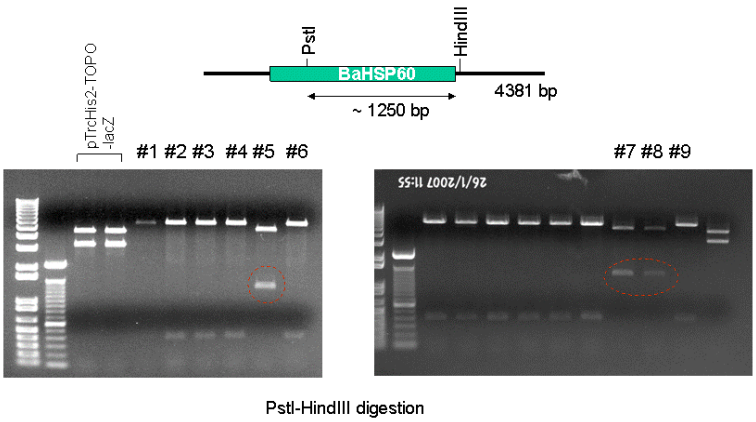

Fig. 41. Construction of BaHSP60 expression vector using pTrcHIS-2-TOPO vector.

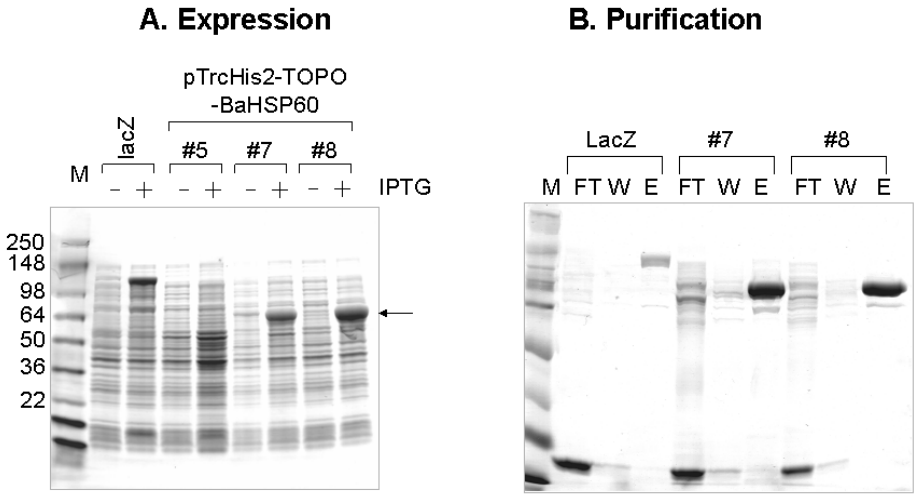

Fig. 42. Expression of recombinant BaHSP60 proteins in *E. coli* DH5α (A) and purification of recombinant proteins by Ni^{2+}-agarose beads (B).

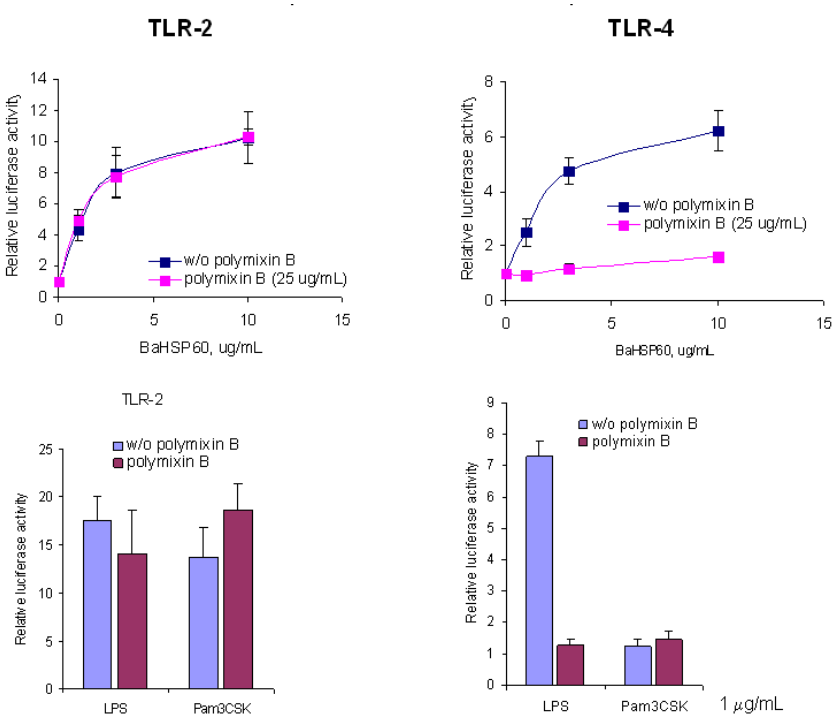

Fig. 43. rBaHSP60 induces NF-kB transcriptional activation through TLR-2. Data represents average of each sample (*n = 4, y axis bar = SD*).

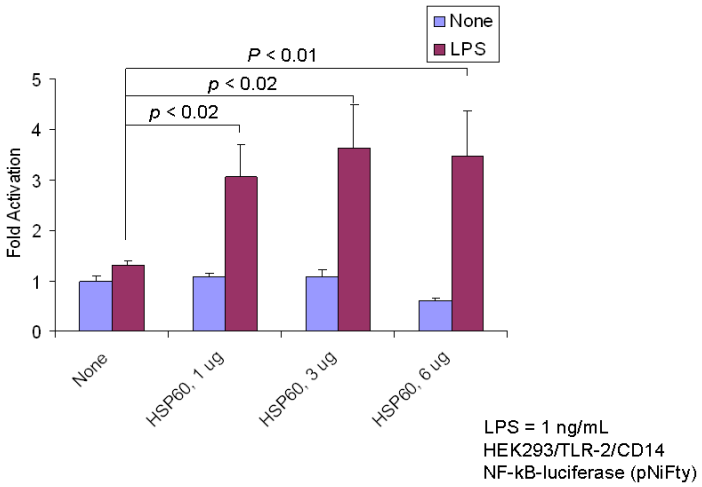

Fig. 44. Synergistic activation of TLR-2 by rBaHSP60 and LPS.

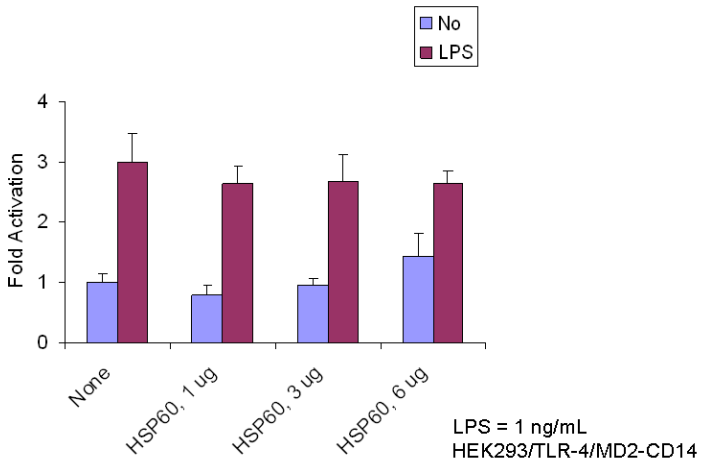

Fig. 45. rBaHSP60 does not activate TLR-4.

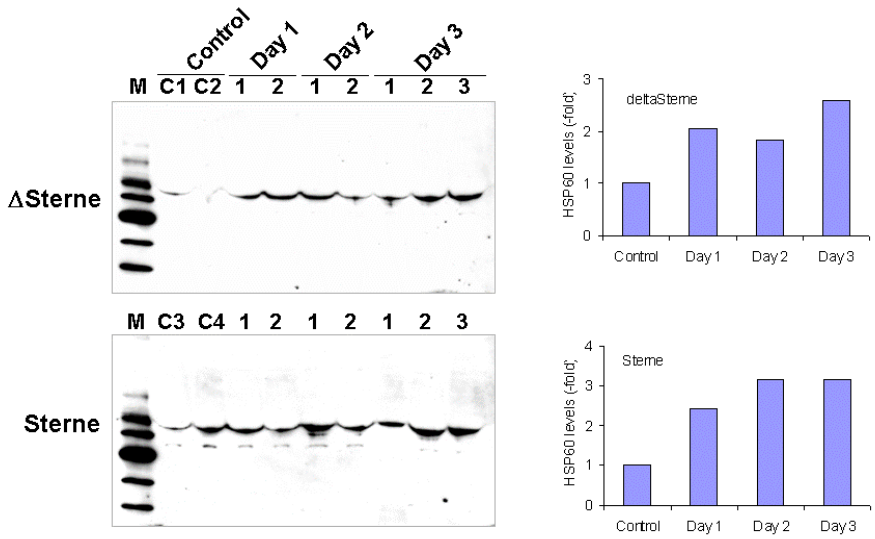

Fig. 46. HSP60 levels in plasma of spore-challenged mice. HSP60 levels represent relative average band intensity to the controls.

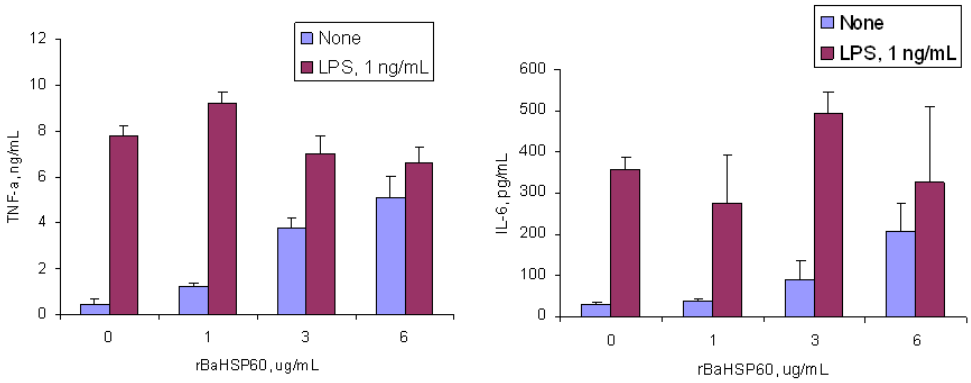

Fig. 47. rBaHSP60 induces proinflammatory cytokines TNF-α and IL6 in murine macrophage RAW264.7 cells in an LPS-independent manner.

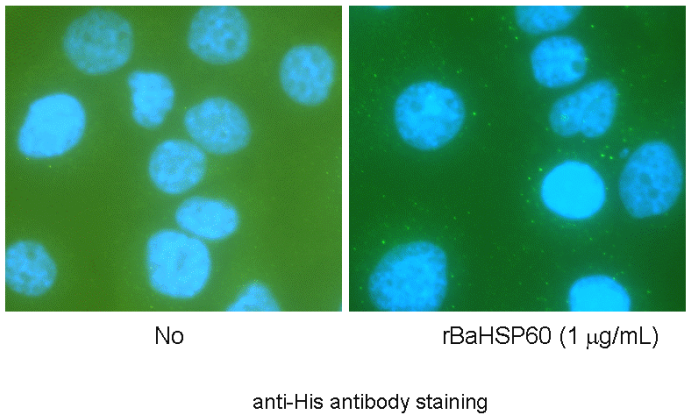

Fig. 48. rBaHSP60 binds to distinct membrane regions on HBMECs.

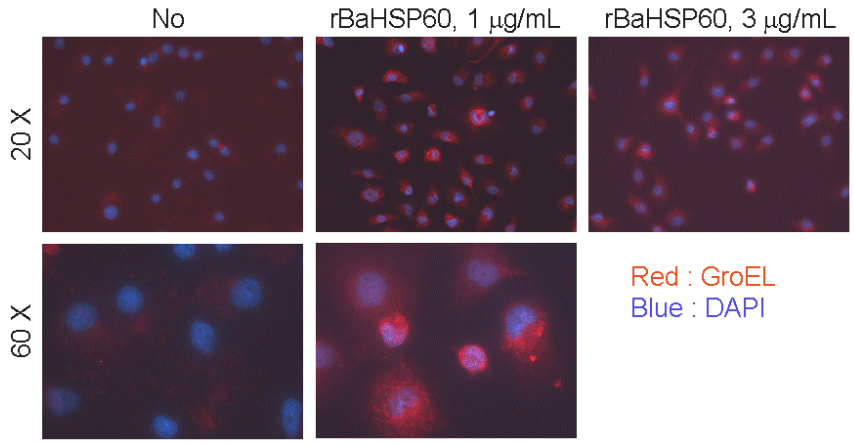

Fig. 49. rBaHSP60 induces binding to HBMECs.

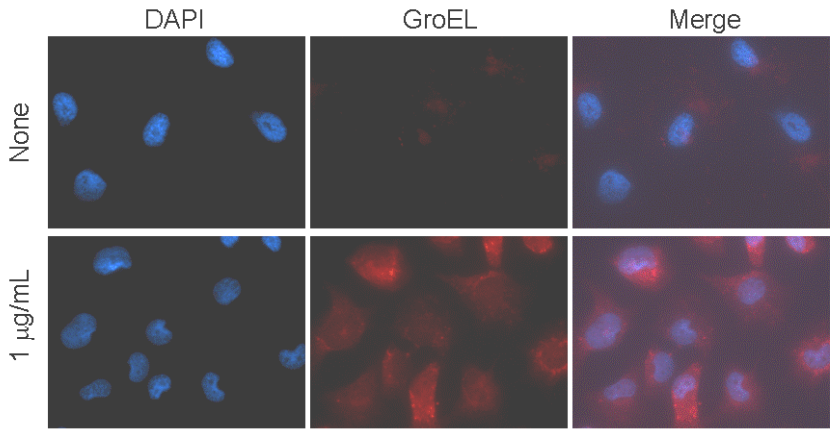

Fig. 50. rBaHSP60 induces apoptosis of HBMECs.

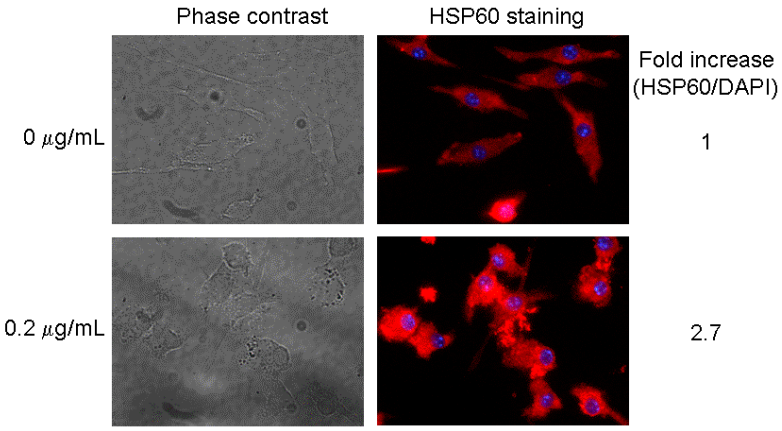

Fig. 51. rBaHSP60 also binds to and induces apoptosis of murine macrophage RAW264.7 cells

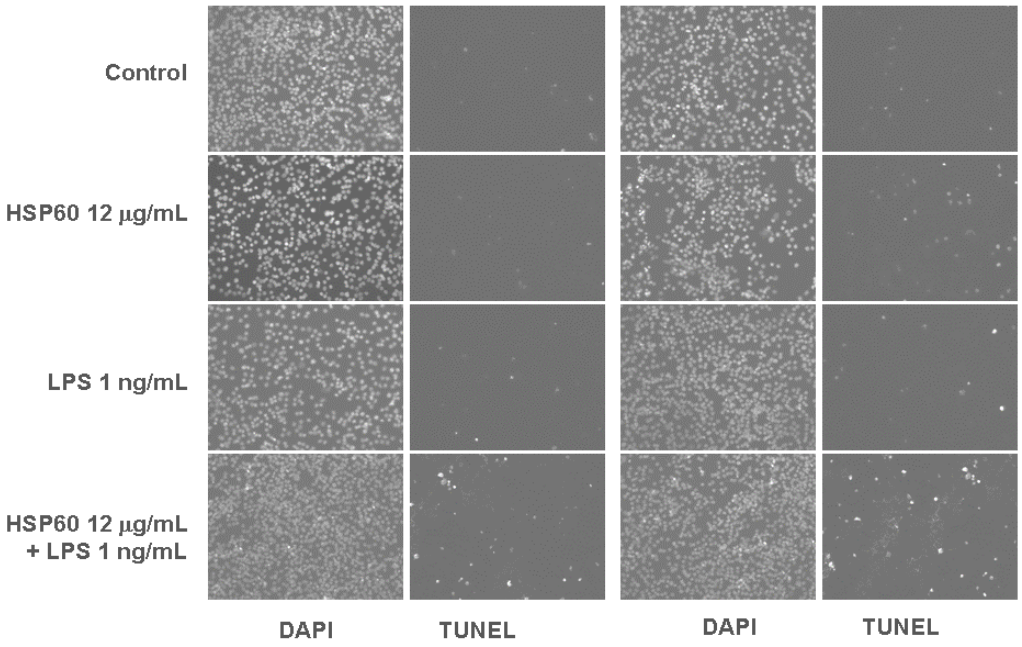

Fig. 52. Synergistic effect of BaHSP60 and LPS on apoptosis of HBMEC.

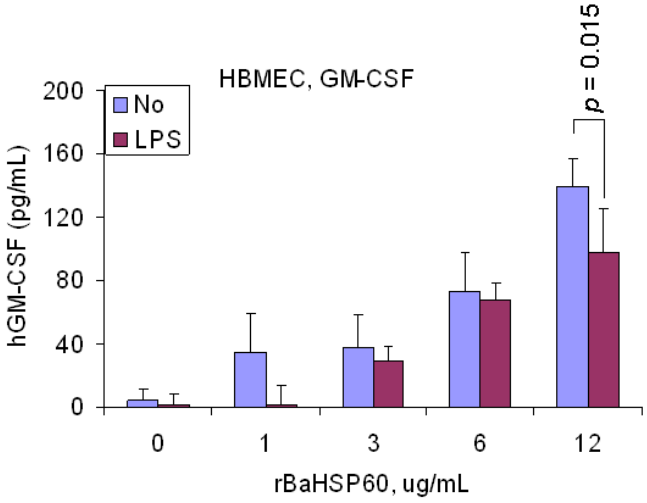

Fig. 53. GM-CSF production in HBMEC treated with rBaHSP60.

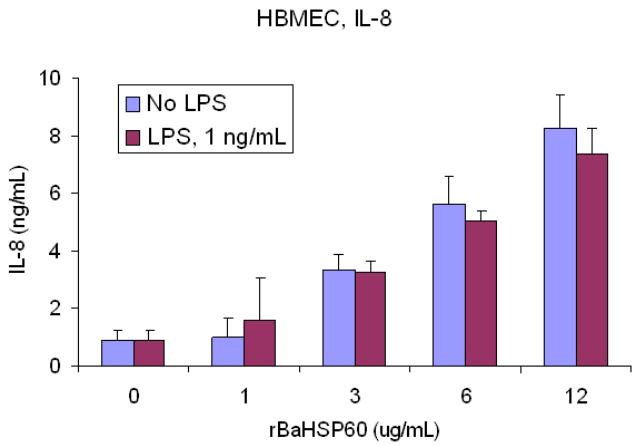

Fig. 54. IL-8 (CXCL8) production in HBMEC treated with rBaHSP60.

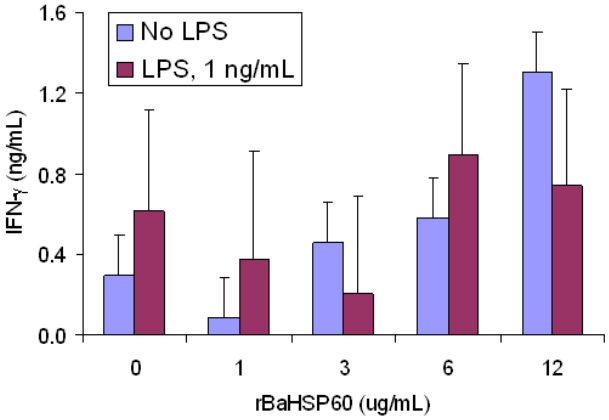

Fig. 55. IFN-γ production in HBMEC treated with rBaHSP60.

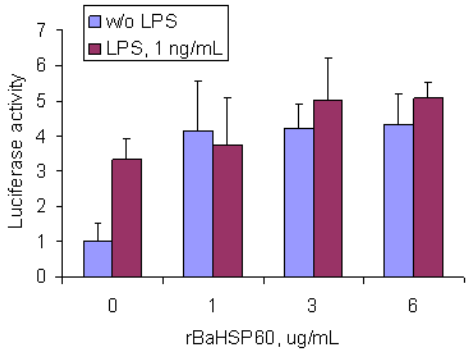

NF-κB-luciferase (pNiFty), 0.2 ug/well
Lipofectamine 2000, 0.5 uL/well

Fig. 56. rBaHSP60 and LPS activate NF-kB transcription activity in HBMEC.

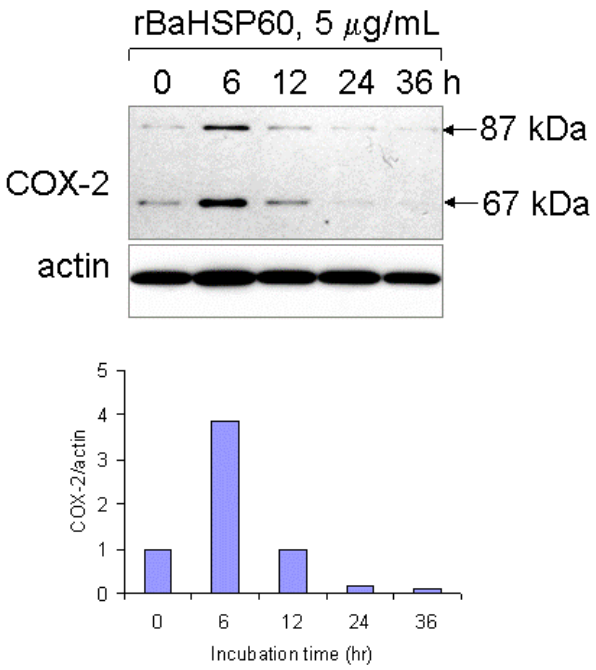

Fig. 57. Induction of cyclooxygenase (COX-2) by rBaHSP60 in HBMEC.

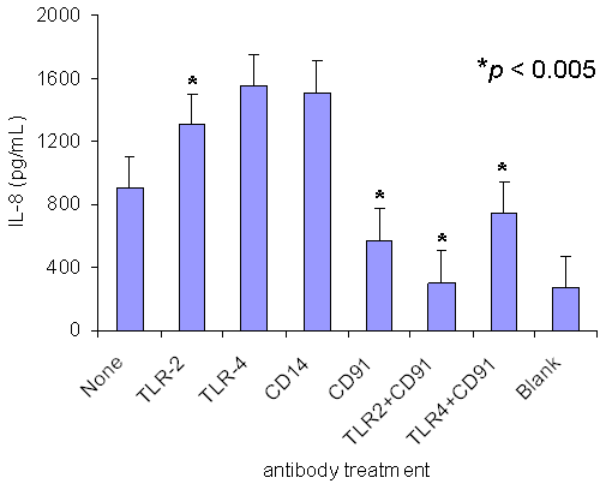

Antibody (10 μg/ml) + HBMEC (96 well) → 2 hrs in CO_2 incubator → add rBaHSP60 3 μg/mL (final) → 24 hrs → collect supt → ELISA (33 μL in 100 μL)

Fig. 58. Identification of receptors for BaHSP60 in HBMEC. CD91 acts as a receptor for BaHSP60 in HMBEC.

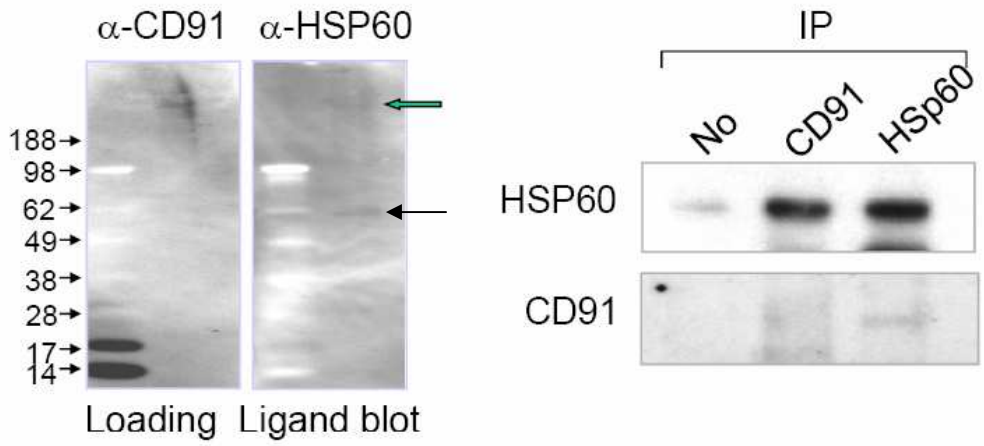

Fig. 59. Ligand blot and immunoprecipitation (IP) analysis for interaction between CD91 and HSP60.

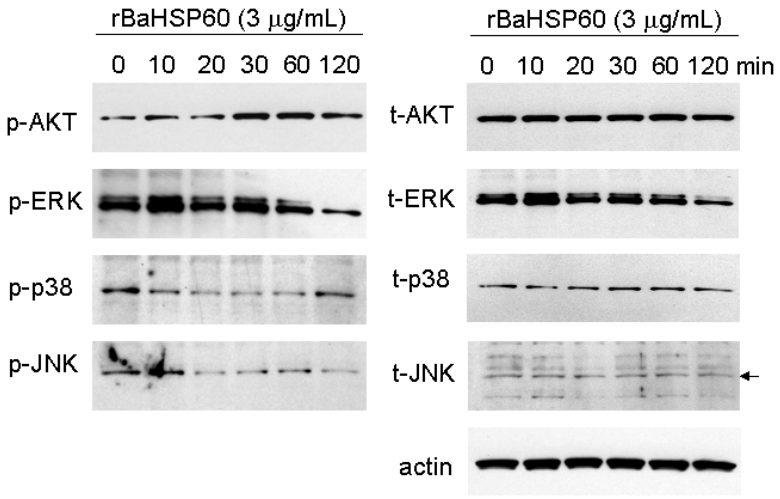

Fig. 60A. Western blot analysis of phosphorylated proteins of HMBEC cells by rBaHSP60 treatment. p-, phosphorylated protein; t-, total protein.

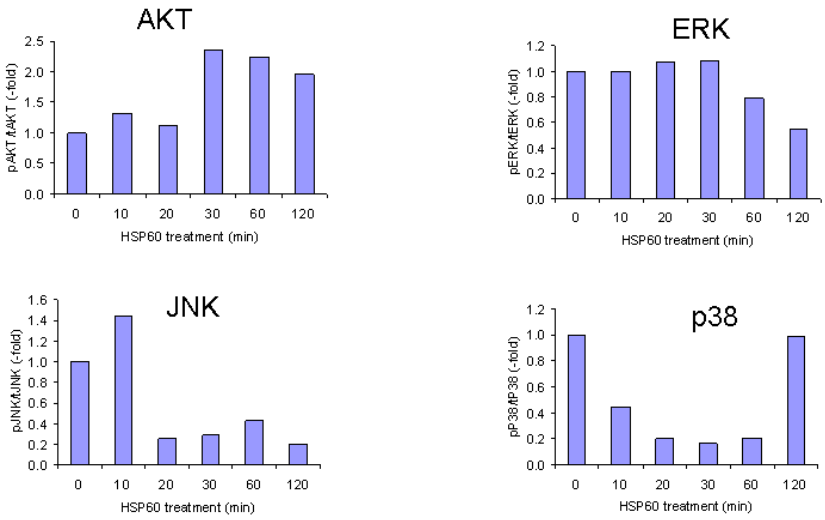

Fig. 60B. Densitometric analysis of phosphorylated proteins of HMBEC cells by rBaHSP60 treatment. Phoshporylated proteins were normalized by total proteins.

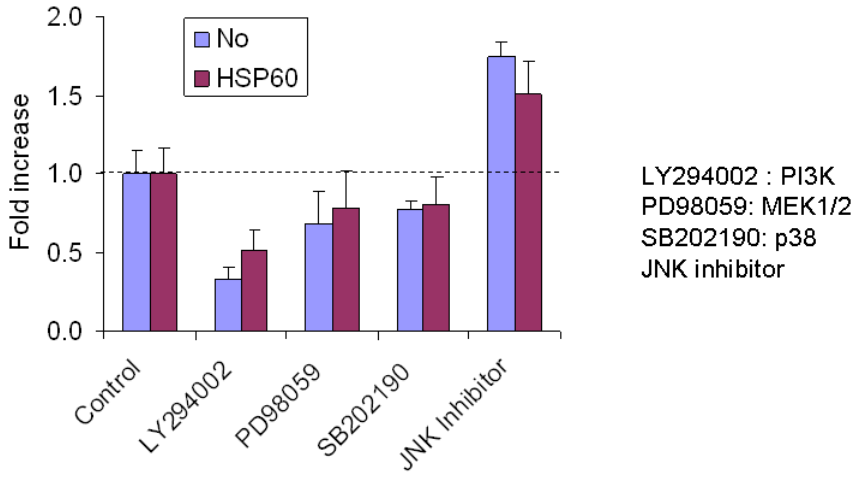

Fig. 61. PI3 kinase inhibitor LY294002 inhibits and JNK inhibitor increases IL-8 production.

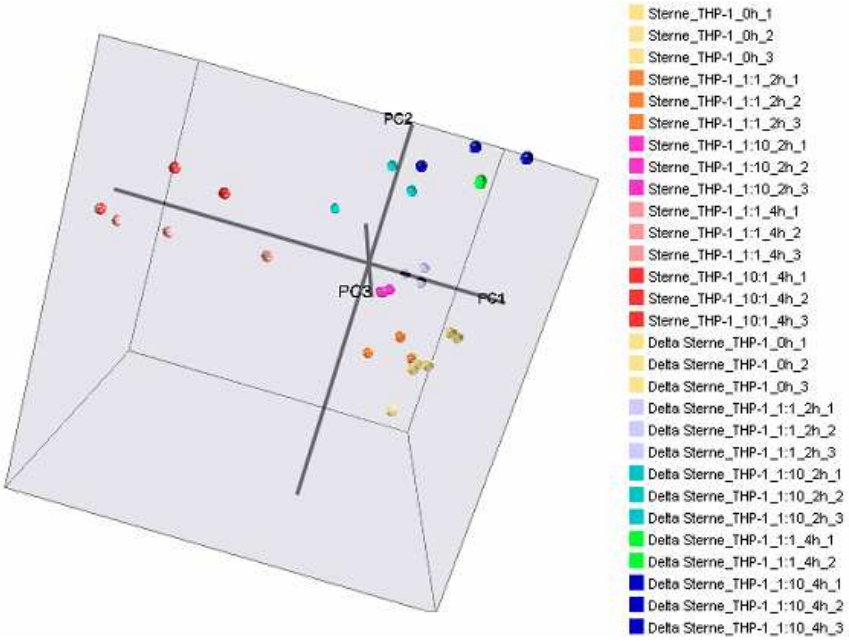

Fig. 62. Principle component analysis of microarrays run in this study confirms groupings of similar treatments, timepoints, and experimental replicates. Each color corresponds to the same experimental treatment, while each point represents a separate chip.

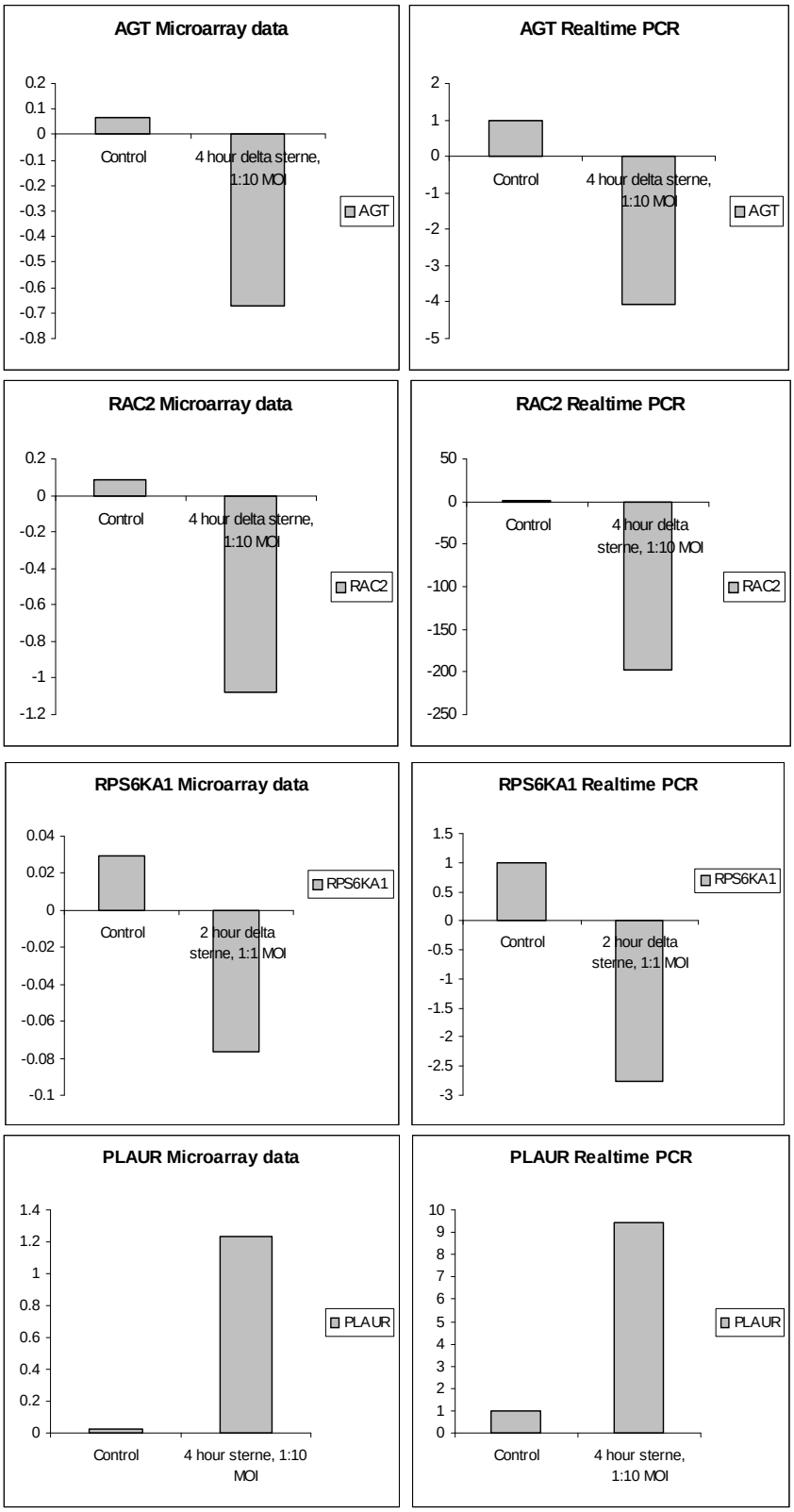

Fig. 63. Realtime PCR of single gene treatments confirms up or down expression trends in the microarray data. Y-axis in microarray data (left) represents expression relative to control samples of THP-1 cells. The Y-axis in realtime PCR data (right) represents the fold change in gene expression in the THP-1 cells within the sample (Expression within the control sample is equal to 1).

A.


sterne
sterne
Control
2 4 2 4 Hours
MOI
activation of MAPKKK
taxis
chemotaxis
immune response
defense response
innate immune response
inflammatory response
response to wounding
regulation of transcription from Pol II promoter
transcription factor
antibacterial humoral response
antibacterial humoral response (sensu Invertebrata)
DNA alkylation
DNA modification
DNA methylation
calcium-dependent protein serine/threonine phosphatase
protein phosphatase type 2A
eicosanoid biosynthesis
protein phosphatase type 2B
myosin phosphatase
oxidoreductase, acting on single donors with incorporation of molecular oxygen, incorporation of
oxidoreductase, acting on single donors with incorporation of molecular oxygen two atoms of oxygen
protein phosphatase type 2C
CTD phosphatase
prostaglandin metabolism
prostanoid metabolism
transforming growth factor-beta receptor ligand
magnesium-dependent protein serine/threonine phosphatase
oxidoreductase, acting on paired donors, with incorporation or reduction of molecular oxygen, miscellaneous
GPI-anchored membrane-bound receptor
eicosanoid metabolism
non-membrane spanning protein tyrosine phosphatase
protein serine/threonine phosphatase
protein phosphatase type 1
oxidoreductase, acting on paired donors, with incorporation or reduction of molecular oxygen
regulation of transcription
regulation of transcription, DNA-dependent
response to oxidative stress
response to pathogenic bacteria
regulation of NF-kappaB protein-nucleus import
negative regulation of protein-nucleus import
regulation of protein-nucleus import
cytoplasmic sequestering of NF-kappaB
negative regulation of NF-kappaB protein-nucleus import
response to stress
response to biotic stimulus

B.

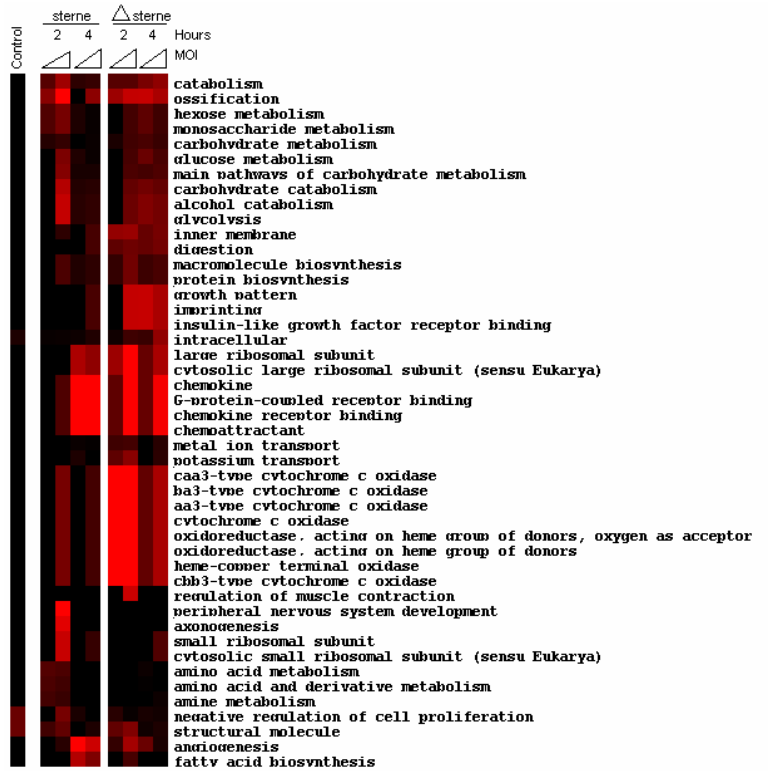
sterne
sterne
Control
2 4 2 4 Hours
MOI
catabolism
ossification
hexose metabolism
monosaccharide metabolism
carbohydrate metabolism
glucose metabolism
main pathways of carbohydrate metabolism
carbohydrate catabolism
alcohol catabolism
glycolysis
inner membrane
digestion
macromolecule biosynthesis
protein biosynthesis
growth pattern
imprinting
insulin-like growth factor receptor binding
intracellular
large ribosomal subunit
cytosolic large ribosomal subunit (sensu Eukarya)
chemokine
G-protein-coupled receptor binding
chemokine receptor binding
chemoattractant
metal ion transport
potassium transport
caa3-type cytochrome c oxidase
ba3-type cytochrome c oxidase
aa3-type cytochrome c oxidase
cytochrome c oxidase
oxidoreductase, acting on heme group of donors, oxygen as acceptor
oxidoreductase, acting on heme group of donors
heme-copper terminal oxidase
cbb3-type cytochrome c oxidase
regulation of muscle contraction
peripheral nervous system development
axonogenesis
small ribosomal subunit
cytosolic small ribosomal subunit (sensu Eukarya)
amino acid metabolism
amino acid and derivative metabolism
amine metabolism
negative regulation of cell proliferation
structural molecule
angiogenesis
fatty acid biosynthesis

C.

Fig. 64. Heat maps of GO-type biological response modules show both similarities and differences in monocytic responses to sterne and delta sterne (Δ sterne). MOIs correspond to a 1:1 MOI at the low end of a triangle, and a 1:10 MOI at the high end of each triangle.

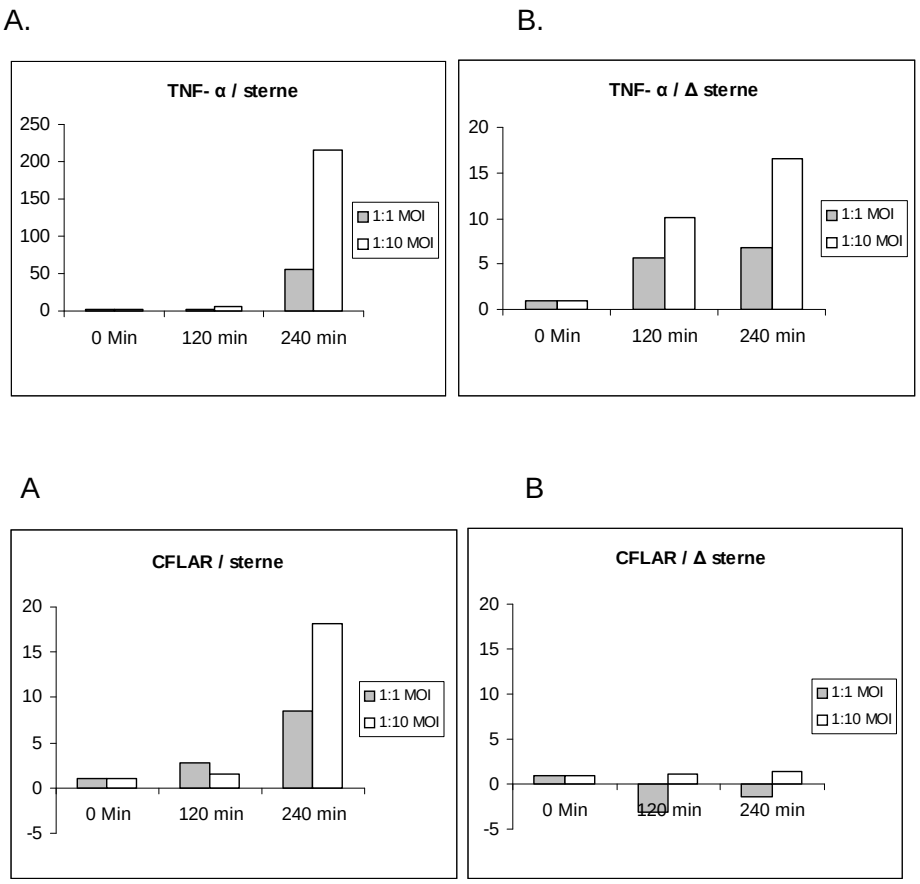

Fig. 65. TNF-α and CFLAR expression in THP-1 cells as measured by realtime PCR. The Y-axis represents the fold change of gene expression relative to the control (where the control expression level is equal to 1). A.) Expression induced by *B. anthracis* Sterne infection. B.) Expression induced by *B. anthracis* delta Sterne (Δ Sterne) infection.

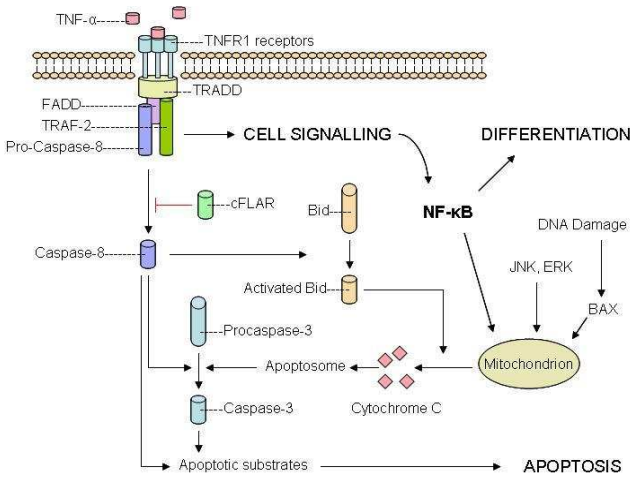

Fig. 66. TNF-α, and mitochondrial damage-dependent apoptotic pathways.